TECHNISCHE UNIVERSITÄT MÜNCHEN

Chemie Department
Lehrstuhl für Physikalische Chemie I

Synthesis, Characterization and Application of Platinum Nanoparticles in Colloidal Hydrogenation Reactions

Patricia Wand

Vollständiger Abdruck der von der Fakultät für Chemie der Technischen Universität München zur Erlangung des akademischen Grades eines

Doktors der Naturwissenschaften

genehmigten Dissertation.

Vorsitzender:	Univ.-Prof. Dr. Sebastian Günther
Prüfer der Dissertation:	1. Univ.-Prof. Dr. Ulrich Kaspar Heiz
	2. Univ.-Prof. Dr. Klaus Köhler

Die Dissertation wurde am 01.06.2016 bei der Technischen Universität München eingereicht und durch die Fakultät für Chemie am 29.06.2016 angenommen.

Abstract

Colloidal ligand-stabilized platinum nanoparticles are applied as model catalysts in the selective hydrogenation of alkynes to alkenes. The throughout characterization of the ligand-stabilized nanoparticles and the systematic study during the catalytic reaction reveal the influence of the ligands binding mode and the structure of the ligand on the hydrogenation. In detail, a new binding mode for amine ligands to platinum nanoparticles is proposed, while a seemingly established one is ruled out. This weak binding mode is reflected by the low stability in catalysis. Thiols, in contrast, lead to stable nanoparticles, but inhibit the catalytic reaction. The activity of thiol-stabilized platinum nanoparticles is enhanced by lowering the ligand coverage, which indeed does not seem to affect their stability. Besides the obtained insights into mechanisms taking place at nanoparticle surfaces, this work supplies a new and important viewpoint for future studies on amines and thiols present during colloid-catalyzed hydrogenation reactions.

Zusammenfassung

Ligandenstabilisierte Platinkolloide werden als Modellkatalysatoren in der selektiven Hydrierung von Alkinen zu Alkenen eingesetzt. Die sorgfältige Charakterisierung dieser Nanopartikel und die systematische Studie der Katalyse legt den Einfluss der Bindungsmodi und der Struktur der Liganden auf die Hydrierung dar. Im Einzelnen wird ein neuer Bindungsmodus von Aminliganden zu Platinnanopartikeln vorgeschlagen, während ein anscheinend etablierter ausgeschlossen wird. Diese, mit dem neuen Modus zusammenhängende, schwache Bindung, spiegelt sich in der niedrigen Stabilität der Nanopartikel bei deren Einsatz als Katalysator wider. Im Gegensatz dazu sind thiolstabilisierte Platinnanopartikel während der Hydrierung stabil, verlangsamen sie jedoch. Die Aktivität von thiolstabilisierten Platinnanopartikeln während der Katalyse wird durch die Verminderung des Bedeckungsgrades der Liganden verbessert, was die Stabilität der Nanopartikel nicht beeinflusst. Neben der gewonnenen Einsicht in konkrete Mechanismen auf Nanopartikeloberflächen, liefert diese Arbeit einen neuen Blickwinkel für zukünftige Forschung bezogen auf den Einsatz von Aminen und Thiolen in kolloidkatalysierten Hydrierungsreaktionen.

Contents

Preface

This dissertation evolved from the last 2.5 years of my work in the physical chemistry group of Prof. Ulrich Heiz. This work is indeed a cooperation project of Dr. Mirza Cokoja and Dr. Martin Tschurl, which includes the work in the fields of the inorganic and physical chemistry. Through this cooperation project I got the opportunity to get insights into different viewpoints of research including the work in the laboratory as well as the interpretation of results. Two written manuscripts for full papers is the countable number of output of this work. One manuscripts, which is not yet accepted for publication, and one accepted paper are the basis for main aspects of chapter 3. The publication entitled "Functionalization of Small Platinum Nanoparticles with Amines and Phosphines: Ligand Binding Modes and Particle Stability" has been accepted by the *Journal of Colloid and Interface Science* (doi: 10.1016/j.jcis.2016.06.003). Furthermore, the manuscript entitled "Influence of Thiol Surfactants on the Selective Hydrogenation of 3-Hexyne to 3-Hexene Catalyzed by Colloidal Platinum Nanoparticles" is in preparation and waiting to be submitted to the Journal *Catalysis, Science and Technology*.

Chapter 1

Introduction

„Nano“ stands for a classification of materials, which is built of one to a hundred nanometers in at least one dimension. This class of materials in the nanoscale has more and more attracted attention in science as well as for everyday life applications due to the exceptional properties these nanomaterials can have. Since nanomaterials fill the gap between bulk materials and molecular structures, their properties correlate with neither of these.[1,2] Instead, size-dependent properties are observed in the nanoscale due to their high surface-to-volume ratio.[2,3] Figure 1.1 illustrates the trend of the reciprocal decrease of the surface-to-volume ratio with an increasing diameter of nanomaterials. This relation reveals the immense influence of the particles dimension on the surface contribution for very small nanoparticles in comparison to the contribution of the bulk. For example, surface plasmons, coherent delocalized electron waves, are a phenomenon found for gold nanoparticles.[4] Their resonance changes with their size and thus, differently sized gold nanoparticles absorb different wavelengths of the visible light, consequently the nanoparticles appear in different colors.[5,6] Quantum size effects are as well observed for the reactivity and catalytic properties of nanomaterials.[1] For very small nanoparticles, also called clusters, the addition or removal of only one single atom can have considerable effects on the catalytic properties influencing the selectivity and activity of a reaction.[7,8] For example, for clusters of platinum a distinct atom by atom dependency for the oxidation of carbon monoxide or the hydrogenation of ethylene was observed.[9,10]

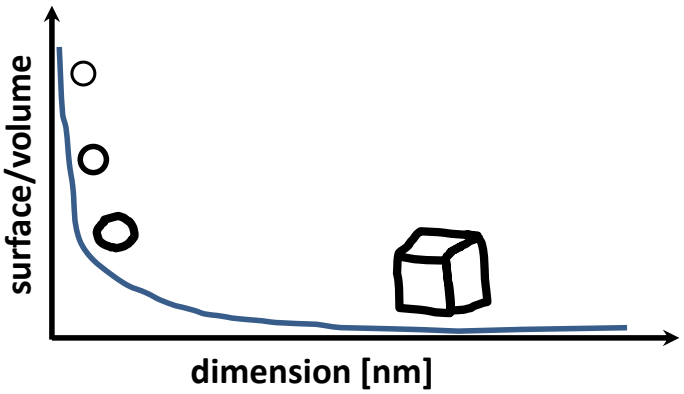

Figure 1.1: Schematic of the surface-to-volume ratio depending on a nanomaterials dimension.

One of the major fields for the application of nanomaterials is indeed catalysis. Industrially, metal nanoparticles present a state-of-the-art group of catalysts used for several reactions, especially hydrogenation reactions.[11,12] Selective hydrogenation reactions of alkynes are especially of interest in the polymer and fine chemical industries.[11] In particular, the hydrogenation of acetylene to ethylene is relevant for purifying ethylene feedstocks for polymerization applications.[13–15] For this reason, catalysts bearing great selectivity and activity for these reactions are needed.

For selective catalysis, the understanding of the mechanisms taking place at the particle surface is inevitable for the design of new nanoparticle based catalysts for industrial application. Fundamental studies are therefore of substantial relevance.[12] In literature, the structure sensitivity of nanoparticle-catalyzed hydrogenation reactions has already been reported.[16,17] Furthermore, the introduction of stabilizing ligands was found to influence the catalytic abilities of a colloidal catalyst to higher selectivities in the selective hydrogenation of alkynes.[18–20]

However, the studies of structure sensitivity and ligand influence on selective hydrogenation reactions only concentrated on either the metal structure or the ligand structure. The interplay of the ligands with the particle surface atoms and the substrate has so far not been analyzed on a molecular level. For catalytically active metal nanoparticles, such as platinum, even the binding modes of ligands to the metal surface are unknown and therefore only interpreted in analogy to complex chemistry.[21] Furthermore, in most of these studies the focus was laid on selectivity and activity rather than on stability of the catalyst. Regarding ligand binding only theoretical studies are known, which focus on the ligand-particle binding mode and the correlating influence on the selectivity and activity of the nanocatalyst.[22,23] The benefit of the knowledge of the exact binding modes of ligands to catalytically active metal

nanoparticles is the recognition of the relation between structure and performance of a nanocatalyst.

On this account, the principal questions of this work are: What are the exact binding modes of organic ligands to catalytically active metal nanoparticles and which effect does the choice of the ligand have on the catalytic reaction?

The approach for answering these questions is the synthesis of defined nanoparticles in a standard procedure followed by the functionalization of the particles in a separate step. Through careful characterization and application of these nanoparticles, the connection between structure and performance is analyzed. This work is therefore divided into three main parts: (i) nanoparticle synthesis and functionalization with organic ligands, (ii) structure analysis for the elucidation of the ligand binding and (iii) the application of the nanoparticles in catalysis. The overview given in the next paragraphs states about state-of-the-art metal nanoparticle synthesis, properties, characterization techniques and limitations as well as the application in the selective hydrogenation of alkynes to alkenes.

1.1 Properties and analysis of metal nanoparticles

For the analysis of a metal nanoparticle as a whole, different aspects have to be considered, as they can be regarded as hybrid nano-objects in themselves due to the presence of ligands at their surface.[24] The metal core and the ligand shell have to be examined distinctly and in combination with each other for the understanding of the interplay of a nanoparticle with its environment. Important aspects in this regard are the particle size, morphology and shape, the binding mode of the ligand with the particle surface and the ligand structure.

1.1.1 Metal nanoparticle synthesis with controlled size and shape

In general, two approaches for generating particles at the nanoscale are known, which are illustrated in figure 1.2. In the top-down approach small pieces are physically separated from a bulk and broken down until the particles are in the range of interest. In the bottom-up approach molecules or atoms undergo agglomeration to form clusters and finally nanoparticles.

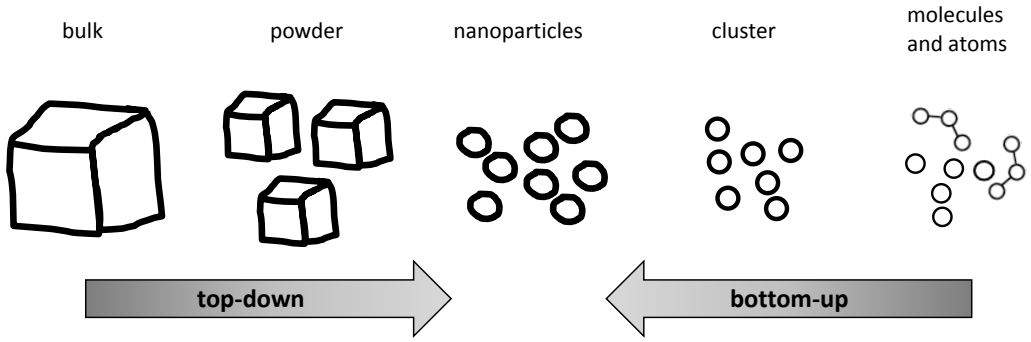

Figure 1.2: Schematic of the top-down and bottom-up approaches of nanoparticle formation.

An example for the top-down approach is the application of a cluster source in ultra-high vacuum (UHV). In this approach small metal clusters can be formed by vaporization of metal atoms from a target by laser irradiation.[25] These atoms are allowed to collide in a formation gas and form size distributed, charged metal clusters. These clusters can be guided to a quadrupole mass filter, in which a specific cluster

size can be selected and guided onto a support. This way, atom precise clusters can be obtained.

During the bottom-up approach a molecular species decomposes to form metal atoms, which stick together upon collision, grow to seeds and finally form metal nanoparticles.[26] The nanoparticle size in this approach is predominantly controlled by the reaction time, temperature and concentration of the substrates. For this approach a variety of synthetic routes are known to produce nanoparticles with controlled size and shape. A prominent example for a colloidal synthesis is the method by Brust and Shiffrin for the formation of gold nanoparticles.[27] As for the physically produced clusters in UHV, it became possible to chemically produce atom precise clusters by the refinement of the Brust-Shiffrin method and by controlling the nucleation step. The resulting atomically precise particles are usually made up of "magic" numbers of atoms, which are certain numbers of atoms tending to occur more frequently than others due to the preferred symmetrical close-packed structures of the respective element.[28] For example, the synthesis of a Au_{55} clusters is known since the 1980s, but reliable analyses to confirm the uniformity of the synthesized particles has never been given.[29] The first wet-synthesis and subsequent crystallization of a size-selected nanoparticle was made by Jadzinsky et al. in 2007.[30] They obtained Au_{102} particles stabilized by 44 *p*-mercaptobenzoic acid molecules. By careful variation of solution conditions during the synthesis, the reduction of $HAuCl_4$ in a water/methanol mixture containing NaOH, the reducing agent $NaBH_4$ and the thiol was carried out to form particles with a sufficiently small size distribution for the crystallization of thin black rods. The crystallization process was carefully screened for each particle preparation to finally form single crystals for which X-ray diffraction (XRD) measurements were performed to determine the exact number and position of atoms.

After this breakthrough a few size selective syntheses were published to obtain single crystals of thiolate protected Au nanoparticles.[31–35] However, these known synthetic routes of atom precise gold nanoparticles could bring up a misunderstanding of the actual research of metal nanoparticles. Gold nanoparticles are extensively studied and the achievements are considerable. Still, other metals are less studied and thus, the accomplishments vary. The first single crystal of a silver nanoparticle, Na_4Ag_{44}(*p*-mercaptobenzoic acid)$_{30}$, was only published in 2013 and for other metals no single crystals could be obtained at all until now.[36]

In the case of platinum no distinct synthetic route for size selected nanoparticles is known. Schmid *et al.* claimed in 1989 to have synthesized one shell (13 atoms), two shell (55 atoms), four shell (309) and five shell (561 atoms) Pt nanoparticles, respectively.[37] However, they admit, that the exact number of metal atoms in these clusters is not precise, as it was only determined via high-resolution transmission

electron microscopy (HR-TEM) images of the particles by counting or rather calculating the exact atom numbers.

Aside from the highly demanding crystallization of metal nanoparticles, the synthesis of a controlled size range is possible. For metal nanoparticles in general, different approaches for the preparation of colloids are widely used, from which the chemical reduction of a metal salt in solution is the most common method applied. Despite hydrogen, carbon monoxide, hydrides, hydrazine or sodium citrate as reducing agents, alcohols are probably the most applied reducing agents for the synthesis of metal colloids.[38] During the synthesis they act as both, reducing agent and solvent. Furthermore, a salt of the respective metal and even stabilizing agents may be present during the synthesis. Table 1.1 summarizes the influences how different reaction parameters may influence the nanoparticle size and dispersity. Thus, it becomes clear, that the size range of the Pt nanoparticles is tunable by carefully choosing the reaction parameters.

Table 1.1: Summary of the influencing parameters of the colloidal synthesis of platinum and palladium nanoparticles by alcohol reduction on the particle size.

parameter	variation	influence on NP size
stabilizing agent quantity[39]	increase	decrease
structure of alcohol[39,40]	increasing boiling point	decrease
alcohol quantity[39]	increase	decrease
metallic precursor quantity[41]	increase	increase
addition of a base[38]	addition of NaOH	decrease
heating[42]	quick heating by microwaves	nearly monodisperse

The control of the form of Pt nanoparticle was first described by Ahmadi *et al.* and attributed to the face-selective growth of crystals.[43] The distribution of the found nanoparticle shapes changed, depending on the variation of the concentration of the capping material polyacrylate with respect to that of the platinum ions. Cubic, tetrahedral, polyhedral and irregular-prismatic particles were formed. These differently shaped nanoparticles proved to have distinct chemical and physical properties, which

are desired to be controlled.[44] One approach concerning this problem was made by Tsung *et al.*, who tried to tune the particles' size and shape at the same time.[45] This challenge was accomplished by controlling the reducing rate of the metal precursors at different stages of the synthesis.

However, in all these synthetic routes for the generation of Pt nanoparticles, a protective agent for the stabilization of the thermodynamic unstable particles is present. In contrast, Wang *et al.* describes a synthesis for "unprotected" Pt nanoparticles with a mean size from 1 to 2 nm.[46] The platinum salt H_2PtCl_6 is simply dissolved in an ethylene glycol/NaOH solution and heated to 160 °C for 3 h. From this synthesis a colloidal solution of Pt nanoparticles weakly stabilized by ethylene glycol is obtained. However, in a recent study the coverage of these particles by adsorbates, other than hydrocarbons was observed, which contradicts with the stabilization by ethylene glycol.[47] It was evidenced by infrared (IR) and nuclear magnetic resonance (NMR) spectroscopy, that the surface of the particles is covered by CO and OH^- species. Nevertheless, these protective species can easily be removed by other ligands by the simple addition of a ligand or the extraction of the particles into a ligand containing phase. Hence, this approach allows for the simple variation of the ligand shell for the same particle size and shape distribution.

1.1.2 Characterization of ligand-stabilized metal nanoparticles

In order to examine the entire structure of metal nanoparticles, two different species have to be considered, the metal particles and the ligated molecules at the particles surface. Different complementary methods are usually applied for the nanoparticle analysis to include the elucidation of: (i) the metal core, (ii) the binding mode of the ligand to the particle, (iii) the structure of the ligand and (iv) the properties of the whole nanoparticle (figure 1.3). [21,48]

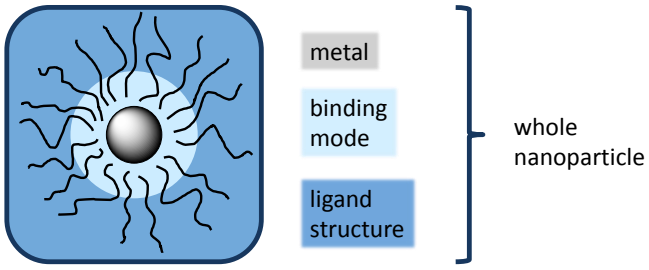

Figure 1.3: Schematic overview of the different aspects that can be analyzed in a nanoparticle.

For different moieties at the nanoparticle, different techniques have to be applied. For example, for the analysis of the size and shape of the metal core (i) transmission electron microscopy (TEM) is a common tool.[49] In an electron microscope the advantage of electrons, exhibiting much lower wavelengths as the visual light (used in light microscopes), is utilized to obtain a highly improved resolution (eq. 1.1). A good light microscope has a resolution of about some hundred nm. In contrast, an average transmission electron microscope can have a device-specific resolution of 2 to 5 Å (0.2 – 0.5 nm).

$$\delta = \frac{0.61\ \lambda}{\mu \cdot \sin\ \beta} \tag{1.1}$$

with δ = smallest distance which can be resolved [nm]; λ = wavelength [nm]; μ = refractive index; β = semiangle of collection of magnifying lens.

Due to the drastic improvement of resolution, TEMs are ideal for mapping nanostructures. In literature the indispensability of TEM analysis for nanostructures is described for the analysis of size and shape.[50] Even atom distributions and structural characteristics may be analyzed. For these reasons, the method is well established in the nano-community and obligatory for any thorough characterization.
For the determination of the size distribution of the hydrodynamic diameter dynamic light scattering (DLS) is a useful tool. However, for monodisperse suspensions only diameters > 20 nm produce reproducible and reliable measurements.[51]
Another method to elucidate the surface structure of metal nanoparticles is X-ray photoelectron spectroscopy (XPS).[52] With this method not the particle shape, but their chemical composition (up to particles of 10 nm) is characterized. For this, X-rays of known energy induce inner electrons to emit from the materials surface atoms. The specific kinetic energy (E_{kin}) of the emitted electron determines its binding energy (E_B) (eq. 1.2).

$$E_B = h\nu - (E_{kin} + \varphi_{spec}) \tag{1.2}$$

with $h\nu$ = energy of X-ray photons; φ_{spec} = instrumental correction factor.

The binding energy is characteristic for each specific orbital of a specific element. Thus, the atoms at the nanoparticle can be distinctly identified. If an identified peak exhibits a so-called “chemical shift”, the oxidation state of the respective element is

different and can also be distinctly identified.[52,53] Hence, with this method the metal core itself and surface species can be elucidated. This measurement allows for the verification of expected compounds as well as the examination of possible contaminations. For nanoparticle analysis this aspect is crucial, because contaminations can interfere with other complementary characterization methods and additionally influence the nanoparticle properties. Furthermore, quantification of the detected atom species and the layer thickness of organic molecules at the particle surface is possible.[54,55] However, for quantification very stable instrumental conditions, clean samples and sometimes even the application of standard materials are necessary.

A complementary method for the quantification of the ligand coverage at the nanoparticle sample is thermogravimetric analysis (TGA). With this method the nanoparticle samples are precisely weighted and then heated up to about 1200 °C, usually under argon. The weight loss (in percent) is detected as a function of the temperature. Often, a mass spectrometer is coupled to the TGA in order to analyze the vaporized species. After heating, the residue only comprises non-volatile components. With this method it can be determined, how much ligand is present at the particle by comparing the mass of the remaining solid with the weight loss. As the metal core is assumed to completely remain solid, the ligand coverage of the nanoparticles can be calculated this way.[56] However, molecular carbon might stay at the solid residue and distort the result. This is, why TGA can only be used as a complementary method to tighten or verify other methods results.

In order to take a closer look at the exact binding situation of a ligand at a nanoparticle surface, different techniques have to be applied. For example, IR spectroscopy can reveal the direct binding of atoms or functional groups.[57] The energy of infrared light lies in the range of the vibrational energy of molecular bonds. If the sample is irradiated by infrared light, particular wavelengths of the spectrum will be adsorbed by the sample due to the excitation of these vibrations. Only the transmitted light is detected and the adsorbed wavelengths can be assigned to distinct bonds or functional.

For nanoparticles it is difficult to obtain clean IR spectra and thus, in literature the spectra are often only described and not shown or only in a small spectral range.[56,58,59] However, the structure of ligands is often analyzed by the comparison of the spectrum of the free ligand and the spectrum of the nanoparticle bound ligand. For example, for thiol ligands bound to gold nanoparticles the S-H peak at 2576 cm^{-1} disappears in comparison to the spectrum of the free thiol ligand.[60] This disappearance is interpreted as the cleavage of the S-H bond and the formation of an Au-S bond instead.[58,60] Similarly for amine-capped Au nanoparticles particular features of the ligand and the particle ligated ligand were found.[56] The observed differences were broadening of peaks and varying relative intensities with respect to the free amine, which were explained

by the proximity of the metal to the vibrating bonds. This explanation hints at the influence of the metal on the ligand structure. However, these comparisons of IR spectra only supply indications to the real bonding situation as the changes in the spectra are small and have to be interpreted based on the common knowledge.

These interpretations can be compared and continued with the help of NMR techniques. Various NMR methods are known for the analysis of materials, each helpful and suitable for different applications. Traditionally, solution NMR has been performed for the elucidation of ligand stabilized metal nanoparticles.[24] In these studies very similar ^{1}H NMR spectra have been repeatedly shown for various metals and ligands and interpreted similarly. [56,61–63] Figure 1.4 illustrates typical ^{1}H NMR spectra of octanethiol-, (b) octylamine- and (c) dioctylamine-capped platinum nanoparticles.

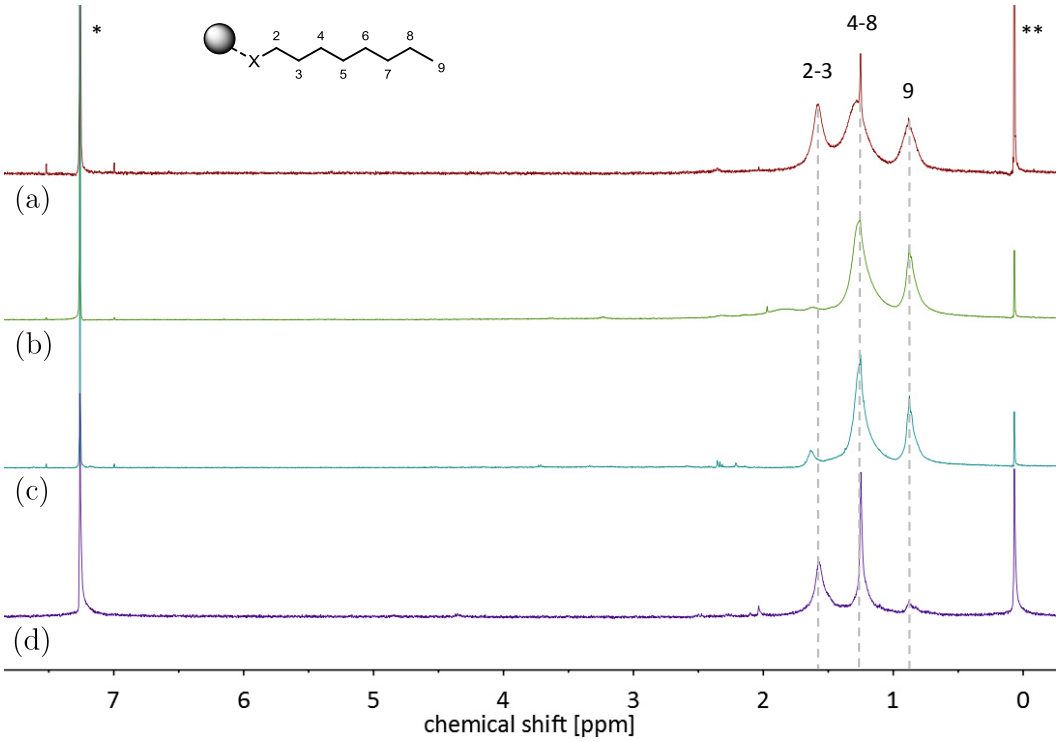

*Figure 1.4: ^{1}H NMR spectra of (a) octanethiol-, (b) octylamine-, (c) dioctylamine- and (d) trioctylphosphine-stabilized platinum nanoparticles in $CDCl_3$ (solvent peaks are marked with *; grease is marked with **).*

The spectra show broad peaks of the nanoparticle-attached ligands instead of the usual sharp peaks obtained by molecular species. For nanoparticle samples, the typical peak broadening and chemical shifts are present in the spectra as well as a change in relative intensities. These differences are attributed to the ligation of the ligands to

the metal surfaces. On the one hand, the metal itself induces differences in the chemical environment of the ligand atoms and on the other hand, the loss of flexibility of the surface bound ligand is assumed to primarily lead to the typical broadening of the peaks.

Furthermore, two-dimensional (2D) NMR techniques can be applied to obtain insights into the ligand arrangement. Nuclear Overhauser effect spectroscopy (NOESY) offers another approach for the analysis of ligand binding and structure of the ligand.[64] In this NMR method, the sign of the cross peaks can be used to determine, if a ligand molecule is bound to a nanoparticle or not. A negative cross peak indicates that bound ligand molecules are present, while a positive cross peak stands for an unbound, tumbling ligand molecule.[65,66] The drawback of this technique is the high amount of sample needed for the generation of significant peaks in the NOESY spectrum.

A further NMR method for the analysis of bound and unbound ligands is diffusion-ordered NMR spectroscopy (DOSY).[64] With this method all signals of the one-dimensional spectrum can be assigned to a certain diffusion coefficient D.[67] Free ligand and solvent peaks are attributed to higher diffusion coefficients as the signals of bound ligands.[68] Even the hydrodynamic radius d_H of the respective species can be determined by this method using the Stokes-Einstein equation (eq. 1.3).

$$d_H = \frac{k_B T}{3\pi\eta D} \tag{1.3}$$

with k_B = Boltzman constant; T = absolute temperature [K]; η = solvent viscosity.

Experiments confirmed the applicability of this equation, as the hydrodynamic radius calculated was found to increase linearly with the diameter of the nanoparticle.[64] This method allows for an easy sample preparation and a straightforward interpretation and is thus a useful tool for nanoparticle analysis. However, for all described NMR techniques a prerequisite is the good solubility of the nanoparticle sample in an NMR solvent.

To avoid this possible problem of sample preparation, solid-state NMR spectroscopy is a convenient tool for NMR analysis of ligand capped metal nanoparticles. The analysis of thiol stabilized Au nanoparticles revealed the typical peak broadening of the signals assigned to the atoms close to the particle surface.[69,70] Furthermore, by using solid state NMR the ligand arrangement, mobility, local environment of the ligands, the ligand dynamics or ligand exchange reactions have been analyzed.[24,69–72] Additionally, Chaudret, Limbach and co-workers analyzed the surface functionalities of ruthenium nanoparticles with regard to its differences after catalysis.[73] They found that during

the hydrogenation of ethylene, Ru-CH_3 surface species were formed indicating the breaking of C=C bonds during this reaction. This was observed for amine and phosphine capped Ru nanoparticles and explained by an alternative, not yet clarified mechanism.[73] These results demonstrate the high potential of NMR spectroscopy in the analysis of ligand stabilized nanoparticles.

The best method for the in depth structure analysis of the whole nanoparticle is the measurement of single crystals by XRD.[21] The XRD method can give detailed insight into the arrangement of all atoms within the particle ligand composite. However, this method can only be applied, if crystals of monodisperse nanoparticles can be obtained. The production of single crystals is up to now only possible for gold clusters containing certain atom numbers stabilized by thiols. For all other metal/ligand combinations single crystals of nanoparticles have not been obtained, yet. This difficulty of obtaining single crystals of nanoparticles represents the limitation of this method. Furthermore, the application of powder XRD instead does not bring up satisfactory results, because the nanoparticles usually contain different facets, which are all measured at the same time. These different facets result into broad reflexes in the diffractogram and thus, an exact structure analysis of the individual atoms is not possible.

In the end, all the described methods together may supply a picture of a possible structure of the whole nanoparticle-ligand arrangement. However, the manifold surface sites on a nanoparticle surface give rise to an even multiplied amount of binding possibilities for the ligands. This makes it more difficult to interpret standard characterization techniques applied for nanoparticle analysis. Nevertheless, if several complementary techniques are applied to analyze and interpret the ligand nanoparticle interactions and compare the results with established theories, insights into the nanoparticles' properties can be gained.

1.1.3 Properties of ligand-stabilized metal nanoparticles

The protecting shell of a nanoparticle certainly governs some of the most important particle properties as e. g. their stability or solubility. This shell can consist of adsorbed anions for electrostatic stabilization, steric demanding species for steric stabilization, a combination of these two types in the form of surfactants or stabilizing ligands for electrosteric stabilization. Common ligands are molecules, which coordinate to the metal surface through a heteroatom.[38] Besides the heteroatom, the ligand is composed of a ligand tail that can form intermolecular interactions with the tails of

the other ligands in the ligand shell or interact with the particle surface. The characteristics of both ligand components, the heteroatom and the ligand tail, are important parameters for the design of particular properties of a colloid.

Binding mode of ligands to metal nanoparticles

The interaction of the heteroatom of a ligand with the metal particle is a debated topic. The analysis of these interactions is very difficult due to limitations of the characterization methods and the complexity of the colloidal systems. Different particle facets can have different binding modes with the ligand. These differences are due to particular coordinating sites of the surface atoms, such as edges, corners or face sites.

For thiols the binding mode was often studied in combination with gold nanoparticles. However, while some believe, that the nature of the thiol binding mode with the nanoparticle surface is clear,[74,75] others do not share this oppinion.[76,77] The accepted two binding modes a the covalent S-Au bond or a chemisorption of the thiol. It was also stated, that the binding strength depends on the surface site.[75] From the time on crystal structures of thiol-ligand stabilized gold nanoparticles were obtained, the binding mode seems to be much better understood. The surprising findings of Jadzinsky et al. reveal a structure, which is very different from the standard models claimed before.[30] They found the sulfur atoms to bind in a bridge conformation to two gold atoms and the outer sphere gold atoms to bind to two sulfur atoms (figure 1.5d).

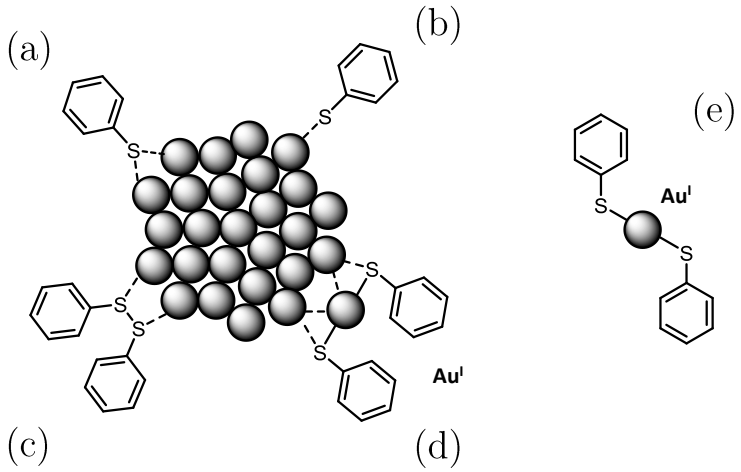

Figure 1.5: Schematic of different models for the binding modes of thiol ligands to gold nanoparticles; (a) chemisorption, (b) covalent bond, (c) covalent bond of a disulfide, (d) binding mode via Au^{I} at the nanoparticle surface[30]and (e) Au^{I} thiolate complex.

These oligomeric Au(I)-thiolate structures are similar to known anionic complexes, which are illustrated in figure 1.5e.[78] This work had an immense impact on understanding of ligand-nanoparticle interaction as since then the gold atoms could be divided into inner and outer spheres with distinct chemical states (Au^0 and Au^I). This bridging motif of thiol ligands was since then observed for several Au nanoparticles.[31,33–35] For very small Au_{11} clusters strong Au-S and Au-P bonds were found, in which the heteroatom only interacts with one Au atom at the particles surface.[32]

For other ligands despite thiols and phosphines no crystal structure of a ligand capped nanoparticle is known until now. Furthermore, only XRD-structures of gold nanoparticles have been obtained so far. These limitations represent the state of the art in research of the exact binding modes of ligands to metal nanoparticles. For all other metals different approaches for the analysis and interpretation the binding modes have to be taken into account.

One approach for this problem is the use of the hard-soft acid-base (HSAB) theory for the prediction of the affinities of ligands to metal particles.[21,79] In this approach hard Lewis-acids and Lewis-bases form strong electrostatic interactions and soft Lewis-acids and Lewis-bases form covalent bonds. The combination of a soft and a hard Lewis-acid and -base leads to a weak interaction of these two. Following this theory, for thiolate protected gold nanoparticles a gold-sulfur bond results, which was disproved by the discovery of the staple motif by Jadzinsky. However, the HSAB theory is still applied for other metal particle/ligand combinations.[21]

Furthermore, the interaction between a metal nanoparticle surface to a ligand molecule is in general seen to be similar to that of a metal ion and a ligand in a metal-organic complex.[21,80,81] From this approach of coordination chemistry, the interactions of the ligands heteroatom and the nanoparticle surface atom is usually specified as a covalent bond. For example, the interaction of a neutral atom containing a free electron pair is proposed to form a covalent bond, in which the lone pair binds to the metal atom of the particle surface. Examples of this ligand type are amines or phosphines. Furthermore, a metal atom can provide electrons for a covalent bond to a neutral ligand with an odd number of valence-shell atoms. These bonds, however, are cleaved heterolytic to form ionic fragments from, for example, carboxylic acids or inorganic salts. These ionic species interact electrostatically with the nanoparticle surface atoms. This categorization is simple and for nanoparticles different other requirements may have to be taken into account. For example, a ligand can interact differently with the face, the edge or the corner atom of a particle, which all exhibit different kinds of coordination. As a consequence, for other ligands than thiols the binding modes are lively discussed.

One example for this are amines, which belong to a group of ligands frequently used for nanoparticle stabilization. For these ligands no agreement for the binding mode to a metal surface has been found, yet. Most common interpretations agree with the metal-organic approach, which suggests the formation of a covalent bond between the amine and the metal surface. For example, Leff et al. state, that this interpretation is in agreement with their systematic characterization of dodecylamine and oleylamine capped gold nanoparticles.[56] Kumar and coworkers define the binding mode of amines to gold nanoparticles more precisely.[74] They claim, that two different binding modes are present, of which one is a weak electrostatic interaction of surface-bound chloroaurate ions with the protonated amine and the other one is a strongly bound [AuCl(NH_2R)]-like species in which the nitrogen atoms coordinate directly with the gold nanoparticles. Furthermore, in a more recent work from 2014, de la Llave et al. describe the binding of amine ligands only vaguely as a direct interaction of the amine functionality with the gold surface.[82] This imprecise way of speaking already makes clear, that the binding mode has certainly not yet been understood and the interpretation of spectroscopic data is not straight forward. Even more, for other metals than gold this interaction is less understood or rather hardly analyzed. In this manner the amine ligand binding to platinum nanoparticles is only compared by the adsorption energies by DFT calculations by Kwon et al.[22]

Overall, this short summary of binding modes of ligands attached to metal nanoparticles in literature reveals the lack of knowledge in this area. The assumed models, which are applied for an easier and better understanding of the binding modes, cannot straightforwardly be applied to nanoparticle systems due to their various surface sites and different electronic properties. The absence of an appropriate method to characterize the particle structure in detail and is presumably the major reason for this lack.

Influence of ligands on nanoparticle properties

In the first place, the purpose of using ligands in nanoscience is to stabilize the nanoparticles and protect them from growth or agglomeration. However, due to their high surface-to-volume ratio the properties of the nanoparticles are predominantly influenced by the surface properties. If ligands are attached to a nanoparticle, the particles' properties will change. Different ligands can influence the particle properties in different ways. In this regard, the physical and chemical properties can be manipulated by the choice of a particular ligand.

A particles stability in a certain solvent is greatly dependent on the ligand attached. Ligands comprising a hydrophobic ligand tail will readily adjust the nanoparticles solubility to nonpolar solvents and hydrophilic ligand-stabilized nanoparticles will be soluble in polar solvents.[83] A special feature of nanoparticles stabilized by ligands with

certain properties is their ability to form pickering emulsions.[84] In such a pickering emulsion nanoparticles, instead of surfactants, are used for the stabilization of the emulsion. The requirement of the nanoparticles is to be partially soluble in both phases. In dependence of the ligand and the coverage degree, the size of the droplets in these emulsions can be tuned.

Important features among others considering the solubility are the ligand coverage or ligand-ligand interactions. By the variation of the ligand coverage the structural arrangement of the single ligand molecules are governed.[85] For example, ligands with long alkyl chains can form a 2D structure at low ligand coverage and a 3D structure at high ligand coverage. In the latter case the order of the ligand layer is maximized for very long chains.[86] One special case of ligand arrangement is the formation of a chiral environment. This intrinsic chirality can be identified by the crystal structure analysis of the nanoparticle and has been proven for Au_{102}(p-MBA)$_{44}$.[30] The phenomenon of chirality of ligand protected clusters has been intensively studied by Bürgi and coworkers, who focused on the transfer of chiral information from the ligand molecule to the nanoparticle.[87] This effect was analyzed by circular dichroism (CD) spectroscopy and various examples have been demonstrated by their group.[88–91] This property opens the door for sensing or catalytic applications. In catalysis, the application of chiral nanoparticles could promote new, highly desired enantioselective syntheses.

1.2 Colloidal metal nanoparticles in the selective hydrogenation of alkynes

The application of stabilized metal nanoparticles in catalysis is especially interesting for selective reactions. The selectivity of hydrogenation reactions of alkynes alkenes can be explained by the reaction scheme in figure 1.6, which is based on the Horiuti-Polanyi mechanism.[92] The reaction proceeds through the consecutive addition of hydrogen to the triple bond obtaining the partial hydrogenated alkene and the fully hydrogenated alkane.[92–94]

A kinetic selectivity favours $k_2 >> k_4$, which means that the hydrogenation would largely stop at the stage of the adsorbed alkene. This case is generally excluded by experimental studies of different metals due to their fast activation of hydrogen to hydrides.[16] A thermodynamic selectivity is obtained when $k_1/k_{-1} >> k_3/k_{-3}$. In this case, the alkyne is preferentially adsorbed from the metal surface prior to the alkene. One way to achieve high selectivities is to reduce the activity of the catalyst by its specific poisons.

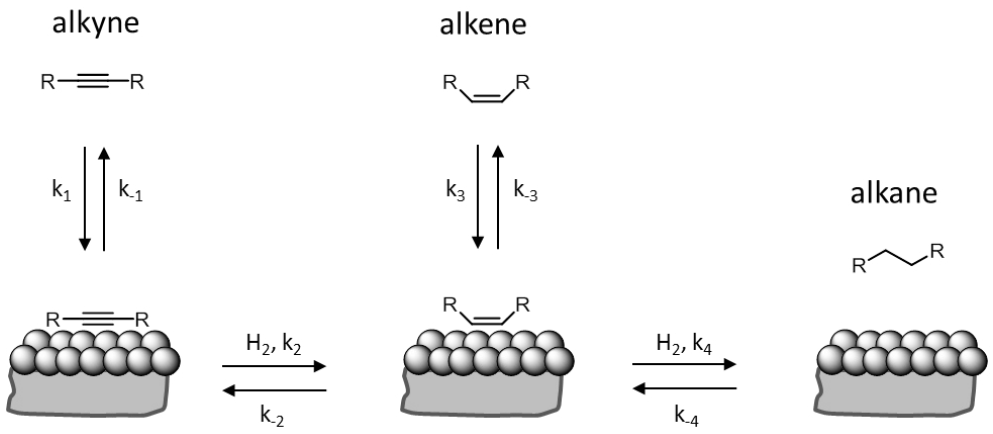

Figure 1.6: Schematic of the hydrogenation mechanism of alkynes on the basis of the Horiuti-Polanyi mechanism; k = rate constants.[92]

In the industry the concepts of the pioneering work of Lindlar, which facilitates this approach in the 1930s, was applied for decades due to the lack of new and innovative contributions. Only lately, Witte et al. presented their designed catalyst NanoSelect™ for the semihydrogenation of alkynes.[95] The catalyst comprises Pd and Pt nanoparticles capped with hexadecyl(2-hydroxyethyl)dimethyl ammonium dihydrogenphosphate and produces comparable selectivities and activities to Lindlar type catalysts in large scale. The concept of using nanoparticles for this reaction is not new, as they present an alternative to heterogeneous catalysts. Furthermore, the application of colloidal nanoparticles in fundamental studies of this kind of reactions might bring insights into the working principle of the catalysts itself without the influence of a support. Table 1.2 summarizes some studies of the selective hydrogenation of alkynes to alkenes applying colloidal metal nanoparticles.

The different fundamental studies about protected metal nanoparticles for the selective hydrogenation of alkynes to alkenes concentrate on different aspects of the catalyst. The ligand influence, the application of ionic liquids (ILs) or the replacement of precious metals with cheaper ones were prospects in focus of these studies.

The influence of the ligand was studied by Pellegatta et al., who investigated the hydrogenation of phenylacetylene catalyzed by polyvinylpyrrolidone (PVP) stabilized Rh colloids.[18] This work illustrates the coordination of phosphines to Rh nanoparticles and the improvement in selectivity in comparison to the nanoparticles without phosphine influences. Furthermore, Kwon et al. investigated in a combined experimental and computational study the influence of amine ligands.[22] For example, the introduction of octylamine to the nanoparticle system increased the yield for 4-octene in the 4-octyne hydrogenation from 0 % to about 90 % compared to the bare Pt nanoparticles. The selectivity was found to be dependent on the degree of surface

coverage with the amine. In addition, different stabilizers were compared. It was found that due to the low adsorption energy of trioctylamine the stabilizer hardly influences the reaction, whereas the high adsorption energy of trioctylphosphine makes it a poison for the catalyst.

Table 1.2: Hydrogenation of alkynes to the corresponding alkenes using colloidal metal nanoparticles[a].

substrate	metal	stabilizer	solvent	NP size	p	T	t	conv.	sel.	ref.
				nm	bar	°C	h	%	%	
phenylacetylene	Rh	PVP, PPh_3	Water	2 - 3	7	60	6	58	93	[18]
phenylacetylene	Rh	PVP, PMe_2	Water	3 - 3	7	60	6	23	83	[18]
1-octyne	Ni	DTBB[b]	THF	2.5 ± 1-5	[c]	25	24	100	85	[96]
4-octyne	Ni	DTBB[b]	THF	2.5 ± 1-5	[c]	25	2	100	99	[96]
diphenylacetylene	Pt	[d]	methanol		13.8	90	16	100	100[e]	[97]
4-ethynyltoluene	Pt	[d]	methanol		13.8	90	4.5	100	88	[97]
diphenylacetylene	Pd	$(C_4H_9)_4NBH_4$	THF	1.8	8	30		100	100[f]	[19]
4-octyne	Pd	$(C_4H_9)_4NBH_4$	THF	1.8	8	30		100	98	[19]
2-hexyne	Pd	$(C_4H_9)_4NBr$	solventless	4 ± 1	2	20		100	71	[20]
1-hexyne	Pd	PVP	ethanol	2.1 ± 0.4	1	25	0.7	95	96	[98]
3-hexyne	Pd	PVP	ethanol	2.1 ± 0.4	1	25	0.5	95	99	[98]
3-hexyne	Pd	IL[g]	IL[g]	7.3 ± 2.2	1	25	1.3	100	92	[99]
diphenylacetylene	Pd	IL[g]	IL[g]	7.3 ± 2.2	1	25	6.5	87	98	[99]
3-hexyne	Pt	1-octylamine	dodecane	3.5	13.8	25	3	100	81	[22]
5-decyne	Pt	1-octylamine	dodecane	3.5	13.8	25	3	100	86	[22]
ethynylbenzene	Ru	PEG2000	toluene	1.6 ± 0.4	20	100	11	98	92	[100]
1-hexyne	Ru	PEG2000	toluene	1.6 ± 0.4	20	100	4	98	95	[100]
diphenylacetylene	Fe	IL[g]	heptane	4 - 5	60	80	44	99	94	[101]
diphenylacetylene	Ni	IL[g]	cyclohexane	7.8 ± 1.1	4	30	16	100	90	[102]
4-octyne	Ni	IL[g]	cyclohexane	7.8 ± 1.1	1	40	17	92	89	[102]

[a] T = temperature, p = hydrogen pressure, t = time, conv. = conversion, sel. = selectivity. [b] DTBB = 4,4'-di-tert-butylbiphenyl. [c] Hydrogen source is ethanol. [d] On ionic liquids (ILs) supportet magnetite NPs. [e] Both isomers together are 100 % in selecticity; trans-isomer has 2% selectivity. [f] Both isomers together; stabilizer/catalyst = 5:1. [g] IL = ionic liquid.

Another type of ligands other than uncharged organic molecules for nanoparticle stabilization are ionic molecules. These charged organic molecules (sometimes ILs) supply electrostatic stabilization, but are at the same time mobile at the particle surface. In the application of the selective hydrogenation of alkynes, the stabilization of palladium nanoparticles by tetrabutlammonium borohydride or tetrabutyl-

ammonium bromide prohibited the over-reduction of the alkene, in contrast to the pure nanoparticles, even after full conversion of the substrate.[19,20] However, precipitation of the colloids was only prevented, when another IL was applied as solvent. In these cases, also recycling experiments revealed the positive effects for the stability and selectivity of the ILs on the catalytic system.[99]

The problem of product separation in the systems was overcome by creating a thermoregulative biphasic condition, in which the product and the catalyst remain in different phases, or by the immobilization of the metal nanoparticles on magnetite nanoparticles, which can easily be separated from the solution by applying a magnet and decanting the products.[97,100]

Furthermore, different metals were applied for the selective hydrogenation of alkynes, which was justified with the need of cheaper catalysts. For example, Ni nanoparticles show the capability of selectively hydrogenating a wide range of internal and terminal alkynes with high selectivities even after full conversion of the substrate.[96,102] Recycling of the nanoparticles under air was possible without loss of activity or selectivity. An even cheaper and more abundant element as nickel is iron. The fundamental study of Gieshoff et al. shows the possible selective hydrogenation of different alkynes and recycling of the nanoparticles.[101]. However, the drawback of iron nanoparticles in this system is the vulnerability to contaminations, such as solvents and air, due to the very fast oxidation of the particle surface.

The trend of catalyst design for the selective hydrogenation of alkynes heads in the direction of green chemistry and convenient catalyst materials. Nevertheless, only theoretical studies take care of the influence of the particles' surface composition on the selectivity so far. However, for a tailored design of novel, green catalysts a detailed understanding of the exact reaction mechanisms, which certainly includes the particles surface chemistry, is inevitable.

Chapter 2

Objective

The introduction gave an overview over the state-of-the art research concerning the structure analysis of ligand stabilized nanoparticles and colloids and their application in catalysis. Apparently, ligand binding modes are not well known, regarding metals other than gold, and no broad agreement for a certain binding mode of amines and phosphines to metal nanoparticles is so far established. However, the detailed knowledge of the mechanisms taking place at a nanoparticles surface is necessary for the volitional tuning of the particles for certain applications, for example in catalysis.
For this thesis the application of ligand-protected platinum nanoparticles in catalysis was chosen for the in-depth elucidation of the ligand binding and the influence of the ligand in catalysis. Platinum nanoparticles are stable under ambient conditions and well-studied concerning hydrogenation catalysis. For this, platinum nanoparticles are synthesized and functionalized in two subsequent processes to obtain nanoparticles of the same size range capped with thiols, phosphines or amines, respectively. With this approach different conditions during functionalization can easily be applied and analyzed. Furthermore, the obtained nanoparticles are characterized thoroughly by TEM, STM, IR, NMR, XPS and TGA analysis. Additionally, the platinum nanoparticles are applied in the form of colloids in the selective hydrogenation of 3-hexyne to 3-hexene. The activity and selectivity of the hydrogenation reaction is monitored and the stability of the colloid after the reaction analyzed by TEM. Moreover, the catalytic reaction is studied more in detail and thus, influences of different ligand concentrations and substituents on the ligand coverage and structure is elucidated. The stability of these particles and the influence concerning selectivity and activity is also analyzed. Figure 2.1 gives a graphical overview of this approach.

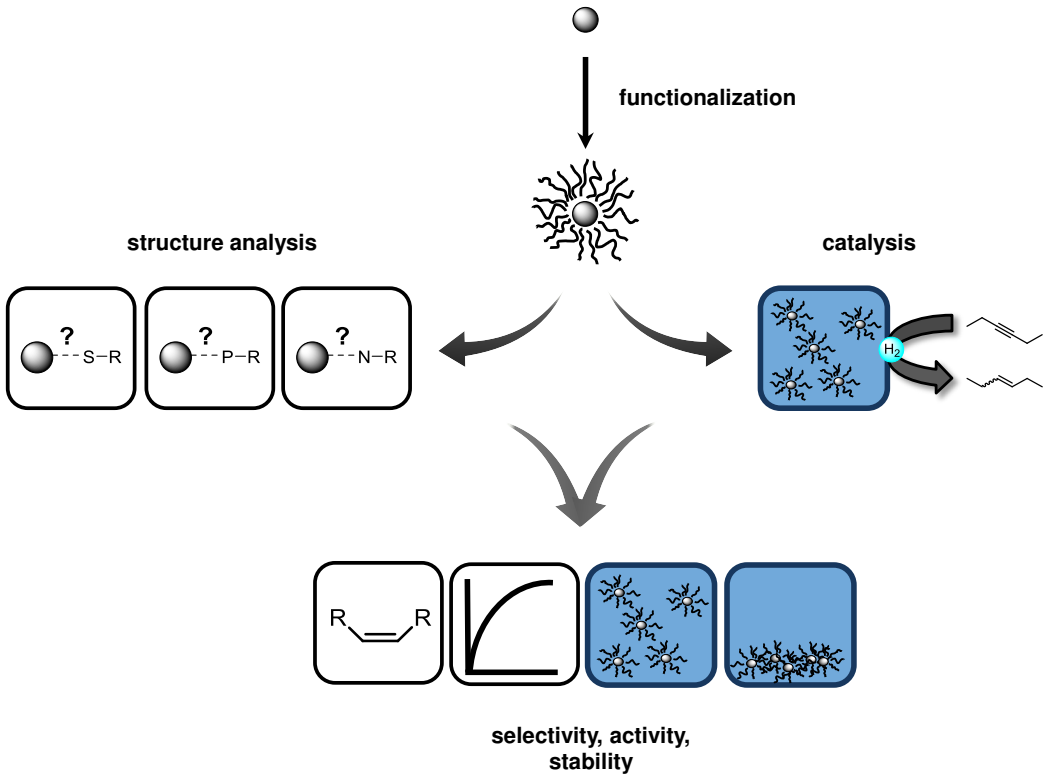

Figure 2.1: Graphical overview of the project plan of this thesis.

The aim of this work is to obtain detailed knowledge about the binding modes of thiols, phosphines and amines to platinum nanoparticles. Furthermore, this knowledge should be the basis for the interpretation of catalytic results. In the end, the prediction of catalytic behavior with respect to the applied ligand should be possible in order to tailor a catalyst with desired properties in the future.

Chapter 3

Results and Discussion

Platinum nanoparticles are investigated thoroughly in order to obtain a detailed knowledge of the binding modes of organic capping ligands and their influence on catalysis. In the structure analysis of platinum nanoparticles, the focus is laid on amine ligands. For the application of platinum nanoparticles in the hydrogenation of alkynes to alkenes, thiol ligands are mostly elucidated.

3.1 Nanoparticle synthesis and functionalization

Due to the considerable effects of the nanoparticles' size on their properties and behavior, the maintenance of the nanoparticle size is substantial for a throughout interpretation of their properties and their interaction with different ligands (figure 3.1). This is, why the polyol method is chosen for obtaining platinum nanoparticles in a confined size regime.[103] The method is slightly modified to one known from literature and a standard procedure for all platinum nanoparticles synthesized during this work is developed.[46]

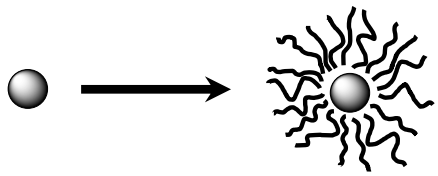

Figure 3.1: Schematic of the particle synthesis and functionalization with an unchanged metal core.

This standard synthesis is easy to carry out and includes an alkaline solution of ethylene glycol and the metal salt chloroplatinic acid. Upon heating to 150 °C and stirring of the reaction mixture, ethylene glycol is oxidized following presumably 3 reaction pathways (scheme 3.2) for the supply of electrons for the reduction of the platinum(IV) salt to platinum(0) atoms.[46,104,105] The platinum atoms form seeds upon collision and grow to nanoparticles until the precursor is entirely used up. When repeating the reaction under the same conditions, the particle size for all syntheses is reproducible. The resulting platinum nanoparticles are usually called "unprotected" due to the fact that they are only weakly stabilized by the solvent. Indeed, the surface is covered by CO and OH^- species.[47]

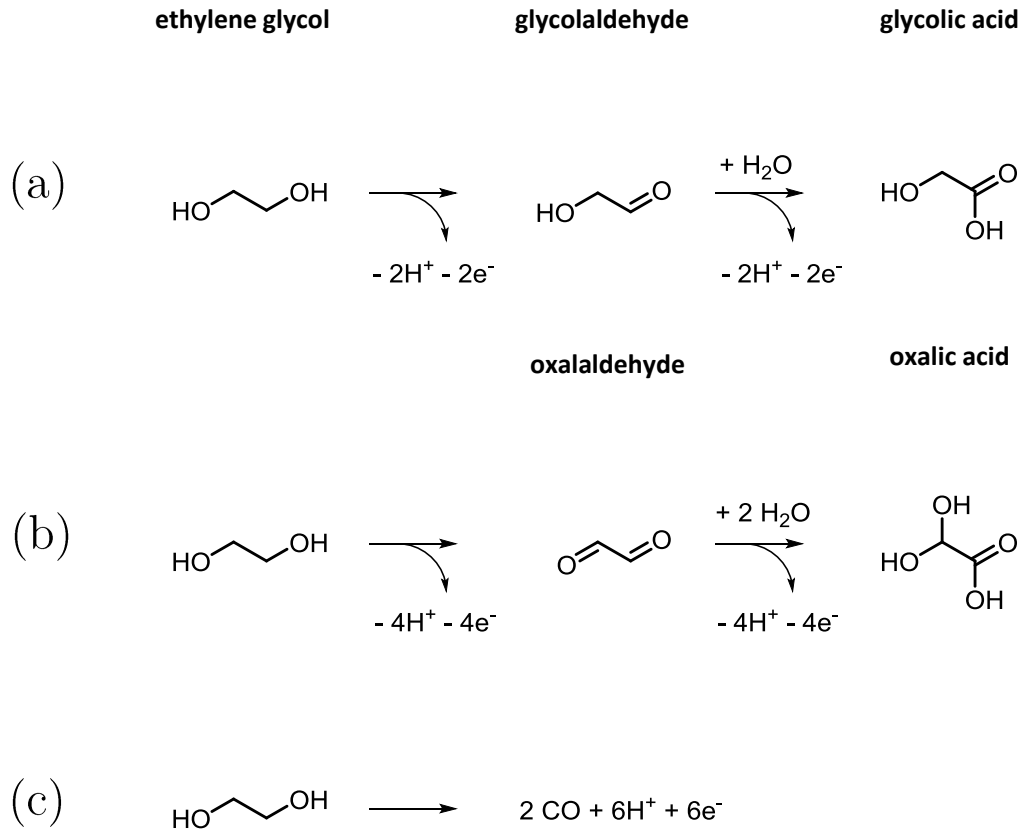

Scheme 3.2: Reaction pathways of the oxidation of ethylene glycol during the polyol synthesis of platinum nanoparticles.

These "unprotected" nanoparticles allow for the preparation of particles with a different ligand shell while the particle size is maintained.[106,107] For this, the functionalization of the "unprotected" platinum nanoparticles is obtained by a phase transfer reaction, which is illustrated in figure 3.3. Organic ligands are dissolved in

toluene, which is added to the alkaline ethylene glycol/platinum nanoparticle solution. The toluene and the ethylene glycol solution form a biphasic system. The two phases mix when they are stirred vigorously and this way the nanoparticles can get in touch with the organic ligands. By the time the stirring is stopped, the toluene and the ethylene glycol phase separate. A successful functionalization of the platinum nanoparticles is indicated by the phase transfer of the nanoparticles into the toluene phase. During this process the ligands build up a ligand shell around the particle and make them soluble in the toluene phase. In this case, the toluene phase turns from colorless to brown and at the same time the brown ethylene glycol phase is decolorized. After the phase transfer reaction, the phases are separated and the nanoparticles precipitated. After this, the particles are washed in order to dispose residual free ligand molecules by alternating centrifugation and redispersing processes. The ligand-stabilized nanoparticles are obtained as a black powder, which is stable for several months and can be dissolved in organic solvents to form stable colloids.

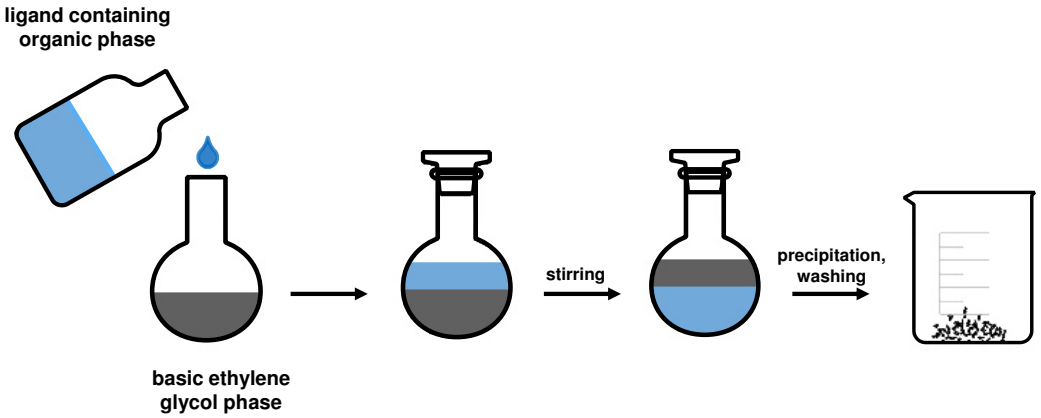

Figure 3.3: Schematic of the functionalization process via phase transfer of platinum nanoparticles.

The comparison of the nanoparticle size before and after the functionalization with octanethiol confirms the maintenance of the particle size of 2.0 ± 0.4 nm, which can be seen from TEM images in figure 3.4. For other ligands this observation is verified in the following chapters.

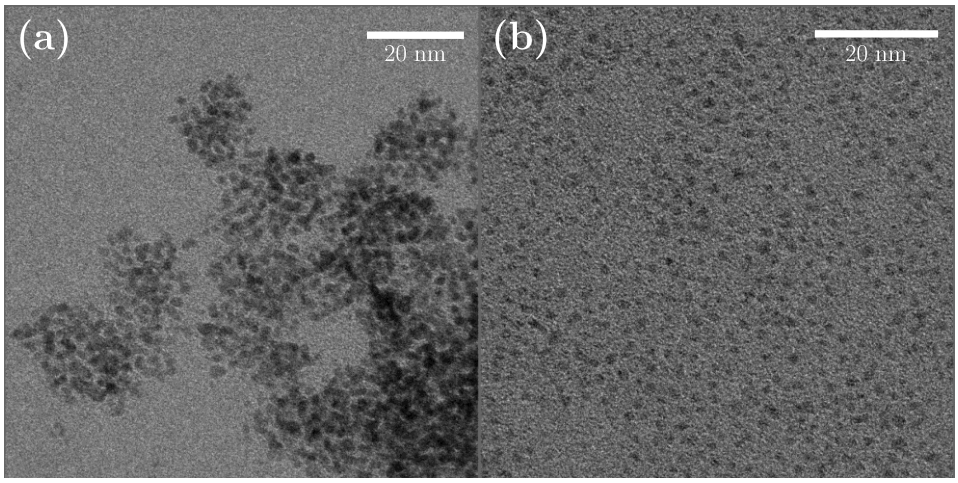

Figure 3.4: TEM images of platinum nanoparticles obtained from the polyol method (a) before and (b) after functionalization with octanethiol.

The separate synthesis and functionalization processes not only allow for the comparison of different ligand shells at the nanoparticle, but also for the easy variation of the functionalization environment without influencing the nanoparticle metal core. Easily modifiable parameters are for example the pH value of the ethylene glycol solution, the type of ligand or the concentration of the ligand. Furthermore, the "unprotected" nanoparticles can be treated prior to the phase transfer to analyze adsorption effects. Such a process may be the application of gases or support material. These numerous possibilities provided by this concept offer the opportunity to study different environmental influences on the binding mode of the ligands to the nanoparticles. Thus, the binding modes can be studied from different viewpoints. Additionally, coverage effects of ligands on the catalytic properties of the platinum nanoparticles can be investigated systematically.
Concluding this, the concept of the nanoparticle synthesis and functionalization in two separate steps provides a high potential tool for the systematic study of ligand binding and the ligand influence on functionalized nanoparticles and is therefore used throughout this work.

3.2 Binding modes of ligands to nanoparticles

In order to elucidate the binding modes of thiols, phosphines and amines to platinum nanoparticles (figure 3.5), the behavior of different ligands during the functionalization process, their IR spectra, NMR spectra, TGA, XPS spectra and finally a first application in catalysis is evaluated and interpreted.

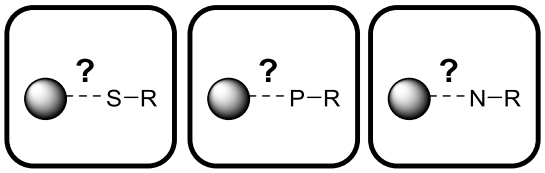

Figure 3.5: Schematic of the unknown exact ligand binding of thiols, phosphines and amines to platinum nanoparticles.

3.2.1 Platinum nanoparticles

Functionalization of platinum nanoparticles

In order to analyze the effect of the heteroatom on the binding mode of platinum nanoparticles, octanethiol (OT), octylamine (OA) and trioctylphosphine (TOP) are studied as ligands to protect platinum nanoparticles synthesized by the polyol method. Furthermore, the influence of substituents is elucidated on the example of the amine by using OA, dioctylamine (DOA) and trioctylamine (TOA) during the functionalization process. The behavior during this process is summarized in table 3.1. For the described standard functionalization process under basic conditions (this is the environment of the particle/ethylene glycol solution directly after the synthesis) only the OT and OA ligands exhibit a fast and complete phase transfer, which is indicated by a decolorization of the ethylene glycol phase. For DOA and TOP only a slow and incomplete phase transfer is observed under the same conditions. For TOA no reaction is observed at all yielding a colorless TOA/toluene solution even after 72 h reaction time. Two sterically less demanding tertiary amine ligands are additionally chosen for the protection of the particles in order to elucidate, if the steric demand of the three octyl chains inhibit the functionalization by TOA. However, triethylamine and

N,N-dimethylhexadecylamine ligands result in the same observation of a negative functionalization process so that a colorless toluene phase results. When adjusting the pH of the TOA phase transfer experiment into an acidic condition (pH ≈ 3) during vigorously stirring, the phase transfer of the platinum nanoparticles into the TOA containing toluene phase is achieved. Also for DOA and TOP a fast and complete reaction occurs under these acidic conditions. A similar trend is observed for TOA and TOP, when the platinum nanoparticles are H_2-activated before the phase transfer. H_2-activation is carried out by the application of molecular hydrogen (2 bar) to the particle containing ethylene glycol solution overnight. After this treatment, even the TOA ligand causes a fast and complete phase transfer of the nanoparticles into the toluene phase.

Table 3.1 Summary of the functionalization process under different reaction conditions (basic, acidic, H_2-treated) for OT, OA, DOA, TOA and TOP.

ligand	environment	phase transfer[a]
OT	basic	fast/complete
OA	basic	fast/complete
DOA	basic	slow/incomplete
DOA	acidic	fast/complete
TOA	basic	no reaction
TOA	acidic	fast/complete
TOA	basic, H_2-treated	fast/complete
TOP	basic	slow/incomplete
TOP	acidic	fast/complete
TOP	basic, H_2-treated	fast/complete

[a] fast = phase transfer in less than 0.5 h; slow = no phase transfer visible for more than 0.5 h; complete = ethylene glycol solution completely decolorized; incomplete = both phases are black even when stirring was continued for 72 h.

After functionalization, the nanoparticles are washed to remove residual free ligand molecules from the sample. These purified nanoparticle samples are used for characterization. First, the analysis of TEM images, shown in figure 3.6, confirm that

the platinum nanoparticle size distribution of 1.9 ± 0.4 nm is maintained during the functionalization process under the standard reaction conditions for all samples functionalized under basic condition. The TEM image and the histogram of the TOA ligand-stabilized particles exhibit a slightly broader size distribution and bigger nanoparticle size of 2.3 ± 0.5 nm.

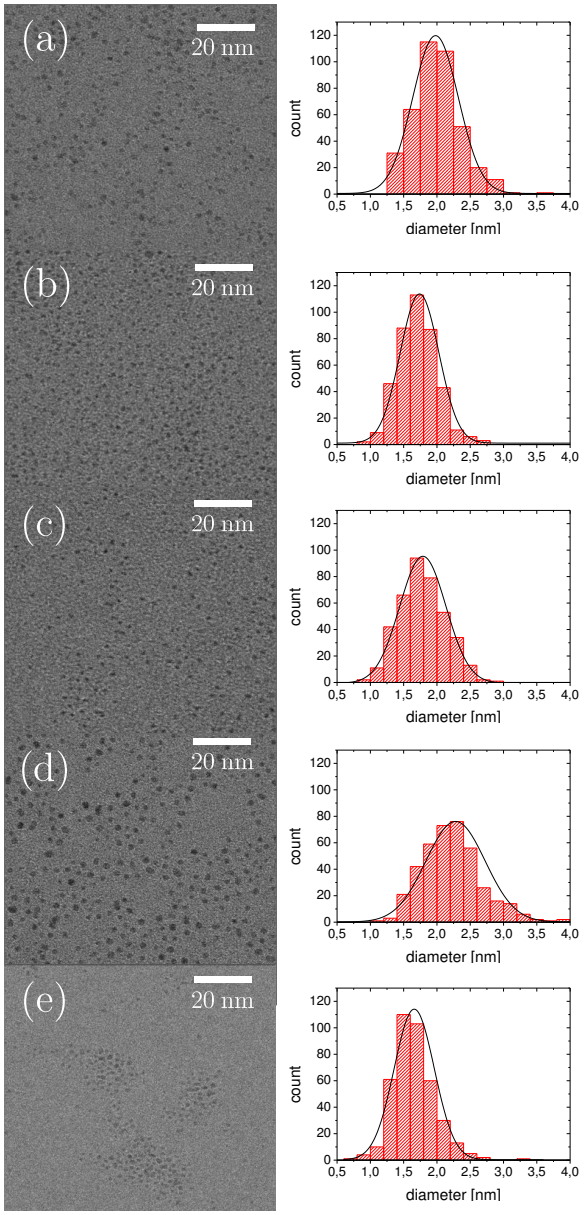

Figure 3.6: TEM images of (a) OT-, (b) OA-, (c) DOA-, (d) TOA[a]- and (e) TOP-stabilized platinum nanoparticles with the respective size distribution.

Scanning tunneling microscopy (STM) measurements (measured in cooperation with Sarah Wieghold) reveal the composition of the platinum nanoparticles at surfaces. On a bare Au(111) surface a flattening of the "unprotected" platinum nanoparticles is

observed directly after deposition. After the fast flattening process an even platinum layer on the gold surface is obtained. When depositing the "unprotected" particles onto a self-assembled monolayer (SAM) of dodecanethiol capped to the gold surface, the particles penetrate through the SAM to reach the gold surface, which is assumed to finally lead to a rearrangement of the platinum particles. The STM images of these samples shown in figure 3.7a and b demonstrate that the particles are arranged in close proximity to each other. Upon stabilization of the particles with either dodecanethiol or OT (figure 3.7c and d) the particles are observed to be stable without rearrangement or coalescence. The height profiles of the different samples in figure 3.7 reveal heights of (b) 2.52 nm, (c) 1.24 nm and (d) 0.26 nm for the marked areas, respectively. However, these apparent heights are difficult to compare, because of the interactions with the gold surface and the relative interaction with the STM tip.

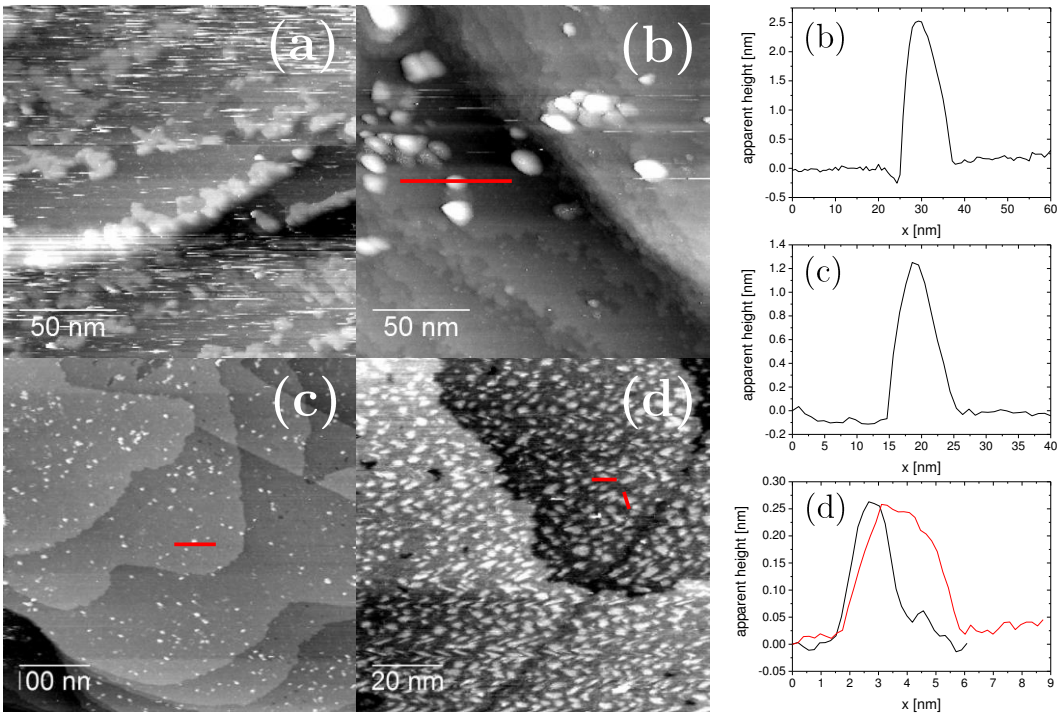

Figure 3.7: STM images of (a) "unprotected" platinum nanoparticles on Au(111), (b) "unprotected" platinum nanoparticles on a self-assembled monolayer of dodecanethiol on Au(111), (c) dodecanethiol-protected platinum nanoparticles on Au(111) and (d) octanethiol-protected platinum nanoparticles on Au(111) and their respective height profiles. Scanning parameters: (a) $I_t = 15\ pA$, $U_t = 900\ mV$, (b) $I_t = 10\ pA$, $U_t = 800\ mV$, (c) $I_t = 15\ pA$, $U_t = 950\ mV$, (d) $I_t = 15\ pA$, $U_t = 950\ mV$.

The results of the STM characterization points out the importance of ligands for the protection of platinum nanoparticles obtained by the polyol method. Although the "unprotected" nanoparticles are stable as a colloid for several weeks, they readily undergo ripening when applied at a metal surface and dried. Even the protection of the surface itself with thiol ligands does not stop the "unprotected" particles from rearranging. Indeed, only the protection of the particles itself allows for them to remain stable upon drying. For this reason it is impossible to apply several characterization methods for the "unprotected" platinum nanoparticles and compare them to the protected ones.
The different behavior of the "unprotected" or ligand protected nanoparticles during the functionalization process and imaging by STM already reveals the impact of the ligand composition on the particles properties. From these results the assumption that different binding situations are present at the particle surface is evident. Thus, a careful characterization could allow for the in-depth elucidation of the binding modes of the different ligands to the platinum nanoparticles.

IR spectroscopy

For the elucidation of the binding mode of ligands to the nanoparticles different characterization techniques are applied. First of all, IR spectroscopy of colloid samples dissolved in carbon tetrachloride is conducted. Figure 3.8 illustrates the recorded spectra.
The comparison of the IR spectra of free and particle-bound OT shows the disappearance of the S−H stretching mode at 2582 cm^{-1} for the bound ligand. This observation is a typical feature of thiol-functionalized nanoparticles.[108] Moreover, a band at 3006 cm^{-1} appears in the spectrum of the bound OT. This feature has already been recognized by Sharma et al. for dodecanethiolate-functionalized gold nanoparticles.[60] In that work the authors mentioned that the position of the band equals the frequency of a C−H stretching transition for C=C groups, but no further interpretation was given. However, this strong blue shift can be interpreted originating from the coordination of a H-atom of the aliphatic carbon chain to the platinum surface. This coordination could consequently lead to a partial C=C bond character and, thus, some of the C−H stretching frequencies are blue-shifted. The phenomenon of pronounced spectral structure above 3000 cm^{-1} and the high relative intensity with respects to the unperturbed C−H stretching modes is even stronger observed in the IR spectrum of the TOP-functionalized nanoparticles (figure 3.8c). Besides this relatively strong interaction of the octyl chains with the nanoparticles, characteristic features are absent in the spectrum, which suggests an otherwise unaltered structure of the ligand.

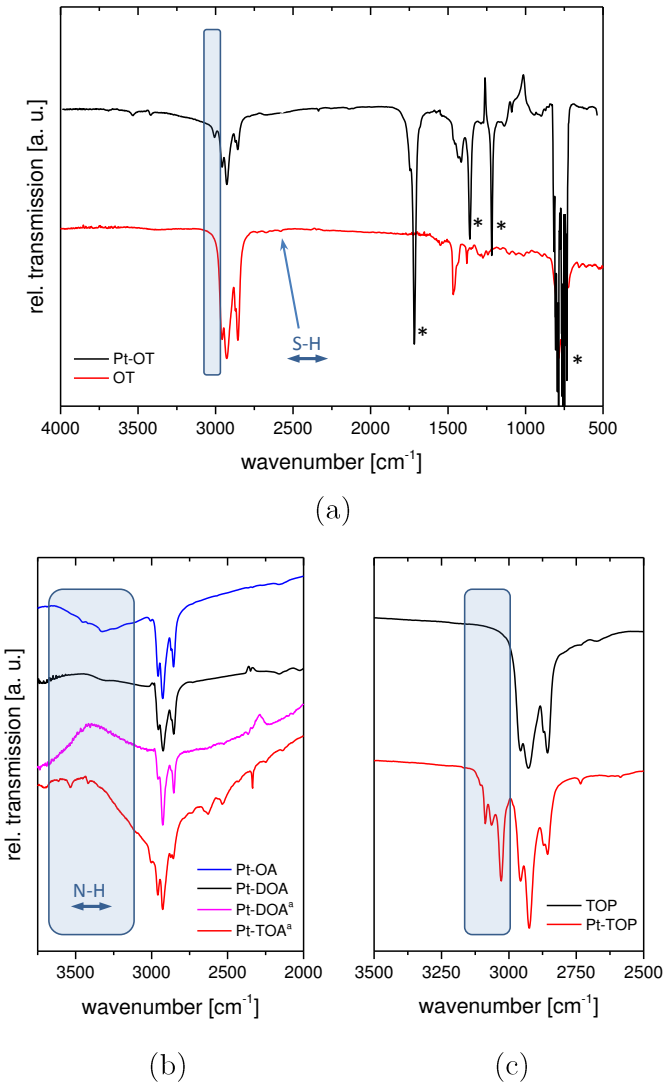

Figure 3.8: IR spectra of (a) OT-functionalized platinum nanoparticles in comparison with the free OT ligand (b) the N—H stretching regime of OA-, DOA-, DOA[a]- and TOA[a]-functionalized platinum nanoparticles and (c) the C—H stretching regime of TOP-functionalized platinum nanoparticles in comparison with the free TOP ligand dissolved in CCl_4.

For the amine-functionalized platinum nanoparticles the typical amine bands at 3335 cm^{-1} are usually broadened and less intense than the ones of the free ligand.[56] These observations of the OA- and DOA-functionalized nanoparticles are confirmed by the IR measurements of these samples (figure 3.8b). The TOA[a]-stabilized nanoparticle sample (acidic condition during phase transfer is denoted by [a]), however, shows an even broader band, which is red-shifted and occurs between 3300 cm^{-1} and

2000 cm^{-1} with a complicated fine structure. Such a band can be assigned to vibrational modes of ammonium cations.[57] Similar broad bands, but with no significant fine structure are found in the spectra of the acid-treated sample of DOA^a-stabilized nanoparticles. The broad band above 3500 cm^{-1}, which is in particular pronounced in the spectrum of DOA^a-protected particles, can be assigned to contaminations of the samples by water species.

NMR spectroscopy

Another valuable tool for nanoparticle structure analysis applied in this work is NMR spectroscopy. Different techniques were used for the elucidation of different characteristics of the platinum nanoparticles. Solution ^1H NMR spectra of all colloidal samples were recorded and analyzed. Figure 1.4 illustrates ^1H NMR spectra of the thiol-, amine- and phosphine-stabilized nanoparticles, which are in good agreement with those reported before.[56,61,62,83,109] The spectra for the thiol-stabilized nanoparticles and the free thiol ligand are shown in figure 3.9.

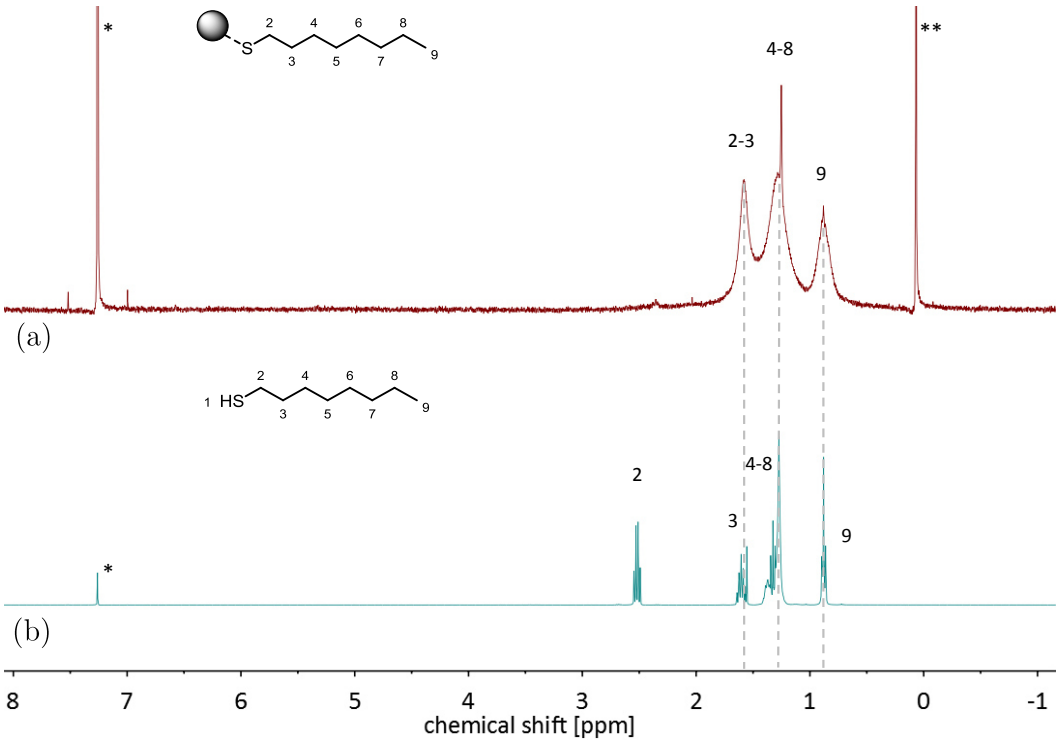

*Figure 3.9: ^1H NMR spectra of (a) OT-stabilized platinum nanoparticles and (b) the free OT ligand in $CDCl_3$ (solvent peaks are marked with *; grease is marked with **).*

From these spectra, the typical features of ligand-stabilized nanoparticles can be easily recognized. The peak broadening is believed to be due to slow Brownian tumbling of the particles in solution, as well as to the distribution of the ligands binding at different types of binding sites at the nanoparticle surface.[62] Other changes in the colloid spectrum are the peak of the α-CH_2 group, which is shifted, broadened and overlapping with the peaks of the other CH_2 groups (from 2.5 ppm (OT), 2.7 ppm (OA) and 2.6 ppm (DOA) to 1.5 – 1.0 ppm) in the particle spectrum. This shift is assumed to be due to the limited rotation degree of freedom of this group, because the α-CH_2 hydrogen atoms interact with the platinum surface.[56]

The ^{1}H spectra of the acidic treated samples of the amines, DOA^a- and TOA^a-stabilized nanoparticles display an additional broad peak at 1.57 ppm, which is absent in the spectra of OA- and DOA-capped particles. In the applied solvent $CDCl_3$ this chemical shift usually indicates the presence of water molecules. However, the temperature dependence of this peak reveals a downfield shift and sharpening for decreasing temperatures (figure 3.10), which is a well-known feature for OH groups.[110,111] Concluding this, the position of the band as well as its temperature dependent behavior in ^{1}H NMR analysis enables its assignment to an OH, OH^- or H_2O species.

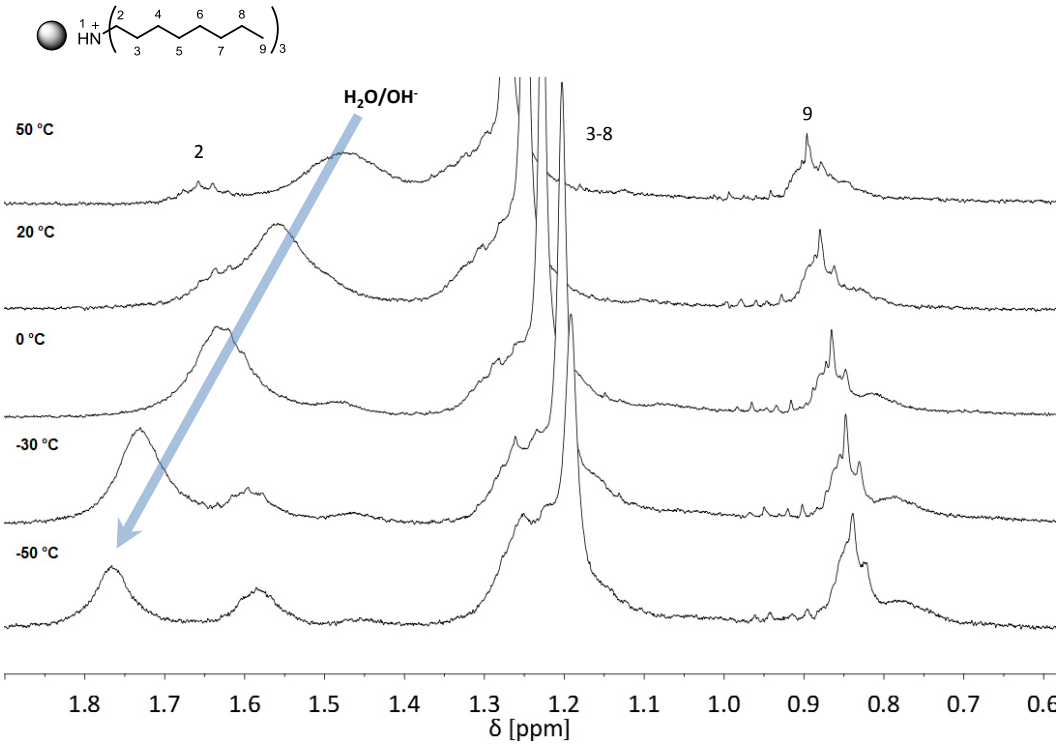

Figure 3.10: ^{1}H NMR spectra of TOA^a-stabilized platinum nanoparticles in $CDCl_3$ at different temperatures.

Besides the measurement in $CDCl_3$, *d*-THF is chosen as solvent for solution NMR measurements, because the exchange of protons is excluded for this solvent in contrast to $CDCl_3$.[112] The spectrum of TOA^a-functionalized platinum nanoparticles in *d*-THF gives rise to an additional peak at 11.1 ppm (figure 3.11). In the spectrum of the acidic treated free TOA^a ligand a similar peak at 11.0 ppm appears. In the spectrum of the ligand-protected nanoparticles this peak is shifted and a significant broadening is observed. An H,H-COSY NMR study of the free TOA^a ligand distinctly reveals the cross peaks of the $R_3N\text{-}H^+$ proton with the $\alpha\text{-}CH_2$ group of the alkyl chain (figure 3.12). COSY cross peaks report the coupling between pairs of nuclei and thus determine, which atoms are bound to each other. In the spectrum all expected cross peaks originating from the alkyl chain are present. Furthermore, this spectrum evidences the assignment of the peak at about 11.0 ppm for the free TOA^a to $R_3N\text{-}H^+$ protons.

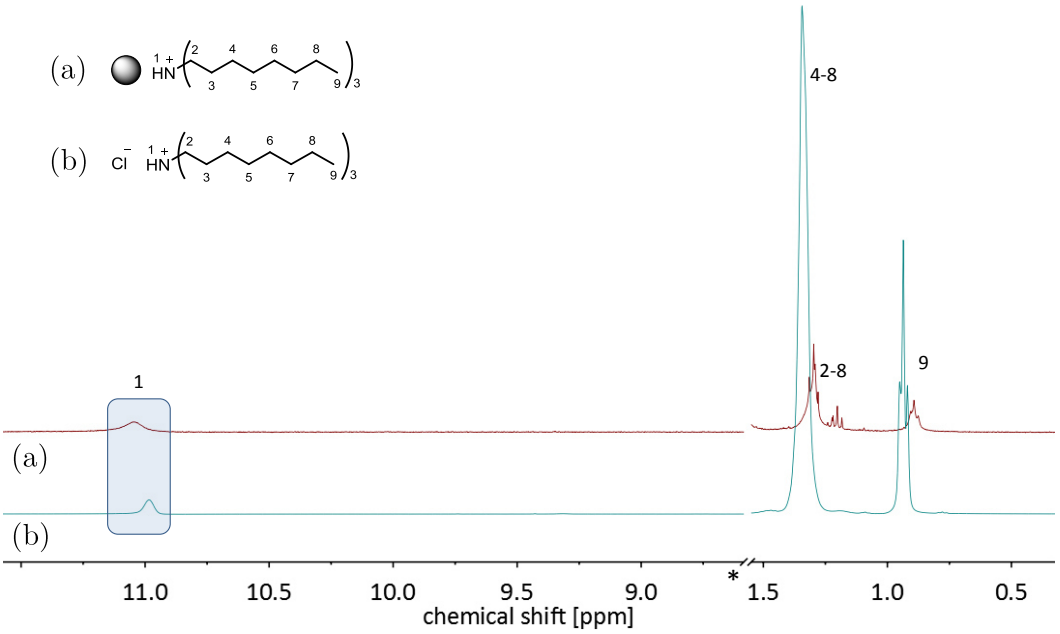

Figure 3.11: ^1H NMR spectra of (a) TOA-stabilized NPs and (b) the free protonated TOA ligand in d-THF (* marks a break in the axis).*

H,H-COSY NMR measurements of TOA^a-stabilized platinum nanoparticles are hampered, because the higher concentration of the sample needed for the measurement of a 2D-NMR (due to the lower sensitivity of the 2D-NMR proton signal) perturbates the experiments due to paramagnetic interferences originating from the platinum metal core. This way, a further evidence of the given assignment cannot

be obtained. However, the peak at 11.1 ppm in the spectrum of the ligand-bound TOA^a may as well be assigned to R_3N-H^+ protons as it is the case for the free TOA^a ligand. This interpretation includes the interaction of the ligand with the metal core resulting in the peak shift and broadening.

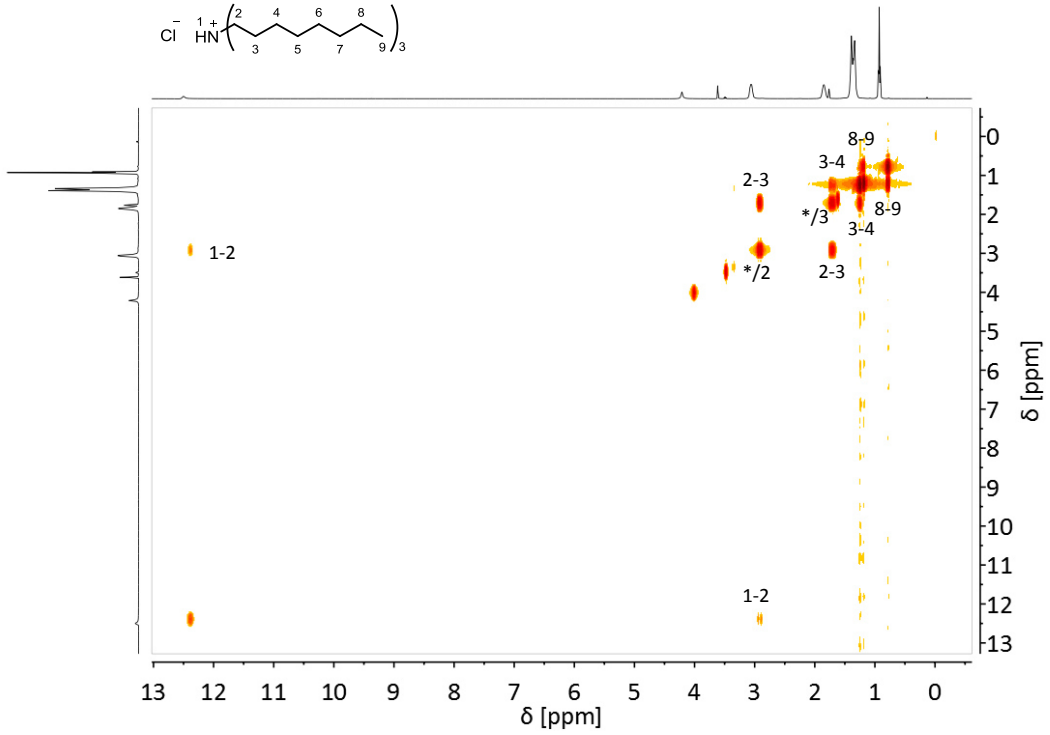

*Figure 3.12: H,H-COSY NMR spectrum of TOA^a in d-THF (solvent peaks are marked with *).*

Furthermore, DOSY NMR experiments are carried out in order to obtain more evidence on the moieties present in close proximity to the platinum surface (figure 3.13). As expected, in the TOA^a ligand spectrum of the free ligand only two species, the ligand molecule and the solvent, are detected. A diffusion coefficient of $4.62 \cdot 10^{-10}$ m^2/s is calculated for the free TOA^a ligand, which is lower than the diffusion coefficient of the solvent and in agreement with the usual diffusion coefficients of molecular species under ambient conditions.[113] Furthermore, the peak at 11.0 ppm correlates with all other peaks of the ligand molecule. For TOA^a- and TOA^H-stabilized platinum nanoparticles (H_2-activation prior to the functionalization is denoted by ^{H}) such a high concentration of the particles in the solvent could not be achieved and thus, the solvent peaks dominate the spectra. Furthermore, the diffusion coefficient of a species in a certain solvent is dependent on its concentration and only the comparison of species within one sample can be compared directly. For the TOA^a-

stabilized nanoparticles several species are detected. The peaks assigned to the alkyl chain (at 0.89 ppm and 1.30 ppm) exhibit the lowest diffusion coefficient of $1.06 \cdot 10^{-9}$ m^2/s compared to a diffusion coefficient of $2.27 \cdot 10^{-9}$ m^2/s of the solvent. However, due to the low concentration, the peak at 11.1 ppm is not detected in the 2D spectrum.

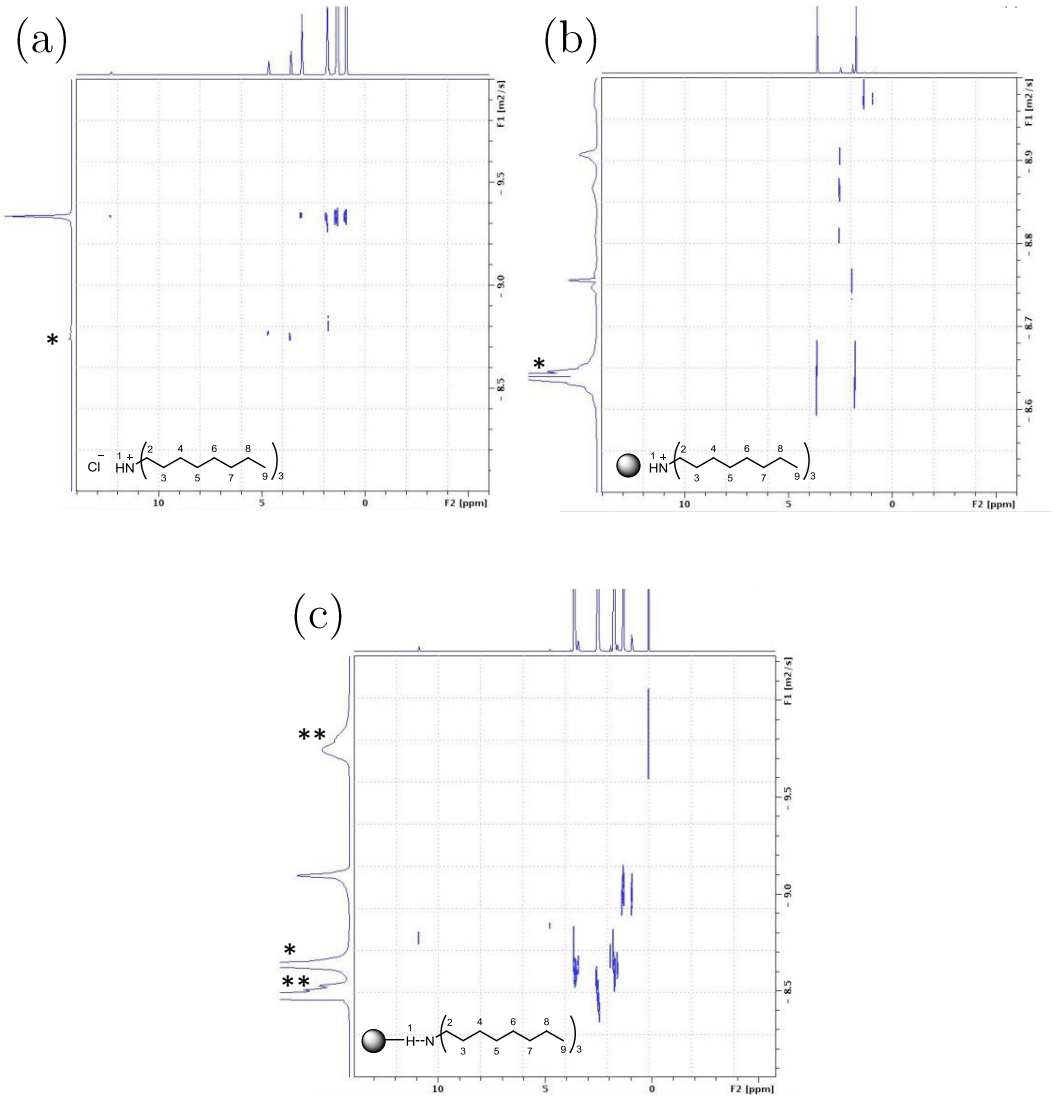

*Figure 3.13: ^{1}H DOSY NMR spectra of (a) free TOA^a, (b) TOA^a-stabilized and (c) TOA^H-stabilized platinum nanoparticles; x-axis: chemical shift [ppm] and y-axis: log diffusion coefficient [m^2/s] (solvent peaks are marked with *, water and grease peaks are marked with **).*

In the spectrum of the TOA^H-stabilized particles, besides peaks from the solvent, peaks from water and grease peaks, the ligand peaks display a diffusion coefficient of $8.02 \cdot 10^{-10}$ m^2/s. The diffusion coefficients of the bound ligands are slightly lower than the one of the free TOA^a ligand, which may exhibit a higher mobility in the solution due to its smaller hydrodynamic radius. However, the diffusion coefficient is dependent on the concentration of the substance in the solvent, which makes a clear interpretation of the different diffusion coefficients difficult.
Furthermore, two small peaks at 4.76 ppm and 10.85 ppm are detected in the measurements of the TOA^H-stabilized particle sample , which do neither correlate with the solvent nor with the ligand signals. In the ^1H NMR spectrum of TOA^H-stabilized particles these two signals are only detected separately from each other. This means, that in a freshly prepared sample of TOA^H-capped nanoparticles the peak appears at 10.85 ppm, while in a measurement of the aged same sample this peak disappears giving rise to the peak at 4.76 ppm (figure 3.14), which is typical for the presence of dissolved H_2.[114] However, the exact origin of these peaks cannot be identified and it seems that they are not related to the platinum nanoparticles.

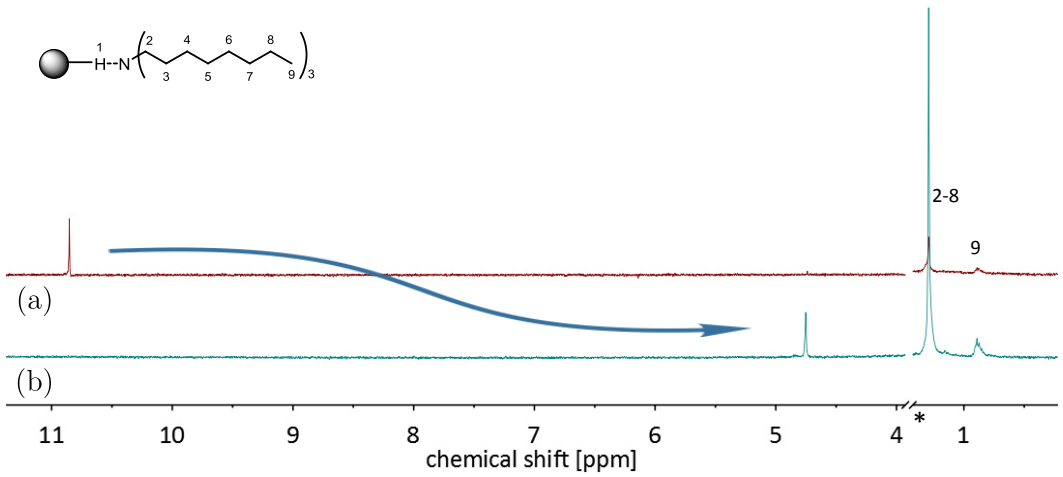

Figure 3.14: ^1H NMR spectra of TOA^H-stabilized platinum nanoparticle sample (a) freshly prepared and (b) after 7 days aging in d-THF; peaks at 10.85 ppm and 4.75 ppm are not attributed to nanoparticle bound moieties.

In addition, the peak at 1.29 ppm, which corresponds to the ligand alkyl chain, gets sharper in the spectrum of the aged sample, which hints to a more flexible alkyl chain. Furthermore, the aging causes precipitation of the sample, which is observed as a black powder at the bottom of the vial. This could be due to agglomeration of the particles. Such a decomposition of the colloidal samples is only observed for the H_2-

activated platinum nanoparticles. In contrast, all other ligand-stabilized samples are found to be stable at room temperature in the form of powder as well as in colloidal solution for several weeks.

The ^{1}H NMR spectra of TOP-stabilized nanoparticles exhibit the same features as the amine- and thiol-stabilized particles concerning the alkyl peaks (figure 1.4). Acid treated TOP^{a}-stabilized nanoparticles result in the appearance of a broad peak at 4.58 ppm, which corresponds to typical P−H shifts of disubstituted phosphines (figure 3.15).[115] The width of this peak is supposedly a consequence of the positive charge of the proton and the proximity to the nanoparticle surface. Another peak at 1.62 ppm is assigned to contaminations by trioctylphosphine oxide (TOPO), which is the oxidation product of TOP.

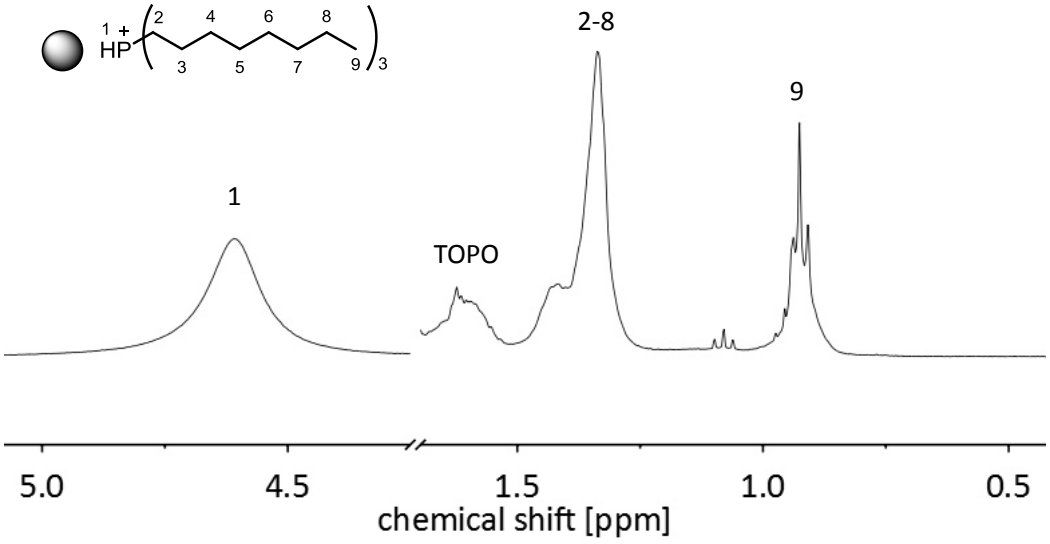

Figure 3.15: ^{1}H NMR spectrum of TOP^{a}-stabilized platinum nanoparticles in d-THF.

Solid state ^{31}P MAS NMR spectra of TOP-capped platinum nanoparticles reveal three different peaks as can be seen in figure 3.16. The signals at 58 ppm and 32 ppm are in agreement with spectra of triphenylphosphine-stabilized gold nanoparticles previously described in literature.[71,72,116] The resonance at 2 ppm has not yet been reported for such systems. However, a final assignment of this species is not possible for this system up to now.

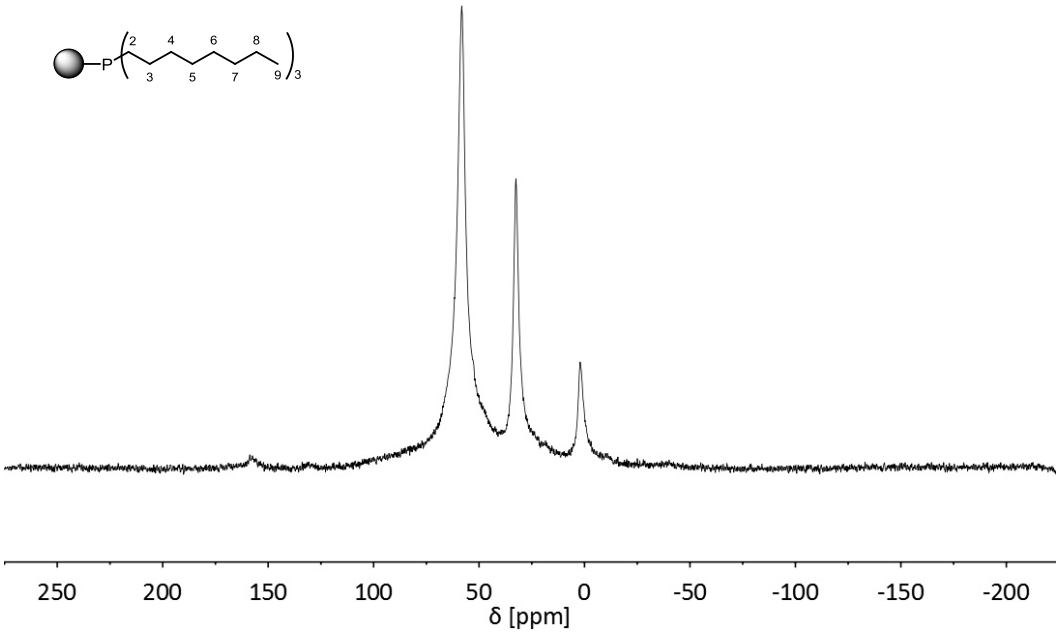

Figure 3.16: ^{31}P MAS NMR spectrum of TOP-stabilized platinum nanoparticles.

Thermogravimetric analysis

TGA measurements allow for the quantification of the amount of ligand at the nanoparticle surface. These data are summarized in table 3.2 for the analyzed ligand-functionalized platinum nanoparticles. OT- and OA-protected nanoparticles have about the same ligand coverage. Protection by DOA leads to a lower coverage possibly due to an increased steric hindrance of the alkyl chains in the secondary amine. For DOA^a-, TOA^a- and TOP^a-capped nanoparticles a significantly lower ligand coverage is found. An extra step of weight loss at 100 – 300 °C is found for these acidic treated samples in comparison to the samples functionalized under basic conditions. This step supports the assumption of the presence of water species at the particle surfaces of all acidic treated samples as already described in the analysis of these samples in the NMR analysis. Furthermore, the significantly lower ligand coverage of these nanoparticle samples is interpreted as a blocking of adsorption sites by the OH, OH^- or H_2O species. Another explanation for this phenomenon could be the repulsive forces of the positively charged ions in proximity to the metal surface.

Table 3.2: Ligand/platinum ratio of functionalized platinum nanoparticles determined by TGA.

sample	ligand/platinum
Pt–OT	0.73
Pt–OA	0.72
Pt–DOA	0.60
Pt–DOA[a]	0.14
Pt–TOA[a]	0.19
Pt–TOP[a]	0.22

XPS spectroscopy

XPS measurements of OA-, OA[a]- and TOA[a]-functionalized platinum nanoparticles are conducted. The overview spectra clearly show that impurities, such as chlorides, are not detected (figure 3.17a). The N 1s spectrum exhibits only one peak at 399.2 eV binding energy (BE), which is independent from the functionalization conditions in basic or acidic environment (figure 3.17b).

The evaluation of the Pt 4f transitions has been reported previously for XPS spectra of platinum particles protected by a primary amine or polyaniline fibers.[117,118] These studies reveal the existence of platinum in several oxidation states in their nanoparticle samples. More insights, however, have only been obtained by the analysis of the N 1s peaks. It has been found, that the pyrolized fibers give several bands.[117] In contrast to that, the results of the primary amine-capped platinum nanoparticles revealed only one band in their XPS spectrum and consequently the presence of only one amine species has been concluded from this measurement.[118] In agreement with that result, the recorded XPS spectra of OA-, OA[a]- and TOA[a]-functionalized platinum nanoparticles exhibit only one peak. TOA[a]-functionalized particles give the same spectrum, but with a strongly reduced signal-to-noise ratio due to the low ligand coverage. Concluding this, the peak position in these spectra neither depends on the functionalization condition nor on the degree of substitution of the ligand. One study, which addresses the interpretation of N 1s spectra was performed on non-noble metals only.[119] However, the assignment of this peak is very difficult due to the lack of available information and no conclusion with respect to the exact binding mode can be drawn from this measurement.

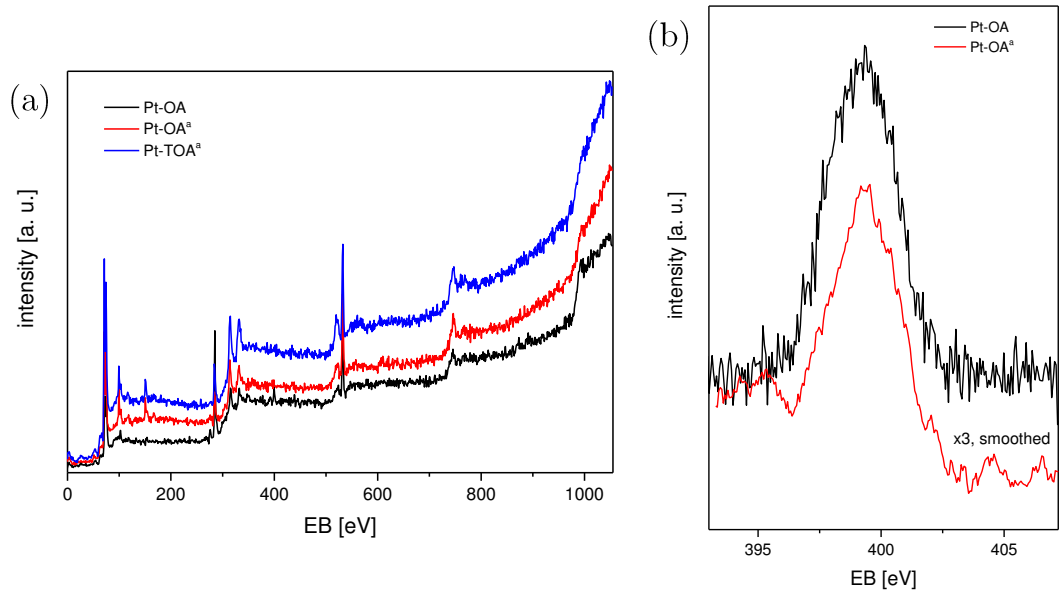

Figure 3.17: (a) Overview XPS spectrum of OA-, OA^a- and TOA^a- and (b) spectrum of the N 1s region of OA- and OA^a-functionalized platinum nanoparticles.

Application in Catalysis

The platinum colloids are applied as catalysts in the selective hydrogenation of 3-hexyne to 3-hexene. Table 3.3 sums up the results of the catalytic reactions under standard conditions in THF. The presented values are at a similar conversion of 87 to 97 % during the reaction for all samples. All reactions exhibit good selectivities in the range of 75 to over 90 %. For all catalytic reactions particularly high values for the selectivity are obtained when the reaction is started, which then decrease during their course. With the exception of the OT-protected nanoparticle, the reactions are fast and give yields over 70 % already after 1 or 1.5 h reaction time. These alkene yields are in good agreement with most literature reports on colloidal nanoparticles studied for this reaction.[19,22,96] While particles stabilized by the amines or the phosphine react fast, the thiol-stabilized nanoparticles only obtain comparable yields after 8 h. However, this strong decrease in the reaction rate does not influence the high selectivity for the alkene during the course of the reaction.

Table 3.3: Summary of yield, selectivity and conversion of the selective hydrogenation of 3-hexyne to 3-hexene (cis- and trans-isomers) under standard reaction conditions (1.5 bar H_2, r. t.).

ligand	time h	yield[a] %	conv.[b] %	sel.[c] %
OT	8	77	88	87
OA	1	80	85	94
DOA	1.5	76	97	78
TOA[a]	1	73	97	75
TOP	1	73	87	84

[a] Defined as the concentration of hexene divided by the sum of the concentration of all products and reactants. [b] Defined as the sum of product concentrations divide by the concentration of all reaction species. [c] Defined as the concentration of hexene with respect to the concentration of all reaction products.

After the reaction a similar trend is observed concerning the colloids stability. The reaction solution of the highly reactive amine- and phosphine-stabilized nanoparticles shows a black precipitate depositing at the bottom of the vials. Only the thiol-stabilized nanoparticles remain as a colloid even after the reaction. The agglomeration of the nanoparticles to larger particles is a reasonable explanation for this observation. These evidences are further verified by TEM analysis (figure 3.18 left) of the reaction solutions after catalysis. While the size of the OT-protected nanoparticles is maintained with a size distribution of 1.9 ± 0.4 nm, the amine- and phosphine-capped nanoparticles agglomerate and exhibit big aggregates. The unaltered size distribution of the OT-protected nanoparticles after catalysis is an evidence for a stable and unchanged catalyst.

Furthermore, an NMR study of the protected platinum nanoparticles after catalysis reveals a similar trend (figure 3.18 right). Thiol-protected particles exhibit the typical broad peaks for ligands attached at nanoparticle surfaces. However, these bands differ slightly in comparison to the bands of the NMR spectrum of the sample before catalysis. At the same time the amine- and phosphine-capped nanoparticles show up a sharp peaks at 1.25 ppm. The sharpening of these peaks hints, like in the case of the aged TOA^H-stabilized particles, to a more flexible alkyl chain in the analyzed system.

These evidences together suggest the assumption that in contrast to particles capped with amines and phosphines, protection by thiols yield particles of high stability.

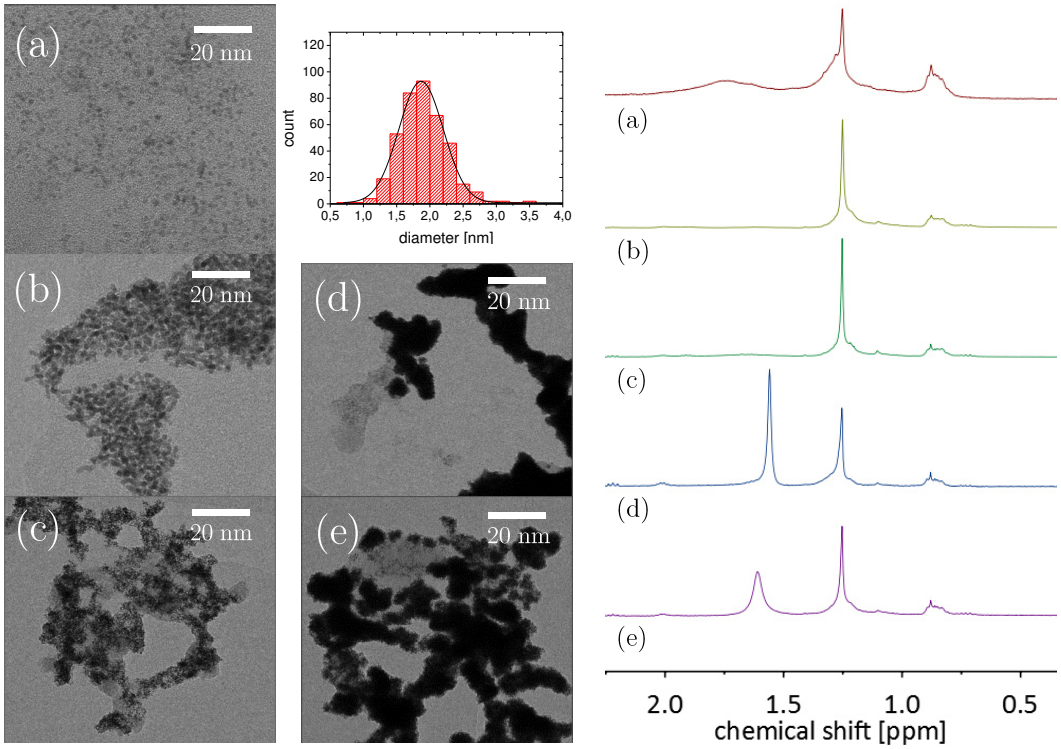

Figure 3.18: TEM images (left) and ^1H NMR spectra in $CDCl_3$ (right) of (a) OT-, (b) OA-, (c) DOA-, (d) TOA[a]- and (e) TOP-stabilized platinum nanoparticles after catalysis; including the respective size distribution for (a) after catalysis.

Discussion

The throughout characterization of ligand-protected platinum nanoparticles helps to understand the binding modes better. It is observed, that the binding of the ligand molecules strongly depends on the functional group and determines the nanoparticle stability and activity. The binding mode for thiols has already been studied well in literature and there is a general agreement that the ligand binds covalently via the sulfur atom to the metal surface.[56] This binding mode is supported by a disappearance of the S—H stretching mode in the IR spectra of thiol-protected nanoparticles as it is also the case for ethanethiol-capped platinum nanoparticles.[108]

For the protection of platinum nanoparticles by amines the binding mechanism is less clear and less studied. In general, two binding modes have been described in literature. In charged systems, the ligand is assumed to mainly interact via electrostatic

interactions with the nanoparticles. This binding mode is proposed for particle protection by quaternary ammonium cations for different metals.[120–123] In these systems the positively charged ammonium ions interact with negative charges at the metal surface and relatively strong interactions result. In this work a similar interaction was found for amines with a lower degree of substitution. The functionalization process of the secondary amine DOA and the tertiary amine TOA in acidic media are even more efficient compared to the functionalization in a basic environment. Even for primary amines a similar observation has been described in literature for the phase transfer of gold nanoparticles in a similar system.[74] They proposed a ligand binding by electrostatic interaction as well as a complexation species at the nanoparticle. In the present work ligand protection of amines at lower pH values yield nanoparticles, which involve a system of ammonium cations, OH^- counterions and water molecules, which is found by IR and NMR spectroscopy. The transition at 11.1 ppm in the NMR spectra of TOA^a-stabilized platinum nanoparticles further suggests a protonation of the ligand molecule, as the free cation exhibits a similar feature at 11.0 ppm. For this peak a distinct evidence for the presence of the proton at the ammonium functional group is given by COSY and DOSY NMR measurements. The broadening of this peak in the NMR spectra of TOA^a-stabilized platinum nanoparticles and its downfield shift indicate that this moiety of the ligand directly interacts with the nanoparticle, as it has been proposed for a similar system of rhodium particles protected by tertiary amines.[124] In that work it was concluded that even the alkyl chain directly interacts with the nanoparticles. The strongly reduced ligand coverage observed by TGA for all nanoparticles functionalized under acidic conditions is assumed to be due to the counterions on the nanoparticles surface blocking surface sites for electrostatic interaction of the ligand cations.

However, for the functionalization in a strong basic environment (i. e. pH = 14) contrasting observations suggest another binding mechanism. By IR and NMR characterization neither the presence of ammonium nor hydroxide species is observed. For nanoparticle stabilization by amines other than ammonium ones, it seems that a binding mode is accepted, in which the amine binds covalently via the lone-pair of the nitrogen atom to the metal nanoparticles.[123,125,126] This is in analogy with the concepts of complex chemistry and the understanding of the binding of amines to gold nanoparticles.[82] XPS analyses of OA-functionalized platinum nanoparticles under basic and acidic conditions do not result in a difference of the N 1s transition and might be interpreted as the same nitrogen species in both samples. However, these results are inconclusive as the behavior during functionalization already revealed that there must be different binding mechanisms. Furthermore, the covalently bound amine species contradicts the observation that the functionalization with TOA or triethylamine ligands fails in a basic environment. Steric effects due to the long octyl chains can be

excluded, because the functionalization under the same conditions with other tertiary amines comprising shorter alkyl chains (N,N-dimethylhexadecylamine and trimethylamine) is also not possible. Additionally, the functionalization behavior puts the binding via the lone electron pair also for the primary and secondary amine in question. The tertiary amine exhibits the highest nucleophilicity of the three studied amines OA, DOA and TOA and should therefore build up a covalent bond to the metal more easily, which is not observed. Furthermore, the secondary amine is also more nucleophilic than the primary, but the functionalization with DOA is incomplete and slower than the primary one. Instead, the number of H-atoms at the amine functional group seems to be involved. An alternative binding mode for amines to platinum nanoparticles and an interaction of the H-atom of the amino group with the metal core may be suggested. First, it is already well known that platinum surface atoms exhibit strong interactions to H-atoms of any kind, even H-atoms of an alkyl chain, which we have interpreted to cause the large blue shift of some C—H stretching transitions of TOP-stabilized nanoparticles. Second, the particles can be functionalized by tertiary amines when they have been treated with molecular hydrogen previously. In the basic environment the platinum nanoparticles are covered with hydrogen so that metal hydrides are formed at the surface. A plausible interpretation could be that the amines interact with these hydrides and bind via the formation of a kind of Pt—H—N moiety to the particle. This binding mode is certainly weaker than the electrostatic one obtained by the functionalization in acidic environment. This could be the reason, why the H_2-treated TOA^H-stabilized nanoparticles are subject to decomposition in solution considerably quickly, which is indicated by precipitation of the colloid after some days.

The reduced stability proven by TEM and NMR analysis of the amine-protected particles with respect to those of the thiol-protected particles during catalysis can be related to this binding mode as well. Similarly to the H_2-treated particles, secondary and primary amines can interact with neighboring surface hydrides so that their initial bond to the particle is weakened, which seems to be the interaction of the amine bound hydrogen atoms to the platinum surface. As a consequence, the ligand is not only more mobile on the surface, but also a dissociation of the molecule becomes probable. This dissociation is even accelerated during catalysis due to the exothermicity of the hydrogenation reaction, which favors the release of ligand molecules from the particles.[127] The binding of amines via the H-atom to the platinum surface has already been discussed in a previous study, where a tertiary amine acted as a modifier.[23] Ab-initio molecular dynamics simulations indicate that no direct binding between the platinum surface and the tertiary amine develops. Instead, it is assumed that an equilibrium exists, in which either the H-atom is strongly adsorbed on the metal surface and only a weak interaction to the amine is formed or the

binding of the H-atom to the amine is strong and to the metal surface only weak.[23] However, while the calculations only simulate the situation during a reaction, they do not include the structure of isolated particles, defects in the particle shells or other undefined side products or contaminations. Nevertheless, this study demonstrates that a binding of the amine via a H-atom is also observed in theory and has to be considered in the study of these systems.

The proposed binding modes for amines to platinum nanoparticles allow for the drawing of conclusions for the functionalization of particles by phosphines as well. Indeed, a binding of phosphonium ions by electrostatic interactions seems very likely. Evidence for such a binding mechanism is found in the ^{1}H NMR spectra, which not only suggests the existence of solvated OH^- species, but may even further supply indications of the protonated phosphine. Similarly to the acidic treated protection by tertiary amines, the TOP-functionalized particles exhibit a strongly reduced ligand coverage. Furthermore, even the catalytic properties are similar to those of amine-functionalized particles. However, TOP-protected particles can be functionalized in a basic environment, in contrast to the functionalization with TOA. These findings suggest that the presence of hydrogen atoms at the phosphorous atom is not prerequisite for their ligand binding to the nanoparticle. However, since the pretreatment of the nanoparticles with hydrogen leads to a more efficient and faster functionalization than the functionalization in basic environment, it seems that a binding via surface hydrides is also a potential binding mode for phosphines. These different types of binding may also explain the occurrence of more than one peak in the ^{31}P MAS NMR spectrum. Due to these evidences, an equilibrium between the interaction of the phosphorous directly with the platinum surface and indirectly via hydrides at the surface is possible.

Conclusion

In this chapter the binding modes of different ligands to platinum nanoparticles are examined. The interpretation of the respective binding modes of thiols, phosphines and amines on the basis of the findings during this work is summarized graphically in figure 3.19.

Amine functional groups are found to bind either via electrostatic interactions or via hydrogen to the platinum surface. Furthermore, the formation of a covalent bond between the platinum particle and the nitrogen's lone pair as suggested in analogy to complex chemistry, can be excluded. Consequently, amines are only weakly bound to the metal surface and stay mobile, which is reflected by their low stability. In a similar manner an additional binding motif of phosphine-functionalized platinum nanoparticles is proposed. While the interaction of non-protonated amines with the

platinum nanoparticle exclusively occurs via a Pt–H–N moiety, an equilibrium between directly Pt–P bound moieties and phosphine interaction to the platinum surface via hydrogen could be possible. In contrast to the thiol-protected particles, which are highly stable in catalysis, but demonstrate a strongly reduced activity, particles protected by the amines and the phosphine are reactive, but show poor stability and a tendency of the catalyst material towards precipitation during the reaction. While thiols bind strongly to the platinum nanoparticles, amines and phosphines can interact with mobile surface hydrides. This interaction does not only increase the ligands mobility on the metal surface, but makes also their release from the particles easier. It is concluded that these catalytic properties are directly related to the type of ligand binding.

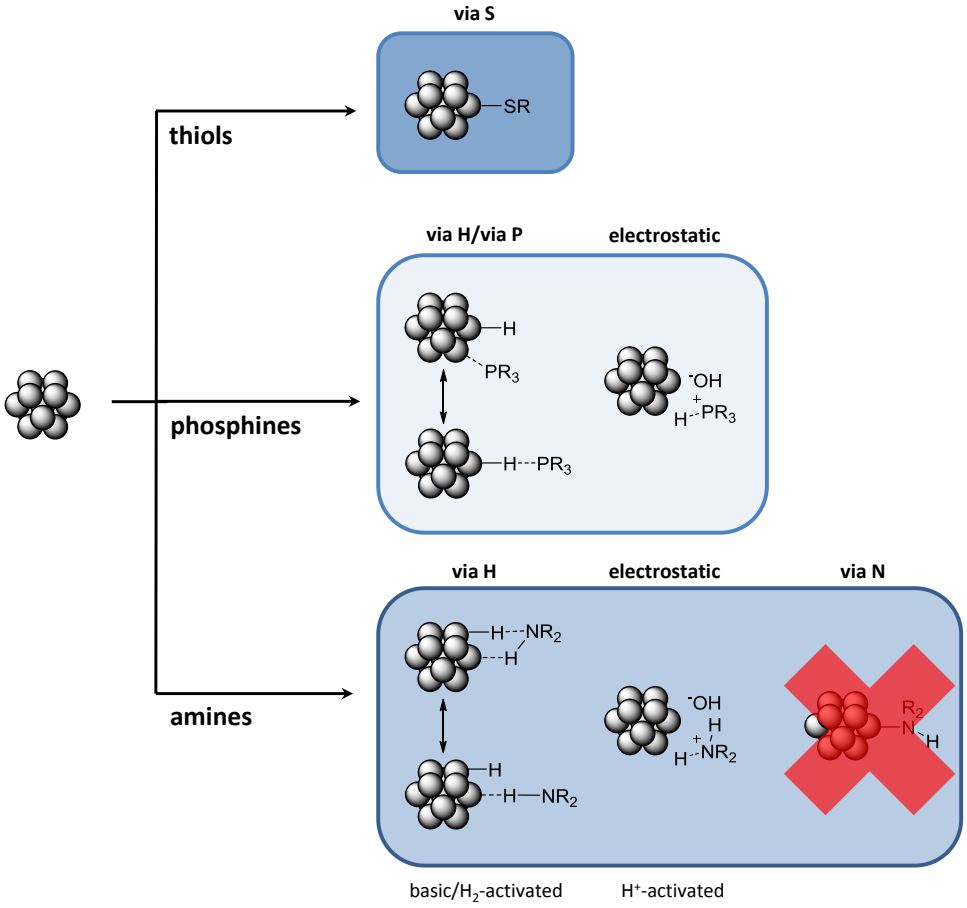

Figure 3.19: Schematic of the proposed binding modes of thiols, phosphines and amines to platinum nanoparticles formed under different functionalization conditions.

3.2.2 Excursus: gold nanoparticles

The elucidation of amine binding modes to platinum nanoparticles reveal new findings, which may be relevant for other metal systems, too. Concerning primary amines, a similar approach of particle synthesis and functionalization through phase transfer has been reported for gold nanoparticles.[74] However, the influence of the degree of substitution of the amines and the application of H_2-activation prior to the functionalization has not been studied. These elucidations are promising for the analysis of the interaction of amines with gold nanoparticles similarly to the new results obtained by the analysis of platinum nanoparticles.

For this, OA, DOA and TOA ligands are applied similarly to the method used for the functionalization of the platinum nanoparticles after the particle synthesis in a separate step during a phase transfer. For the nanoparticle synthesis the Brust-Shiffrin method, from which monodisperse gold nanoparticles can be obtained, is not suitable for this application, because the synthesis involves a two phase process, in which thiol ligands are already present during the particle formation.[27] The synthesis of gold nanoparticles in a water based single phase reduction of a gold salt by citrate is a better suited method. This procedure was introduced by Turkevich et al. and has already been described in literature for the synthesis and functionalization of gold nanoparticles by primary amines.[74,128–130]

In this work, gold nanoparticles are synthesized following the Turkevich method and obtained in a violet aqueous solution stabilized by citrate molecules with a mean diameter of 5.9 ± 1.0 nm (figure 3.20a). As a proof-of-principle, a first functionalization attempt of the approach is carried out by adding an OT ligand containing toluene solution to the gold colloid. This approach is carried out under both, acidic and alkaline environment. A subsequent phase transfer of the particles is observed for both approaches. However, the color of the acidic OT^a-stabilized gold nanoparticles changes and the plasmon resonance determined by UV/VIS spectroscopy results in a peak shift from 512 nm of the "unfunctionalized" gold nanoparticles to 522 nm in the spectrum of the OT^a-functionalized particles (figure 3.21). This redshift indicates the change of the nanoparticle size, the electronical environment or influences by the solvent.[131] For the alkaline OT-stabilized particles no change of plasmon resonance was detected by UV/VIS.

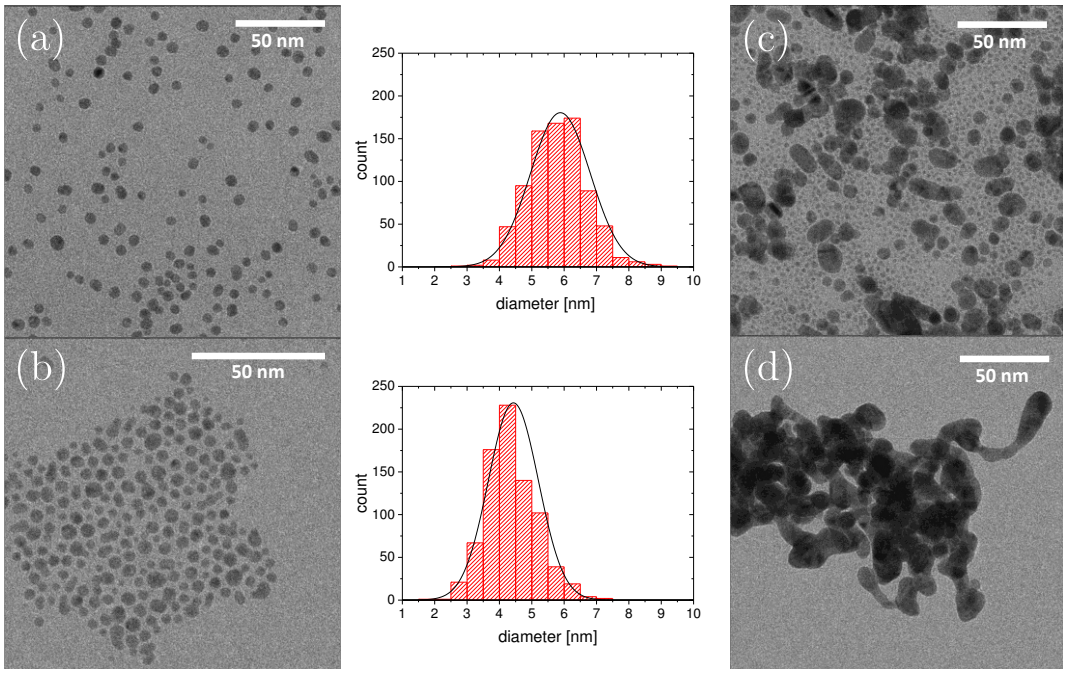

Figure 3.20: TEM images of gold nanoparticles stabilized by (a) citrate, (b) OT[a], (c) OT and (d) OA ligand molecules and the respective size distributions for (a) and (b).

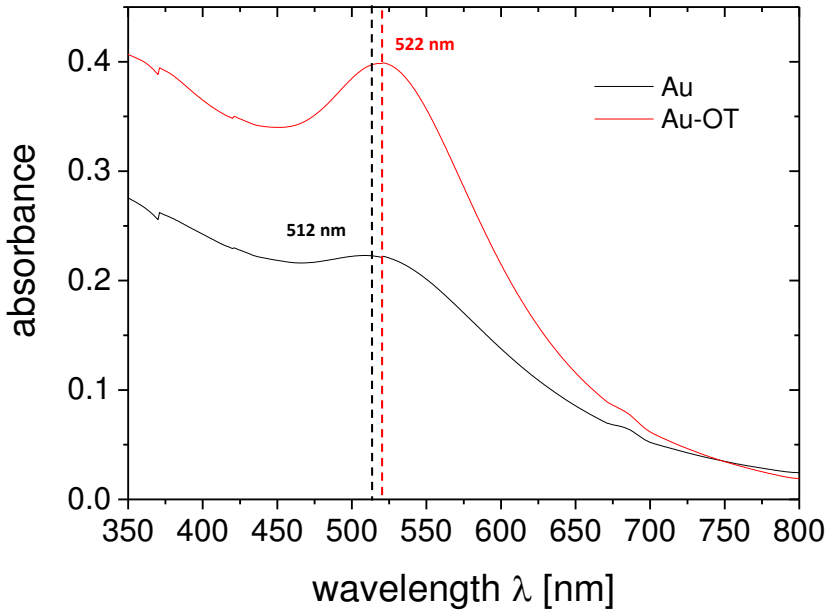

Figure 3.21: UV/VIS measurement of gold nanoparticles stabilized with citrate molecules in aqueous solution (red) and stabilized by octanethiol ligands in toluene (black).

However, TEM images of both samples reveal inconclusive results with regard to these UV/VIS measurements (figure 3.20). The OT[a]-functionalized particles preserve the size of the unfunctionalized particles even after the functionalization, while the OT-functionalized particles exhibit two different size ranges of particles (figure 3.20b and c). One particle species is significantly smaller than the "unfunctionalized" gold particles, while the other species shows coalescence of some particles to bigger aggregates. These images suggest different mechanisms during the functionalization. Furthermore, the attachment of the OT ligand is proven by NMR spectroscopy, for which the typical peak broadening and shift of nanoparticle capped ligands is observed (figure 3.22a).

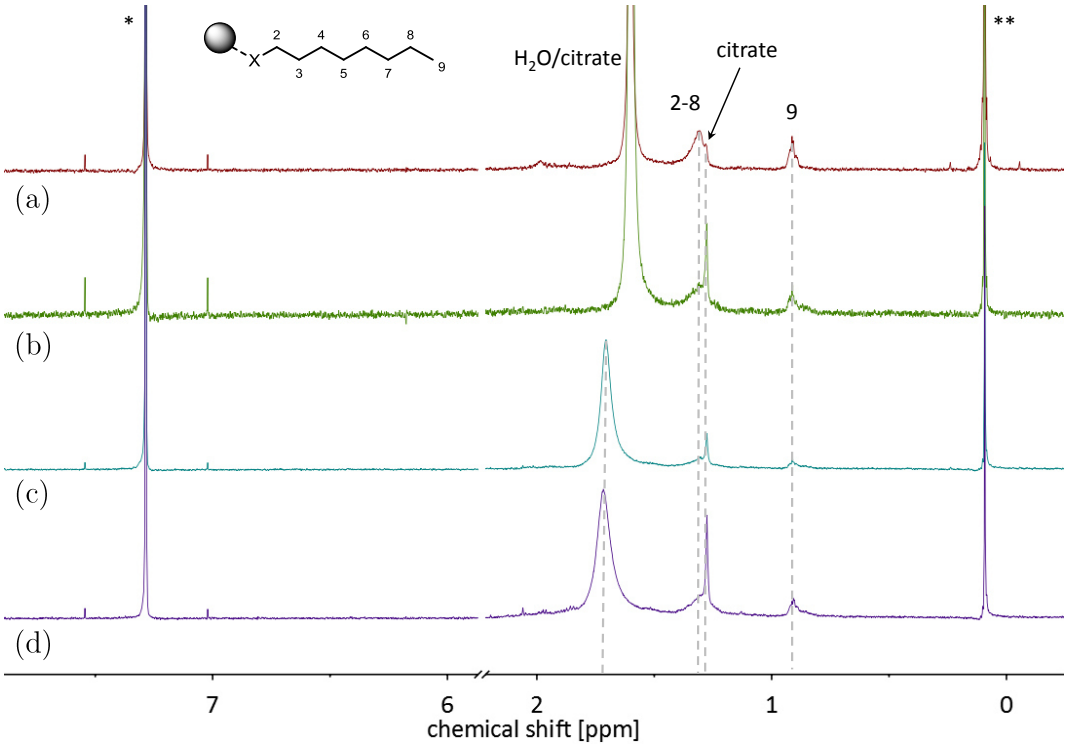

*Figure 3.22: NMR spectra of (a) OT-, (b) OA-, (c) DOA- and (d) TOA[a]-functionalized gold nanoparticles in $CDCl_3$ (solvent peaks are marked with *, grease peaks are marked with **).*

After the feasibility of the functionalization method by the phase transfer reaction and characterization techniques for gold nanoparticles is studied with the thiol, the different amines are applied similarly. However, the functionalization process is not as straight forward for amine ligands as for the thiol ones. The OA ligands causes a color change from violet to black during the functionalization under acidic or basic conditions after some time of reaction. The black particles are situated at the interface

of the two phases. After washing and cleaning of these particles no dissolution is possible in different organic solvents, e. g. toluene or hexane. TEM images of the OA-capped gold nanoparticles indicate their coalescence of the nanoparticles (figure 3.20d). However, the NMR spectrum of these particles exhibit small, but broad signals of the ligand (figure 3.22b). The functionalization with the DOA ligand results in the same results as observed for the OA ligand. Furthermore, no phase transfer is observed at all upon the application of TOA during the functionalization process under acidic or basic environment. NMR spectra of DOA and TOA ligand-treated gold particles exhibit an broad peak additional peak at 1.72 ppm (figure 3.22c and d).
The results obtained by the functionalization of gold nanoparticles with amine ligands reveal the substantial differences caused by some changes in the system. The functionalization of all samples in basic environment leads to coagulation of the gold particles. This observation is made independently for all ligands and the reason seems to be attributed to the "unprotected" gold nanoparticles, which are indeed protected by easily replaceable citrate molecules. The ripening process under basic condition is probably to be due to the rearrangement of the citrate molecules at the particle surface. Under acidic condition the citrate molecules are present as di- or tri-protonated citric species, from which the protonated carboxylic groups may be adsorbed at the gold surface.[132] Further citrate molecules are dangling in a second layer at the particle due to intermolecular hydrogen bonds of the COOH groups.[133] These dangling citrate molecules can be removed by adjusting the pH to higher values (≈ 9) due to the repulsive forces of the deprotonated COO^- groups.[134] Upon further increase of the pH value a further rearrangement of the citrate ligands likely occurs.[133] This rearrangement presumably leads to a reduced stabilization of the nanoparticles and a higher probability for fragmentation or coalescence upon the collision of two particles. During functionalization, a small number of ligand molecules are able to be attached at the particles surface, which is detected by NMR, but the amount of ligand at the surface of the nanoparticles seems to be insufficient for stabilization. The observations under basic conditions are in good agreement with the findings of Kumar et al.[74]
However, they have also reported that the subsequent functionalization by primary amines under acidic condition results in stable colloids, which could be washed, dried and redissolved in chloroform, which differs to the findings of the present work. In the present work, even under acidic condition the amine ligands do not induce a phase transfer of the gold particles and precipitation is observed after some time. Kumar et al. proposed ammonium species as the stabilizing moieties, which is in agreement with the earlier proposed binding modes of amine-stabilized platinum nanoparticles. This explanation seems reasonable as well for the stabilization of gold nanoparticles. However, in this work the coalescence of the gold particles could be due to

contaminations in any of the used chemicals or an insufficient choice of the ratios between amine, gold or citrate molecules or solvent volume. The ripening of the gold nanoparticles during amine-functionalization hampers the analysis of the binding modes with amines under the applied conditions.
The excursus of the functionalization of gold nanoparticles leads to the conclusion, that the applied method for platinum nanoparticles is not similarly applicable for this system. The weakly stabilizing agent citrate bears, in contrast to ethylene glycol, difficulties during the phase transfer process leading to a ripening of the particles. Thus, a throughout characterization of the ligand binding of amines with different degrees of substitution was so far not possible.

3.2.3 Excursus: ruthenium nanoparticles

The results obtained by the synthesis and functionalization of gold nanoparticles very well demonstrate the sensitivity of such systems to the change of parameters, such as the weakly stabilizing species present during the particle synthesis. Due to the fact that ruthenium nanoparticles, which are generally applied as catalysts, can be obtained by exactly the same polyol method as for the synthesis of platinum nanoparticles, this approach seems also very well suited for the elucidation of the ligand binding mode to these particles. Furthermore, ruthenium is a very active metal in the catalysis of hydrogenation reactions in general and thus, the functionalized nanoparticles can as well be applied in the selective hydrogenation of 3-hexyne to 3-hexene.[135,136]
In analogy to the synthesis and functionalization of ligand protected platinum nanoparticles, ruthenium nanoparticles are synthesized by the polyol method.[50] The functionalization by OT, OA, and DOA is conducted in basic environment, while the functionalization with TOA does not result in a phase transfer under these conditions. Thus, TOA[a]-protected ruthenium nanoparticles are produced under acidic conditions. TEM analysis of OT-capped ruthenium nanoparticles shows the size of the particles in a range of about 2 nm (figure 3.23). Similarly to the protection of platinum nanoparticles a constant mean diameter is expected for all samples of functionalized ruthenium nanoparticles.
NMR spectra of these ruthenium nanoparticle samples (figure 3.24) reveal the typical broad peaks of ligand protected nanoparticles at 0.88 ppm and 1.25 ppm. Furthermore, a sharp peak at 1.56 ppm in the spectra of the basic treated samples hints at water species, which are not coordinated to the particles surface. These samples have probably not been dried sufficiently. Furthermore, the broad peak at the same chemical shift in the spectrum of the TOA[a]-functionalized particles indicates, in

analogy to TOA[a]-capped platinum nanoparticles, OH^- or water species in close proximity to the ruthenium surface.

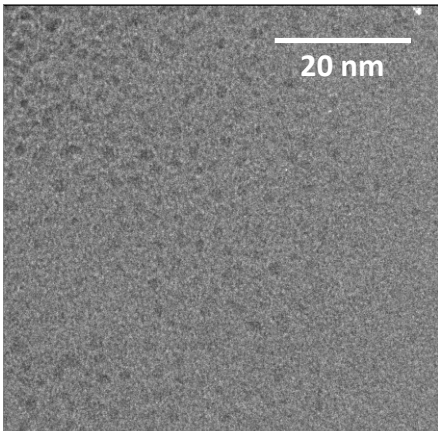

Figure 3.23: TEM image of OT-stabilized ruthenium nanoparticles obtained by the polyol method.

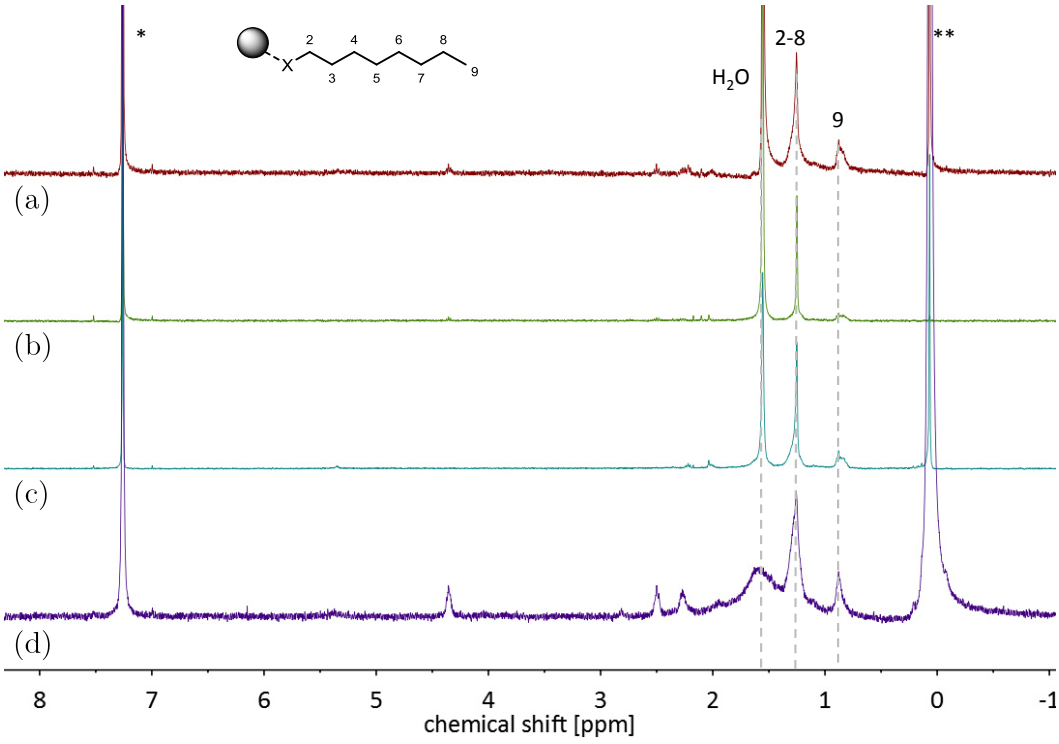

*Figure 3.24: NMR spectra of (a) OT-, (b) OA-, (c) DOA- and (d) TOA[a]-functionalized ruthenium nanoparticles in $CDCl_3$ (solvent peaks are marked with *, grease peaks are marked with **).*

Since a similar behavior of TOA ligands during the functionalization process and similarities of the NMR spectra of the TOA[a]-functionalized ruthenium nanoparticles to that of the respective platinum nanoparticles have been observed, a similar binding mechanism is proposed. This means, that a covalent and strong S—Ru bond is formed, while amines interact only in the form of protonated ammonium species electrostatically or via interaction with hydrogen atoms, in analogy to the binding modes of thiols and amines to platinum nanoparticles illustrated in figure 3.19. This assumption is in agreement with the findings of a previous study about ruthenium nanoparticles stabilized by thiols or primary amines.[137] In that study, stable colloids have been formed upon functionalization with thiols. In contrast, the functionalization by primary amines revealed rapid exchange reactions between the bound amines and the free amines in solution. Note, that the synthesis and functionalization of the ruthenium particles occurred in one step in organic solution under 3 bar hydrogen. These conditions facilitate the binding of amine ligands via a hydrogen interaction, especially when primary amines are used. Furthermore, the rapid exchange of amine ligands correlate with the mobility of surface hydrides and the amine ligands associating with the proposed amine binding mode.

The functionalized ruthenium nanoparticles are applied as catalysts in the selective hydrogenation of 3-hexyne to 3-hexene. During the catalytic reactions no conversion is obtained even after 3 h reaction time for all ligand-stabilized ruthenium nanoparticle samples. These results are surprising, because ruthenium nanoparticles in general and ruthenium nanoparticles obtained by the polyol method in particular are common catalysts for hydrogenation reactions.[135,136,138] An explanation for this result may be the oxidation of the particles and the formation of inactive RuO_2 at the particles surface. Indeed, upon addition of water to the polyol synthesis of ruthenium nanoparticles RuO_2 nanoparticles result, whereas under inert conditions (i. e. the absence of water and oxygen) active ruthenium nanoparticles are obtained.[138,139] According to these observations and due to the fact that the synthesis is not carried out under inert conditions, the probability of traces of water during the particle synthesis is high. Thus, the formation of RuO_2 species at the nanoparticle seems very likely. The presence of RuO_2 may be confirmed with XPS measurements in comparison with the synthesis of ruthenium nanoparticles carried out following the same approach under an inert atmosphere in future studies.

Concluding the results, similar binding modes of thiol and amine ligands are indicated by the evidences obtained during functionalization and characterization. Furthermore, it was found that the polyol synthesis for ruthenium nanoparticles is sensitive to water and oxygen, leading to the oxide contaminations at the nanoparticles. The reactivity of the ruthenium oxide particles reveal a strongly reduced activity in comparison to

pure metal nanoparticles. Catalysis with pure ruthenium nanoparticles are assumed to catalyze the hydrogenation of alkynes to alkenes instead of the oxidized ones. However, more experiments have to be carried out in order to confirm the assumption of similar binding modes of ligands to ruthenium nanoparticles as to platinum nanoparticles. Furthermore, the presence of air and water during the nanoparticle synthesis should be excluded in order to avoid the contamination with oxides. These pure ruthenium particles may obtain a higher reactivity than the oxide ones. However, due to the high oxidation potential of ruthenium nanoparticles, they are not as useful for application in catalysis as platinum nanoparticles.

3.3 Application of ligand-protected platinum nanoparticles in catalysis

Based on the findings of the different binding modes of different ligands to platinum nanoparticles, it becomes clear that the protection by thiols strongly reduces the particles activity, but their use seems to be a requisite for a high stability of the catalysts in colloidal hydrogenation reactions. Since stable and defined systems are of interest for the tailoring of a selective catalyst, thiols seem to be the system of choice for the protection of platinum nanoparticles in the selective hydrogenation of alkynes to alkenes. The hydrogenation of 3-hexyne to 3-hexene serves as a model system for the selective hydrogenation of triple bonds to double bonds. The catalytic reaction takes place under colloidal condition of the ligand-protected nanoparticles dissolved in THF, as illustrated in figure 3.25. For the hydrogenation, a Fischer-Porter bottle is used as a reactor and molecular hydrogen at 1.5 bar is applied. A septum on top of the reactor facilitates the withdrawal of samples for GC analysis during the course of the reaction.

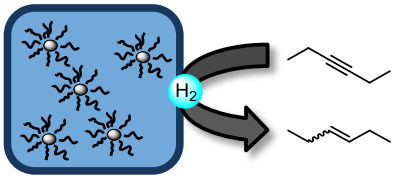

Figure 3.25: Schematic of the selective hydrogenation of 3-hexyne to 3-hexene in a colloidal solution of ligand-protected platinum nanoparticles with molecular hydrogen.

3.3.1 Thiol-stabilized platinum nanoparticles

The stability of thiol-functionalized platinum nanoparticles in catalysis is their advantage in comparison to particles functionalized by amines or phosphines. However, the low reactivity remains a challenge to be solved. The main questions in this regard are: (i) how can the particles be tailored to be more active, (ii) are active thiol-functionalized platinum nanoparticles still stable, (iii) does the higher activity influence the selectivity of the reaction and (iv) can different substituents at the thiol ligand directly influence the activity and selectivity of the hydrogenation reaction?

One approach for obtaining a higher activation of the particles is the reduction of the ligand coverage in order to create a path for the substrates to reach the active platinum surface. This approach is elucidated more in detail in this work. For this, the standard synthesis of platinum nanoparticles in analogy to the polyol method is used to obtain nanoparticles in the same size regime of 2.0 ± 0.4 nm, as described earlier in the synthesis part of this work.[46] After subsequent functionalization under different conditions the particles are tested in the selective hydrogenation of alkynes to alkenes.

Functionalization

Another advantage of the synthesis and functionalization of nanoparticles in two separate steps, in addition to the application of different pH conditions during the phase transfer or pre-conditioning of the particles, is the convenient application of different ligands or ligand concentrations. This way, only the ligand shell is altered and the catalytically active nanoparticle core remains unchanged, which is a prerequisite for the comparison of the different nanoparticle samples regarding catalysis.

In order to obtain a varied ligand coverage of the platinum nanoparticles, two different approaches are applied. During the functionalization process different concentrations of the OT ligand and thiols with different substituents other than the octyl chain are elucidated. Concerning the variation of the OT concentration during functionalization 0.05, 0.5, 1, 5 and 25 equiv. of OT with respect to the applied amount of platinum are used. A rapid phase transfer of the nanoparticles into the OT containing toluene phase is obtained for all samples. The phase transfer indicates the successful binding of the thiol ligand to the particle surface. Samples prepared with less than 0.5 equiv. OT undergo a phase transfer during the functionalization, but upon redissolution in an organic solvent, they precipitate. In contrast, samples with higher concentrations than 0.5 equiv. of OT applied during functionalization are stable after washing and drying in the form of powders as well as colloids after redissolution in THF for several weeks.

Furthermore, the platinum nanoparticles are functionalized with phenylethanethiol (PET), diphenylmethanethiol (DPMT) and cyclohexanethiol (CHT) ligands (figure 3.26) with an excess of 5 equiv. of the ligand with respect to the amount of platinum. This excess is chosen, because the bulky ligand DPMT was not transferred into the ligand phase when a lower ligand concentration is applied. For triphenylmethylthiol, an even bulkier ligand, no phase transfer of the nanoparticles is observed at all, even for very high concentrations of the ligand (i. e. 50 equiv.). In order to be able to compare the influence of the different substituents of the thiol ligands with each other, the functionalization conditions are kept constant for all functionalization processes. All thiol-protected nanoparticle samples are stable after redissolution in THF.

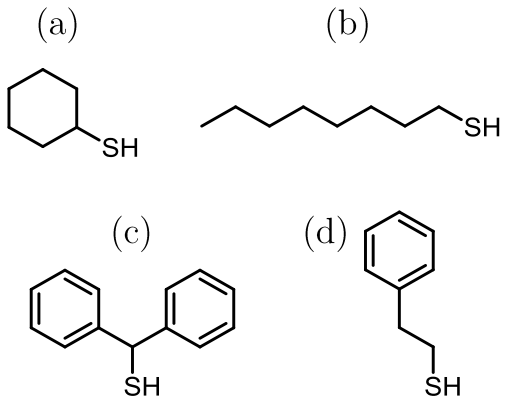

Figure 3.26: Schematic of the structures of the applied ligands for the stabilization of platinum nanoparticles: (a) cyclohexanethiol (CHT), (b) octanethiol (OT), (c) diphenylmethanethiol (DPMT) and (d) phenylethanethiol (PET).

The ligand coverage degree of all platinum nanoparticle samples is determined by elemental analysis, from which the percentage by mass of sulfur and platinum in the samples is given. These values are calculated in order to obtain the ratio between sulfur and platinum atoms. From the "magic" number approach, it is estimated that approximately 54 % of the total number of platinum atoms (Pt_t) are located at the surface of the nanoparticle.[140] With this approximation the ratio between sulfur and platinum surface atoms (Pt_s) was determined, leading to the ligand/Pt_s values when the presence of one sulfur atom in one ligand molecule is considered (table 3.4). The ligand/Pt_s ratio gives the coverage degree of ligands at the platinum nanoparticles after the functionalization. For an easier reading, the nanoparticle samples are abbreviated due to their ligand and ligand concentration applied during functionalization (e.g. OT0.5 for the sample functionalized with an octanethiol concentration of 0.5 equiv.).

These results of the elemental analysis confirm the expected order of coverage degrees in correlation with the different applied OT ligand concentrations during functionalization, as it can be seen in table xxx a higher ligand concentration results in a higher coverage degree and *vice versa*. For nanoparticle samples with different ligands applied, the coverage degree on the particle surface differs for each ligand, which is as well summarized in table 3.4.

Table 3.4: Summary of calculated ligand/Pt_s ratio of thiol-functionalized platinum nanoparticles obtained by elemental analysis.

sample	ligand	equiv.	ligand/Pt_s
$OT_{0.05}$[a]	OT	0.05	0.11
$CHT_{0.5}$	CHT	0.5	0.35
$OT_{0.5}$	OT	0.5	0.38
CHT_5	CHT	5	0.47
CHT_{25}	CHT	25	0.48
$DPMT_5$	DPMT	5	0.53
PET_5	PET	5	0.60
OT_1	OT	1	0.68
OT_5	OT	5	0.88
OT_{25}	OT	25	0.97

[a]Not stable upon redissolution in THF.

These differences are expected to originate from different steric demands of the substituents, which may also be a considerable factor in affecting the coverage density at the particle surface. Due to the steric hindrance, the side chains of the thiols may interfere with each other. This way, the bulkier thiols favor a less dense ligand coverage and non-bulky thiols support a higher ligand density. Comparing the data obtained from elemental analysis, this expected trend is confirmed by the high ligand coverage of OT_5-stabilized platinum nanoparticles (0.88) in contrast to the lower ligand coverages of the nanoparticles stabilized by the bulkier thiols containing phenyl- or cyclohexyl-groups. Surprisingly, the bulkier $DPMT_5$-covered particles exhibit a lower ligand coverage (0.53) than the PET_5-stabilized particles (0.60). One explanation for this phenomenon could be the rigidity and in connection with this the chain length of the ligand. In this work a trend is observed, in which longer chains and thus more flexible ligands result in higher ligand coverages. For shorter alkyl chains between the thiol functionality and the bulky phenyl- or cyclohexyl-groups, these bulky groups are located closer to the surface of the nanoparticle. Thus, a further ligand molecule cannot get close enough to neighboring platinum surface atoms to interact with them. For more flexible ligands, the ligand can adapt its position and thus, bind to a surface atom close to another bound ligand molecule. The CHT_5-stabilized nanoparticles exhibit the lowest ligand coverage (0.47) in comparison to the other samples after application of 5 equiv. ligand, which is in agreement with

this explanation. Upon the further decrease of the CHT ligand to 0.5 equiv. during functionalization, the resulting nanoparticles exhibit an even lower ligand coverage of 0.35 ligand/Pt_s compared to the CHT_5 sample. Nevertheless, the particles are stable in colloidal solution. A lower ligand concentration as 0.5 equiv. of CHT during the functionalization process did not lead to a sufficient phase transfer of the nanoparticles, indicating a "critical" concentration of CHT. Essentially, it is expected that the ligand coverage at the platinum nanoparticle surface is dependent on the ligand concentration applied during functionalization, the bulkiness of the ligand, the chain length and the rigidity of the ligand, which is consistent with previous observations in literature.[141,142]

TEM images of OT_5-, $OT_{0.5}$-, PET_5-, CHT_5- and $CHT_{0.5}$-stabilized platinum nanoparticles reveal the uniformity of the particles size for all applied ligand concentrations and different substituents at the thiol ligands of 2.0 ± 0.4 nm (figure 3.27). These results confirm that the standard particle synthesis followed by a subsequent functionalization of the particles produces thiol-stabilized platinum nanoparticles, for which only the ligand shell is altered, but the size of the metal core is preserved.

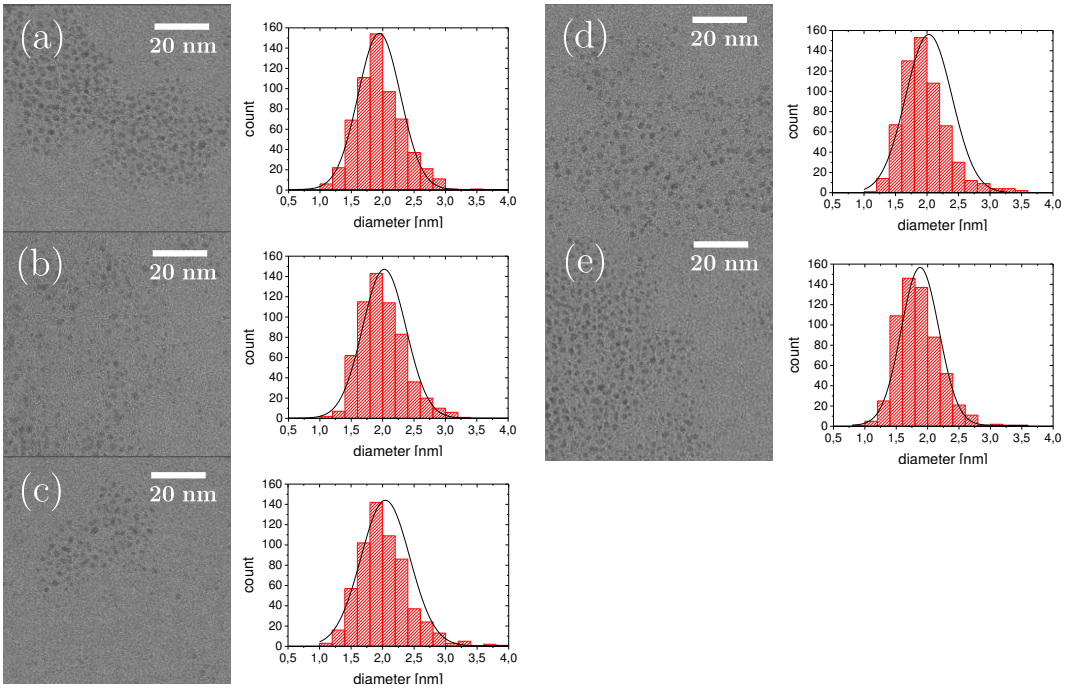

Figure 3.27: TEM images of (a) OT_5-, (b) $OT_{0.5}$-, (c) PET_5-, (d) CHT_5- and (e) $CHT_{0.5}$-stabilized platinum nanoparticles with the respective size distribution.

In summary, all synthesized thiol-functionalized platinum nanoparticles reveal similar properties regarding the nanoparticle size and stability. The obtained nanoparticle samples with a concentration of 0.5 equiv. or higher during functionalization are in the size range of 2.0 ± 0.4 nm and are redissolvable in THF after washing and drying to form stable colloids. A minimal ligand coverage of 0.35 ligands/Pt_S is obtained by $CHT_{0.5}$-functionalize nanoparticles.

Selective hydrogenation of 3-hexyne to 3-hexene

After confirming the comparability of the produced platinum nanoparticles exhibiting different ligand shells, they are applied in the selective hydrogenation of 3-hexyne to 3-hexene, which functions as a model catalytic reaction (figure 3.28).

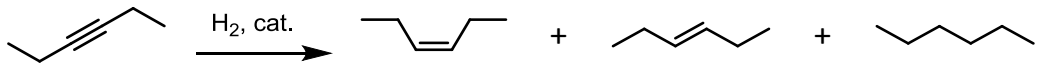

Figure 3.28: Reaction equation of the hydrogenation of 3-hexyne with the reaction products cis-3-hexene, trans-3-hexene and hexane.

For the hydrogenation reaction, the nanoparticle samples are dissolved in THF and pressurized with 1.5 bar hydrogen. The reaction is then initialized upon the addition of 3-hexyne to the colloid via syringe. The course of the reaction is followed by taking aliquots of the reaction mixture via a syringe and the analysis of these aliquots with GC-FID. From the analyses the conversion of 3-hexyne, defined as the sum of product concentrations divided by the concentration of all reaction species, and the selectivity for 3-hexene, defined as the concentration of hexene with respect to the concentration of all reaction products, are calculated. Furthermore, turnover frequencies (TOFs) are obtained for the respective particles considering the moles of platinum contained in 1 mg of sample (from elemental analysis) and the average number of platinum surface atoms (calculated from the particles diameter and the "magic" number approach[140]). Figure 3.29 shows typical chromatograms for a hydrogenation reaction after 8 %, 33 %, 89 % conversion and after 99 % conversion of 3-hexyne with separate peaks for each reaction substrate and product. After full hydrogenation of 3-hexyne and 3-hexene, only the alkane peak is monitored, which allows for the exclusion of side reactions other than the simple addition of hydrogen to the molecules. However, trace amounts of side products, such as oligomers or cyclization products, may be present, which are below the detection limit of the GC-FID.

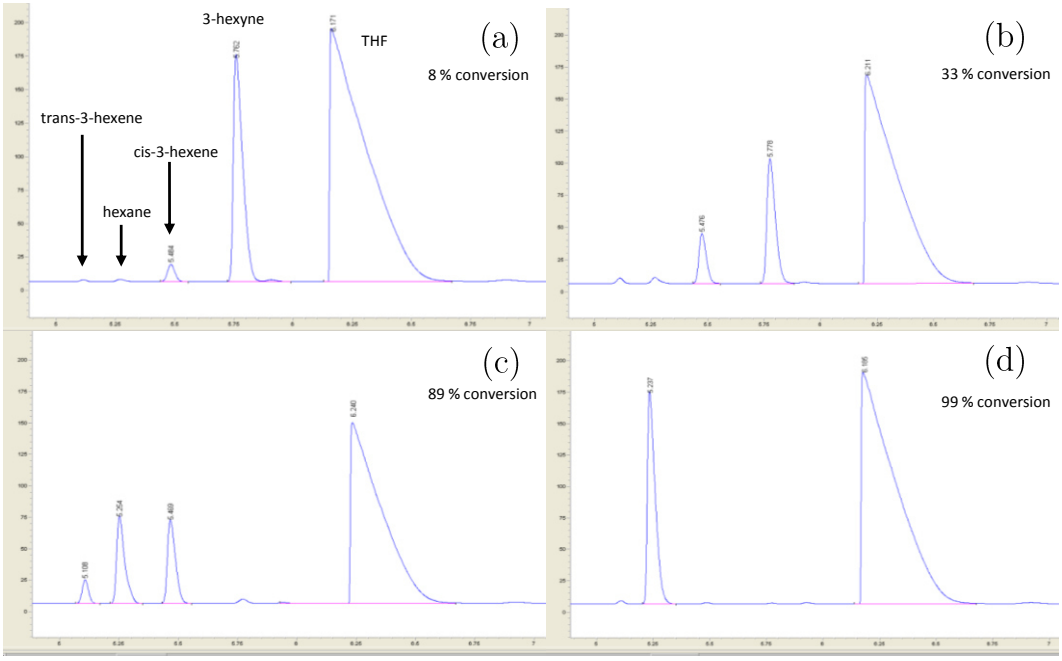

Figure 3.29: Chromatograms of the hydrogenation of 3-hexyne after (a) 8 %, (b) 33 %, (c) 89 % and (d) 99 % conversion of 3-hexyne; retention times: 5.11 min trans-3-hexene, 6.25 min hexane, 5.49 min cis-3-hexene, 5.78 min 3-hexyne and 6.21 min THF.

The results of the hydrogenation applying the OT-stabilized platinum nanoparticles with different ligand coverages show that an increase of the coverage degree leads to a decreased reaction rate (figure 3.30), which is in agreement with literature findings.[143] This difference in catalyst activity is assumed to be due to the absolute number of blocked active surface sites, for which a lower coverage degree corresponds to a lower number of blocked sites. Consequently a lower coverage degree results in a higher reaction rate.[141] At the same time the selectivity for 3-hexene lies in a range of 84 - 90 % for all OT coverage degrees for high conversions (table 3.5). This observation is different to a catalytic system, which has recently been described for the selective hydrogenation of alkynes to alkenes with ligand-stabilized platinum nanoparticles as catalyst.[22] In that case the ligand coverage degree influences the selectivity due to the change of adsorption properties of the particle. Furthermore, for Lindlar-type catalysts it is assumed that the high selectivity for alkenes before alkanes is caused by a surface poison, either by interactions with ligands or lead modification.[144] However, this trend is not observed for the system studied in the present work. Only an increase in activity is observed while at the same time the selectivity remains constant.

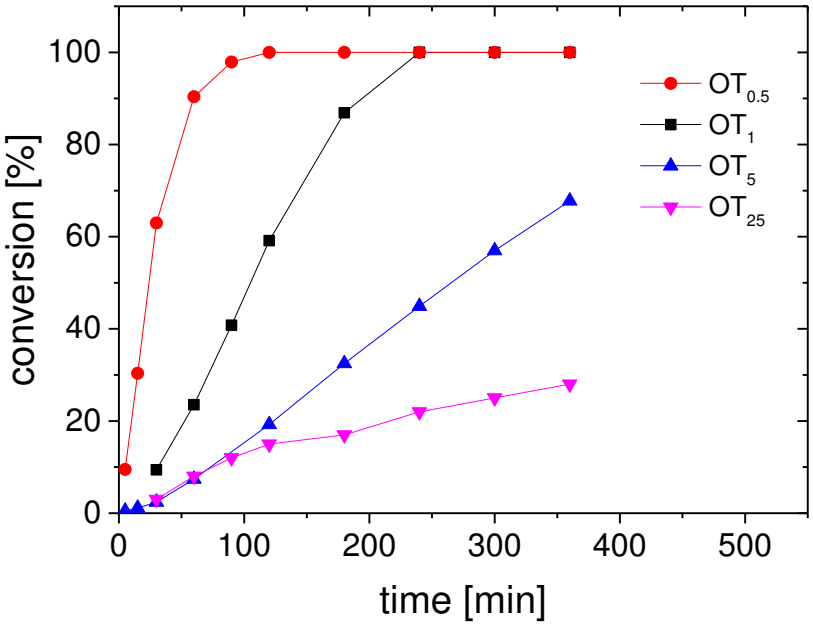

Figure 3.30: Conversion vs. time graphs of the hydrogenation of 3-hexyne for different ligand coverages of OT-stabilized nanoparticles applied as catalysts.

When applying the platinum nanoparticles protected by different thiol ligands in the hydrogenation of 3-hexyne to 3-hexene, the different substituents similarly influence the reaction rate (figure 3.31), but not significantly the selectivity (87 – 90 %) (table 3.5). The tuning of the selectivity by capping ligands to active metal nanoparticle sites has been described by Medlin and coworkers and attributed to steric effects, active-site selection, molecular recognition and electronic effects caused by the thiol head group.[145] However, the difference in selectivity was found to be independent of the ligands' substituents. This independence is also confirmed by the present study. One difficulty in the hydrogenation of 3-hexyne to 3-hexene is the absence of any functional group, which could interact with the ligand and lead the reaction into a certain direction. This is the case in other studies, which report the dependence of the ligands substituents on the selectivity in hydrogenation catalysis.[145] However, in the present study the selectivity of the hydrogenation of alkynes to alkenes is comparable to other catalytic systems, where ligand-protected colloidal metal nanoparticles are applied as catalysts.[144]

While a higher TOF for a lower ligand coverage is observed for the CHT_5-protected particles, particles functionalized with PET_5 and $DPMT_5$ reveal the opposite behavior. The PET_5-functionalized catalyst exhibits a higher ligand coverage, but also obtains a higher TOF than the $DPMT_5$-functionalized catalyst. Cliffel and coworkers have discussed a similar trend, for which the bulkiness of the ligands was made responsible

for the slower reaction due to blocking the substrate from the catalyst surface.[141] In this context, the bulkier DPMT ligand with its two phenyl substituents is more efficiently blocking the diffusion of substrate molecules to the active sites at the nanoparticle surface than the PET ligand with its single phenyl substituent. The OT_5 ligand-protected particles possess the highest ligand coverage and the lowest TOF. This observation again correlates with the number of blocked surface sites by the thiol head group.

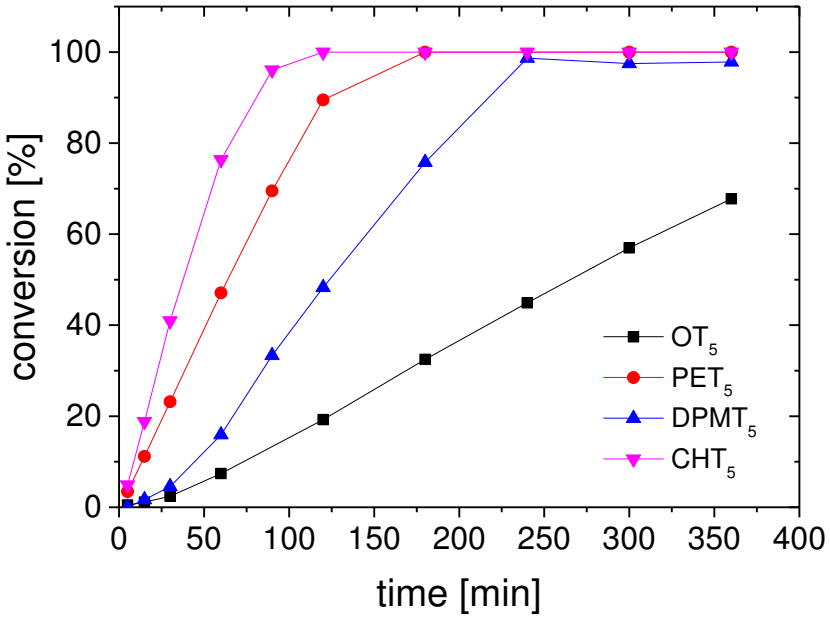

Figure 3.31: Conversion vs. time graphs of the hydrogenation of 3-hexyne for different substituents of thiol-stabilized nanoparticles applied as catalysts.

Additionally to the study of the influence of the different ligand substituents, the CHT ligand, which exhibits the highest activity for the hydrogenation reaction, is chosen for further studies. The CHT-functionalized nanoparticles are further analyzed by altering the ligand concentration during the functionalization. Surprisingly, the CHT_5-nanoparticles and CHT_{25}-nanoparticles possess an almost similar coverage degrees of 0.47 and 0.48, respectively. This result may indicate the almost maximal coverage degree of the platinum nanoparticles for the CHT ligand is already reached at this ligand concentration for the functionalization. Furthermore, a reduction of the ligand coverage is obtained by a lower CHT concentration during the functionalization process, resulting in a coverage degree of 0.35 for $CHT_{0.5}$-nanoparticles.

Table 3.5: Summary of the calculated TOF, conversion and selectivity for thiol-stabilized platinum nanoparticles.

sample	ligand/platinum	sel.[a] %	conv.[a] %	TOF[b] h^{-1}
$CHT_{0.5}$	0.35	91	85	3996
$OT_{0.5}$	0.38	89	90	3514
CHT_5	0.47	89	96	2051
PET_5	0.48	90	97	1188
OT_1	0.53	84	93	722
$DPMT_5$	0.60	87	99	610
CHT_{25}	0.68	86	71	279
OT_5	0.88	89	68	219
OT_{25}	0.97	90	34	170

[a] TOF = mmol substrate/(mmol catalyst · reaction time); considering the moles of Pt contained in 1 mg of sample (from elemental analysis) and only the platinum surface atoms. [b] From GC-FID.

In the hydrogenation reaction, the $CHT_{0.5}$ platinum nanoparticles exhibit the highest TOF of 3996 h^{-1} in comparison with the $OT_{0.5}$ nanoparticles with 3514 h^{-1} and the CHT_5 nanoparticles with 2051 h^{-1}, which give the highest TOF for the study of the OT ligand coverage degree and the study of the influence of the substituent, respectively. The value of these TOFs correlates with the found ligand coverage degrees of the respective nanoparticles. A higher coverage of one particular ligand leads to a lower TOF and *vice versa*.

The comparison of the obtained TOF of 3996 h^{-1} for the $CHT^{0.5}$ nanoparticles in the selective hydrogenation of 3-hexyne to 3-hexene to TOF values from literature is difficult, because the environment of the hydrogenation reactions is often very different and only few references even name this particular value. For example, Ohkuma et al. reached an exceptionally high TOF of 12500 min^{-1}, when applying colloidal palladium nanoparticles (1.7 nm) in combination with tetrabutylammonium borohydride at 8 atm hydrogen and 30 °C for the selective reaction from 3-hexyne to 3-hexene.[19] However, as the metal, the particle size, the stabilizing ligand and the hydrogen pressure strongly influence the hydrogenation reaction, the TOF values are difficult to compare. Another study, which is more similar to the present work, has been conducted by Cliffel et al., who achieve a TOF of 13 h^{-1} for hexanethiol-capped platinum nanoparticles in the hydrogenation of double bonds under similar reaction conditions (room temperature, atmospheric hydrogen pressure).[141] In a further study,

Dupont et al. studied the TOF of the 3-hexyne hydrogenation in an ionic liquid medium for palladium nanoparticles (7.2 nm) and a TOF of 1282 h^{-1} under similar reaction conditions was found.[99] Furthermore, in this study, only the exposed metal atoms on the nanoparticle surface were considered for the calculation of the TOF values, similarly to the present study. These data reveal that the $CHT_{0.5}$-functionalized platinum nanoparticles applied as catalyst in the present study outperform the (largely comparable) systems of Cliffel and Dupont et al. in terms of the TOF.

Furthermore, another influence of the ligand on the selective hydrogenation reaction may be the involvement of the substituents itself in the reaction. The hydrogenation of the respective unsaturated ligand during the catalytic reaction has already been described in literature and it is a possible reaction pathway for unsaturated ligands in the present study.[73] As a result, the hydrogenation of the alkyne is competing with the hydrogenation reaction of the unsaturated ligand. In the present study the phenyl substituents of the DPMT and PET ligands can be hydrogenated forming cyclohexyl-groups. These groups possess a higher steric demand as the planar phenyl rings due to their chair- or boat conformation. This way, an even higher steric hindrance results. This assumption is supported by conditioning experiments using the $DPMT_5$-capped nanoparticles. In these experiments the catalyst was exposed to molecular hydrogen (1.5 bar) for different time intervals prior to the hydrogenation reaction (figure 3.32).

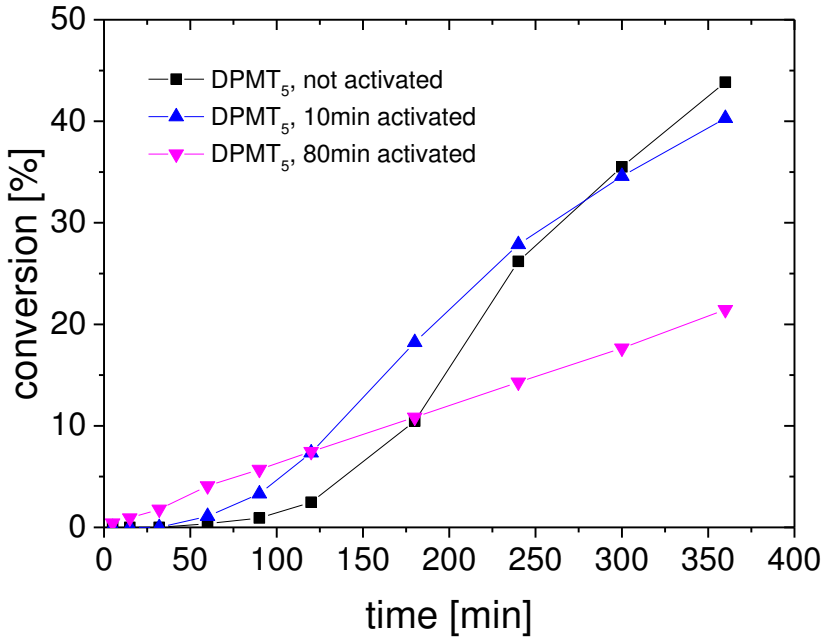

Figure 3.32: Conversion vs. time graphs of the hydrogenation of 3-hexyne for DPMT-stabilized platinum nanoparticles with different activation times (application of 1.5 bar hydrogen prior to hydrogenation).

The results show, that the activated $DPMT_5$-capped nanoparticles (80 min activation time) initially catalyze the hydrogenation reaction followed by a constant reaction rate. The non-activated catalyst needs time for conditioning in the initial phase of the reaction until the hydrogenation starts and then shows a higher activity for the reaction. From these results it can be interpreted that the hydrogenation of the ligand in the initial phase of the reaction is followed by the hydrogenation of the substrate after this initial phase (figure 3.33).

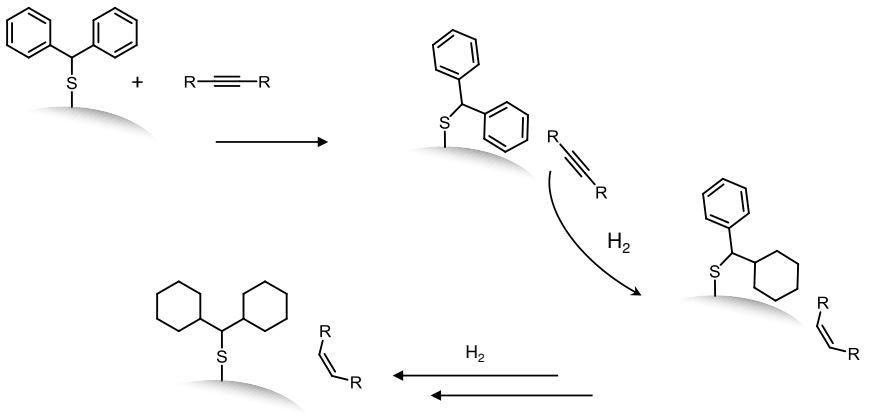

Figure 3.33: Schematic of the proposed reaction pathway taking place for the DPMT ligand during the initial phase of the hydrogenation reaction.

Furthermore, the work of Medlin *et al.* supports this assumption of unsaturated thiols undergoing partial hydrogenation under hydrogen atmosphere at platinum nanoparticle surfaces.[146] They observed that the difference in the chemical structure of the ligands influences the hydrogenation reactions significantly. In case of the CHT ligand no hydrogenation of the ligand is possible and thus, no competition reaction or change of the structure of the ligand is supposed to influence the catalytic hydrogenation of 3-hexyne. Due to the low solubility of $DPMT_5$-functionalized nanoparticles in the deuterated NMR solvents, an NMR study is carried out for the PET ligand in order to study the hydrogenation of the phenyl substituent of the ligand molecule (figure 3.34).

First, the PET_5-stabilized platinum nanoparticles are measured by ^1H NMR in $CDCl_3$. The spectra show the typical broad peaks, which are characteristic for ligand stabilized nanoparticles. The peak of the aromatic group at about 7.21 ppm, which is usually found in the range of 6.5 – 7.5 ppm, is very broad and overlaps with the solvent peak of $CDCl_3$ at 7.26 ppm. Additionally, water species are detected at

1.55 ppm. The sample is then exposed to 3 bar hydrogen, stirred for 17 h and measured again by ^{1}H NMR spectroscopy. In addition to the peaks described before, this spectrum shows a peak at 4.62 ppm, which is characteristic for dissolved H_2. Furthermore, the water peak is broadened and shifted downfield, which may hint that water interacts with surface hydrides at the particles. For the peaks corresponding to protons, which are situated closely to the nanoparticle surface, at 0.84 ppm and 1.26 ppm additional peaks are detected at 0.88 ppm and 1.21 ppm. These additional peaks suggest a change in the structure of the ligand. When stirring the sample under atmospheric conditions the hydrogen peaks disappears due to degassing of the solution. No further changes in the spectrum are detected. After this, the sample is again pressurized with 3 bar hydrogen for 17 h and measured by ^{1}H NMR. This spectrum again reveals the features already described for the first spectrum of the hydrogen treated sample. For all spectra a change of the peak at 7.21 cannot be observed due to the broadness of the peak and the overlap with the solvent peak. However, the additional peaks at 1.21 ppm and 0.88 ppm also indicate a change of the sample structure, which may be related to hydrogenation of the aromatic ring of some of the ligand molecules.

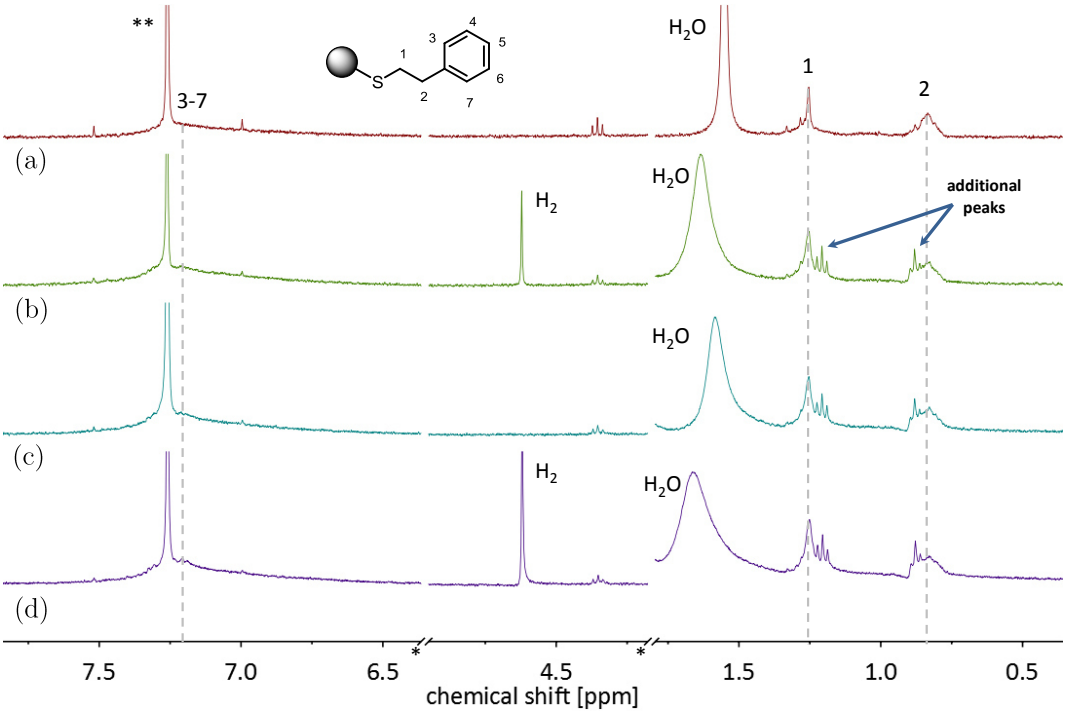

Figure 3.34: NMR spectra of (a) PET-stabilized platinum nanoparticles, (b) after H_2 exposure (3 bar) for 17 h, (c) after stirring of the H_2 treated sample for 17 h and (d) after another H_2 exposure (3 bar) for 17 h in $CDCl_3$ (marks a break in the axis; ** marks solvent residual peaks).*

Another investigation of the nanoparticles concerns their stability in the reaction, as it was found that the highly thiol-covered particles already exhibited a high stability. The stability of a platinum nanoparticle with a lower ligand coverage may assumed to be lower, because the reduction of the number of ligands at the particles surface potentially leads to a higher probability of agglomeration of two particles on collision. During the hydrogenation reaction all nanoparticles are colloids, even the $OT_{0.5}$ stabilized catalyst with the lowest ligand coverage of 0.38 ligands/Pt_S, are stable during the course of the reaction. TEM images before and after catalysis (figure 3.35) show that the particles retain their size and do not agglomerate. These results reveal that the activity of the platinum nanoparticles can be tuned by simply reducing the amount of thiol molecules at the surface. At the same time the particles stability is maintained. However, a minimum thiol coverage on the nanoparticles has to be achieved for their stabilization. If the thiol ligand coverage is too low, the particles do not form stable colloids even before catalysis. From these observations it becomes evident that thiols, which are often marked as catalyst poison,[141,147,148] are capable of both, stabilizing a nanocatalyst and largely preserving its activity.

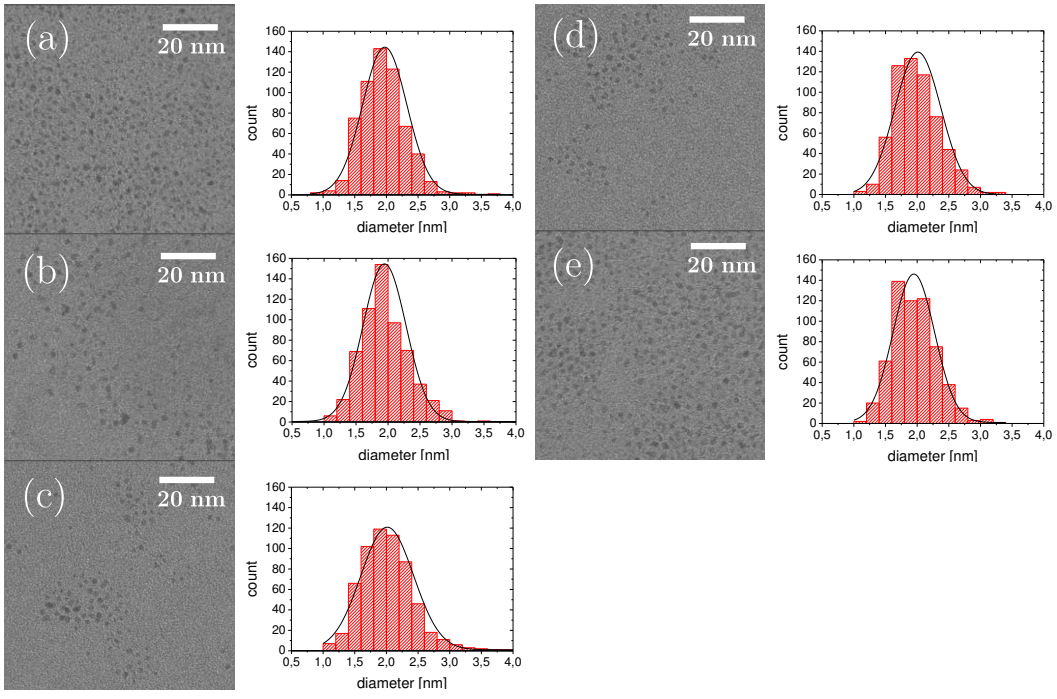

Figure 3.35: TEM images of (a) OT_5-, (b) $OT_{0.5}$-, (c) PET_5-, (d) CHT_5- and (e) $CHT_{0.5}$-stabilized platinum nanoparticles after catalysis with the respective size distribution.

Recycling (see chapter 5.5.1) is tested for the platinum nanoparticles obtaining the highest TOF, $CHT_{0.5}$-functionalized platinum nanoparticles. After a reaction time of 1 h, a conversion of 98 % is reached with 82 ± 5 % selectivity for 3-hexene (figure 3.36). The recycling of the catalyst for 8 runs without significant loss of selectivity and activity reflects its high durability. Additionally, TEM images of the nanocatalyst after the recycling experiments reveal high stability of the nanoparticles during several runs of the catalytic hydrogenation reaction without agglomeration or coalescence (figure 3.37). After 8 runs the mean diameter of the nanoparticles is still found to be 2.1 ± 0.4 nm.

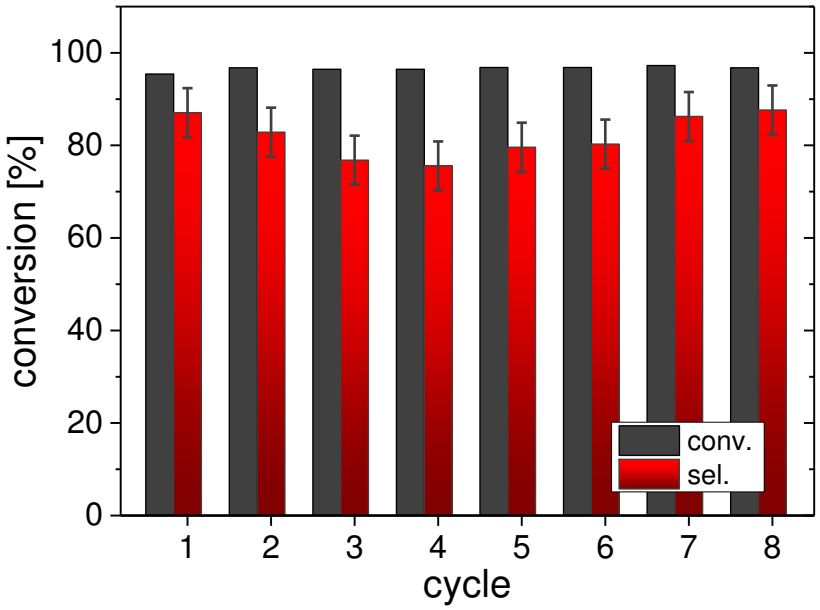

Figure 3.36: Conversion and selectivity of the hydrogenation of 3-hexyne to 3-hexene for 8 recycling runs applying $CHT_{0.5}$-stabilized platinum nanoparticles as catalyst.

A recent study about ligand-protected palladium nanoparticle catalysts revealed a ligand insensitivity concerning the activity and selectivity for certain substrates and for the same ligand a sensitivity for other substrates during hydrogenation catalysis was found.[142] This means, if the chosen substrate reacts independently from the ligand substituents, another substrate might be influenced by it. This is, why the present study is extended to the elucidation of the catalysis of thiol-protected platinum nanoparticles for the sterically demanding terminal alkyne phenylacetylene in the hydrogenation reaction to selectively form styrene.

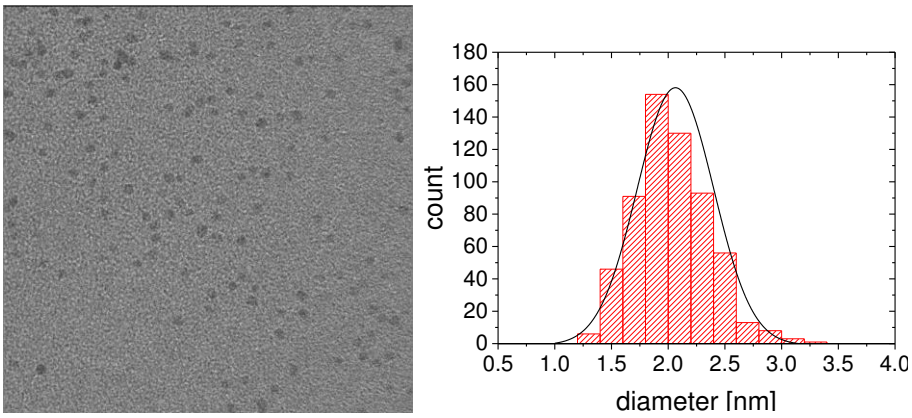

Figure 3.37: TEM images of $CHT_{0.5}$-stabilized platinum nanoparticles after recycling the particles for 8 runs.

Hydrogenation of phenylacetylene

The selective hydrogenation of phenylacetylene to styrene is carried out in analogy to the hydrogenation of 3-hexyne. Possible products of the phenylacetylene hydrogenation are styrene, ethylbenzene and ethylcyclohexane, as shown in figure 3.38.

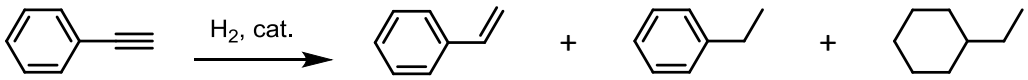

Figure 3.38: Reaction equation of the hydrogenation of phenylacetylene with the reaction products styrene, ethylbenzene and ethylcyclohexane.

As catalysts for this reaction two nanoparticle samples, $CHT_{0.5}$- and $OT_{0.5}$-stabilized platinum nanoparticles, are chosen, which exhibit the lowest ligand coverage degrees and give the highest TOF for the 3-hexyne hydrogenation. Figure 3.39 shows the comparison of the reaction rates of both catalysts and the course of the reaction of the $OT_{0.5}$-nanoparticle catalyzed hydrogenation reaction. Surprisingly, the $CHT_{0.5}$-protected nanoparticles exhibit only 3 % conversion after 300 min, while the $OT_{0.5}$-sample obtain 51 % conversion of phenylacetylene after the same reaction time. This effect may be attributed to the steric demand of the substrate. In contrast to 3-hexyne, phenylacetylene contains a bulky phenyl group, which may sterically interact with the CHT ligand. As a consequence, the phenylacetylene triple bond is

not able to reach the platinum surface, where the hydrogenation reaction takes place. In case of the $OT_{0.5}$ catalyst, the octyl chain of the ligand is flexible and rearranges so that the entire molecule with the phenyl groups can access the surface and the triple bond can be hydrogenated.

The progress of this reaction shows the typical course of the selective hydrogenation of phenylacetylene, in which styrene is the main product, ethylbenzene is formed in small amounts during the reaction and the fully hydrogenated product ethylcyclohexane is not obtained.[18]

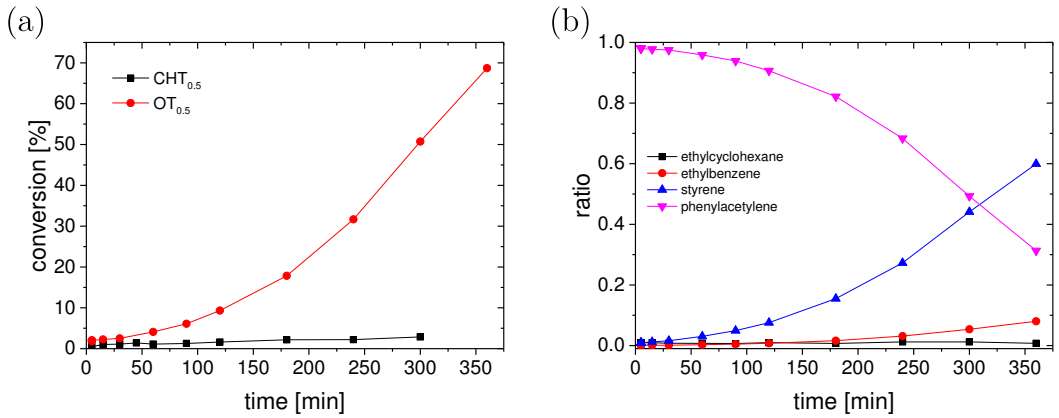

Figure 3.39: (a) Comparison of the reaction rate of $CHT_{0.5}$- and $OT_{0.5}$-stabilized platinum nanoparticles and (b) course of the reaction of $OT_{0.5}$-stabilized platinum nanoparticles in the phenylacetylene hydrogenation.

In conclusion, this experiment confirms the influencing effect of the ligands substituents on the hydrogenation of phenylacetylene. In contrast to the hydrogenation of 3-hexyne, this catalytic reaction is sensitive to a steric demand of the stabilizing ligands. Furthermore, these results point out the difficulty of the selective hydrogenation of a substrate, which lacks the presence of functional groups, because these groups could steer the reaction into a specific direction by the interaction with ligand moieties.

Conclusion

The application of thiol-functionalized platinum nanoparticles in catalysis obtained information about the influence of the ligand shell on the stability, activity, selectivity and substrate sensitivity of the reaction (figure 3.40).

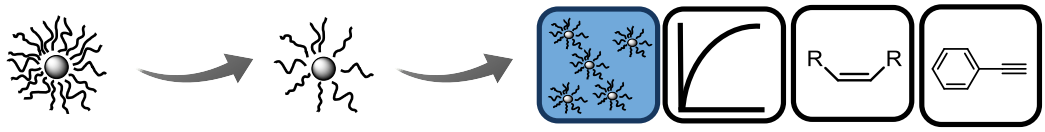

Figure 3.40: Schematic of the influence of altering the ligand coverage at platinum nanoparticles on the nanoparticle stability, activity, selectivity and the substrate sensitivity of the selective hydrogenation of alkynes to alkenes.

The tuning experiments of platinum nanoparticles for catalytic applications demonstrate the ability to control the ligand coverage degree of thiol-stabilized platinum nanoparticles by altering the ligand concentration during the functionalization process or by varying the ligand properties. Furthermore, the influence of the coverage degree and the ligand characteristics on the catalytic reactivity are analyzed. The CHT-ligand supplies platinum nanoparticles with the lowest ligand density, which can only be varied in a small regime by the ligand concentration applied during functionalization. This property is attributed to the bulkiness of the cyclohexyl group in connection with the rigidity of the ligand. Furthermore, it is found that unsaturated ligands tend to hinder the hydrogenation of 3-hexyne at the surface of the platinum nanoparticle, since they may act as a competitive substrate and the unsaturated group is hydrogenated. Another effect of this unwanted hydrogenation is that the ligands phenyl groups may become more bulky.

The hydrogenation of phenylacetylene exhibits another ligand effect of the substituents. For a bulky and rigid ligand, the hydrogenation is very slow, while for a more flexible ligand the hydrogenation is significantly more active. Surprisingly, the selectivity of the hydrogenation of alkynes to the respective alkenes is not influenced by any change in the ligand shell of the nanoparticles.

The highest TOF for the 3-hexyne hydrogenation of 3996 h^{-1} is achieved by $CHT_{0.5}$-protected platinum nanoparticles with 91 % selectivity. During all hydrogenation reactions the stability of the nanoparticles is maintained, which makes thiols ligands potential candidates for well-defined nanocatalysts in hydrogenation catalysis.

3.3.2 Excursus: Al_2O_3-immobilized ligand-stabilized platinum nanoparticles

Despite the use of platinum nanoparticles in catalysis as colloids, they may as well tested be as heterogeneous catalysts immobilized on a support (figure 3.41). The advantage of heterogeneous catalysis is the easy separation of the catalyst from the products and is for that reason often used in industry.[149] This approach is carried out in a cooperation project (in particular with Imke Schrader), in which platinum nanoparticles functionalized with hydrophilic ligands are immobilized onto Al_2O_3 and applied in the selective hydrogenation of 3-hexyne to 3-hexene as a model reaction.

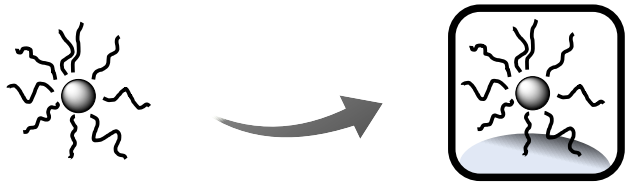

Figure 3.41: Schematic of the immobilization of ligand protected platinum nanoparticles onto a support for application in catalysis.

An advantage of applying supported hydrophilic ligand-stabilized nanoparticles in organic solvents is the exclusion of any redispersion of the nanoparticles from the support into the solvent. This way, leaching of the catalyst is not a problem.[107] Earlier studies on immobilized platinum nanoparticles stabilized by chiral hydrophilic ligands revealed a high chemoselectivity and activity in the selective hydrogenation of acetophenone to phenylethanol.[126] Indeed, an enhanced reaction rate towards the selective product has been found for proline-functionalized nanoparticles in comparison to the "unprotected" platinum nanoparticles, for which the side products methylcyclohexylketone and cyclohexylethanol have also been obtained. In the present work the influence of ligands of a similarly prepared catalyst on the selective hydrogenation of 3-hexyne to 3-hexene is elucidated.
The "unprotected" platinum nanoparticles obtained by the polyol method described before are transferred into the organic solvent cyclohexanone prior to functionalization. To the resulting colloid, a ligand containing aqueous solution is added and stirred vigorously. A phase transfer of the platinum nanoparticles into the aqueous phase indicates the successful stabilization of the nanoparticles by the

ligands. To a solution of these hydrophilic nanoparticles Al_2O_3 is added and the solvent evaporated to obtain the heterogeneous catalyst.
A prerequisite for former studies with these catalyst is the exclusion of diffusion limits of the heterogeneous catalytic system. This can be achieved by the determination of real reaction rates by adjusting the reaction conditions so that the conversion was kept close to 10 %.[126,150] Under these conditions the stirring rate as well as a pestling of the catalyst should not influence the conversion. These requirements are tested for the proline-functionalized catalyst, as listed in table 3.6. The reaction conditions of the catalysis are the use of 20 mg catalyst (0.2 wt% platinum), 5 mmol 3-hexyne (3-hexyne/platinum ≈ 2439), 5 mL THF, 3 bar hydrogen at room temperature.

Table 3.6: Summary of the testing of diffusion limitations applying Al_2O_3 immobilized ligand-functionalized platinum nanoparticles in the hydrogenation of 3-hexyne to 3-hexene[a].

entry no.	rotational speed rpm	t min	conv. %	sel. %
1	500	30	15	92
2	250	30	14	92
3	1000	30	16	92
4	250	300	99	93

[a]20 mg proline-functionalized platinum nanoparticles immobilized onto Al_2O_3 (0.2 wt% platinum), 5 mmol 3-hexyne (3-hexyne/platinum ≈ 2439), 5 mL THF, 3 bar hydrogen at room temperature.

L-Proline-functionalization enhances the selectivity and activity of the catalyst for the selective hydrogenation of acetophenone to phenylethanol in comparison to the "unprotected" catalyst (L-proline structure shown in figure 3.44). The same comparison for the hydrogenation of 3-hexyne is carried out resulting in the same selectivity of 92 – 93 % for both catalysts. The comparison of the reaction rate is illustrated in figure 3.42a.

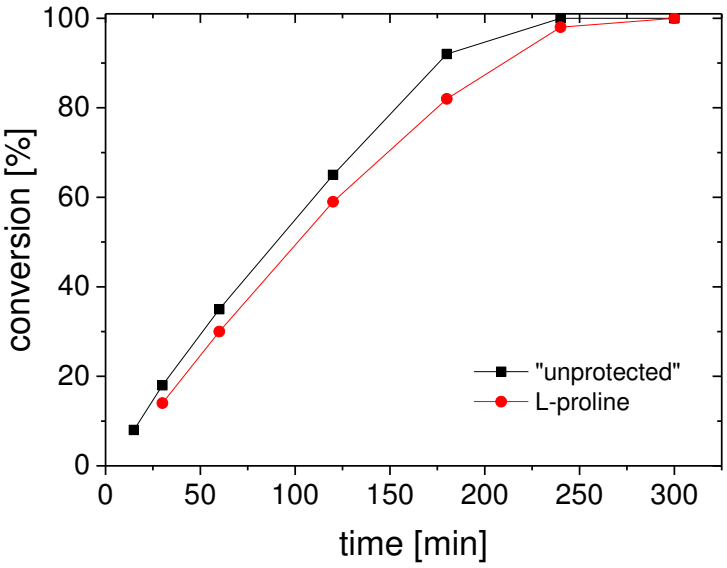

Figure 3.42: Conversion vs. time graphs of the hydrogenation of 3-hexyne to 3-hexene for L-proline-functionalized and "unprotected" platinum nanoparticles immobilized onto Al_2O_3 (0.2 wt% platinum); conditions: 20 mg catalyst, 5 mmol 3-hexyne (3-hexyne/platinum ≈ 2439), 5 mL THF, 3 bar hydrogen and room temperature.

This comparison reveals a similar conversion during the reaction for both catalysts. An influence by the addition of L-proline on this reaction is, thus, not evidenced. Furthermore, table 3.7 reveals the insensitivity of the "unprotected" catalyst for different solvents. In all cases of conversions under 99 % the selectivity is constant at 93 %. Above 99 % overreduction of the alkene takes place reducing the selectivity.

Table 3.7: Summary of the testing of diffusion limitations applying Al_2O_3 immobilized ligand-functionalized platinum nanoparticles in the hydrogenation of 3-hexyne to 3-hexene[a].

entry no.	solvent	t min	conv. %	sel. %
1	THF	30	18	93
2	THF	300	100	76
3	toluene	30	13	93
4	toluene	300	85	93
5	cyclohexane	30	16	93
6	cyclohexane	300	99	87

[a]20 mg proline-functionalized platinum nanoparticles immobilized onto Al_2O_3 (0.2 wt% platinum), 5 mmol 3-hexyne (3-hexyne/platinum ≈ 2439), 5 mL THF, 3 bar hydrogen, 250 rpm at room temperature.

For the analysis of the influence of the solvent, L-(+)-a-phenylglycine, a ligand exhibiting a phenyl group (structure shown in figure 3.44B), is applied during functionalization of the platinum nanoparticles. However, this functionality shows a significant influence on neither the selectivity (92 – 93 %), nor the activity when the hydrogenation is carried out in THF, toluene or cyclohexane, respectively (figure 3.43). Only the reaction in cyclohexane proceeds slightly faster.

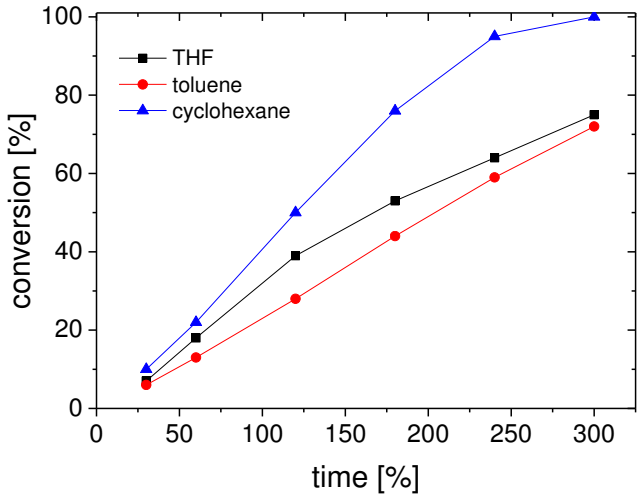

Figure 3.43: Conversion vs. time graphs of the hydrogenation of 3-hexyne to 3-hexene for L-(+)-a-phenylglycine-functionalized platinum nanoparticles immobilized onto Al_2O_3 (0.2 wt% platinum) in different solvents; conditions: 20 mg catalyst, 5 mmol 3-hexyne (3-hexyne/platinum ≈ 2439), 5 mL solvent, 3 bar hydrogen and room temperature.

In another experiment, different ligands are applied for the functionalization of platinum nanoparticles and tested during the hydrogenation of 3-hexyne. Figure 3.44 shows the structures of the applied ligands L-proline, L-alanine, L-(+)-a-phenylglycine, (R)-3-pyrrolidinol, L-serine, L-threonine, L-4-thiazolidinecarboxylic acid and L-cysteine.

The results of these catalytic experiments are illustrated in figure 3.45 for conversions after 30 min and 300 min. A peculiar decrease in activity of sulfur containing ligands is obtained in comparison to ligands with only amine and carboxylic acid groups. This observation indicates an interpretation similar to thiol ligands attached to colloidal platinum nanoparticles. It can be assumed that the strong covalent binding mode of sulfur to platinum nanoparticles passivates the metal surface by blocking both, the substrate sterically with the substituents at the sulfur head group and the active sites

at the particles with their covalent bond. A reduction of the coverage degree of the sulfur containing ligands may lead to an enhanced activity of these catalysts.

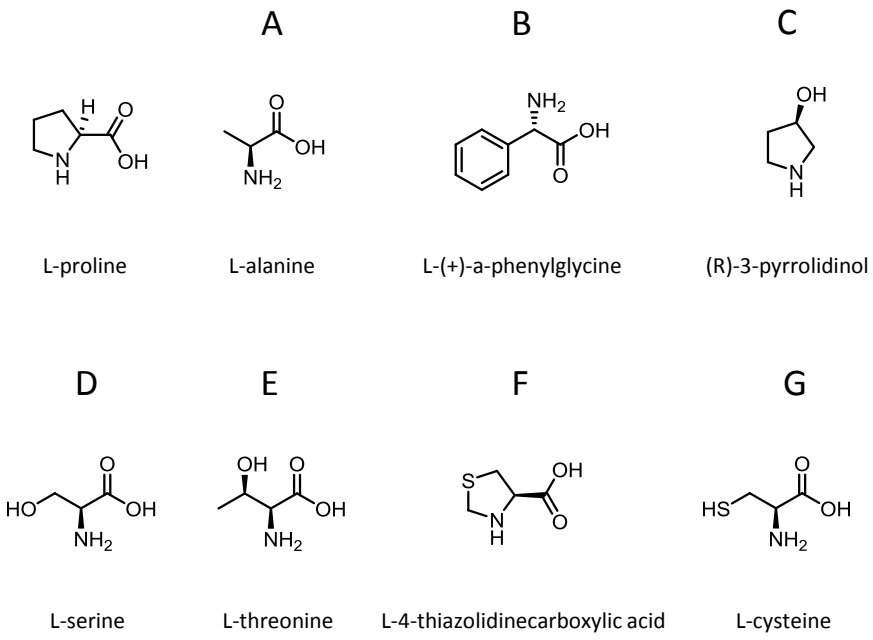

Figure 3.44: Structures of the hydrophilic ligands applied for the functionalization of platinum nanoparticles.

However, as the stability of the particles is supposed to be high as ligand leaching is avoided in this system, the use of thiols as ligands is not as advantageous as for purely colloidal systems. Furthermore, the selectivity of all hydrogenation reactions compared in figure 3.45 is similar at 92 – 93 %. This result is in agreement with the previously described ones, which address the influence of different ligands on the selectivity for the colloidal catalytic system (chapter 3.3.1). The ligands seem to only influence the stability, solubility and the activity of the platinum nanoparticles, but not the selectivity. However, the selectivity for the supported nanoparticles slightly exceeds the selectivities found for the colloidal systems (84 – 91 % selectivity). An interpretation for this result may be an influence of the support material on the catalytic properties of the platinum nanoparticles.

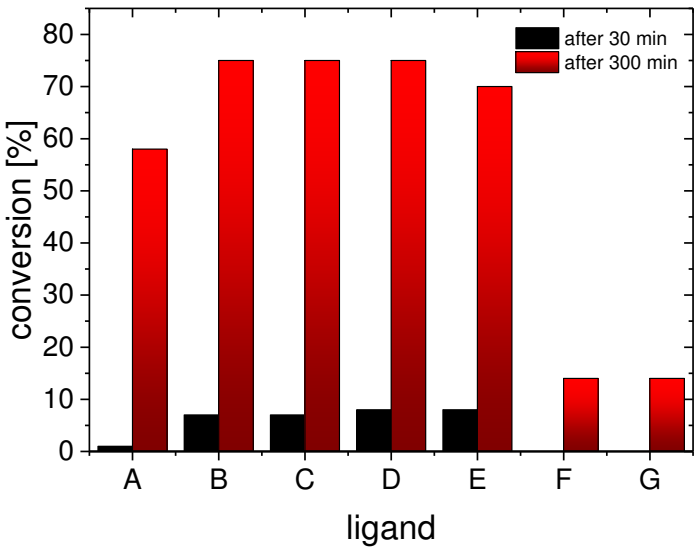

Figure 3.45: Comparison of the conversions during the hydrogenation of 3-hexyne to 3-hexene for (A) L-alanine (B) L-(+)-a-phenylglycine (C) (R)-3-pyrrolidinol (D) L-serine (E) L-threonine (F) L-4-thiazolidinecarboxylic acid and (G) L-cysteine–stabilized platinum nanoparticles immobilized onto Al_2O_3 (0.2 wt% platinum) after 30 min and 300 min reaction time; conditions: 20 mg catalyst, 5 mmol 3-hexyne (3-hexyne/platinum ≈ 2439), 5 mL THF, 500 rpm, 3 bar hydrogen and room temperature.

In conclusion, the immobilization of the ligand-protected platinum nanoparticles reveals a high potential of the catalysts for being successfully applied in the selective hydrogenation of 3-hexyne to 3-hexene. In contrast to the hydrogenation of acetophenone to phenylethanol, the selectivity of the selective hydrogenation of 3-hexyne is not influenced by the choice of the ligand. For all samples selectivities of 92 – 93 % are achieved. The reaction is furthermore largely independent from the choice of the solvent. Only the application of sulfur-containing ligands result in a decrease of the reaction rate, which is in total agreement with the findings of similar ligands in colloidal hydrogenation systems. Additionally, this work shows, that the immobilized nanoparticle systems are applicable catalytic reactions other than the ones already described in literature.[126]

Chapter 4

Summary and outlook

In this work the binding modes of different ligands to metal nanoparticles and the application of ligand-protected platinum nanoparticles are elucidated. In order to be able to study the nanoparticles systematically, they are obtained by a standardized synthesis. In a subsequent step, functionalization of the different nanoparticle samples leads to ligand-protected nanoparticles with altered ligand shells and equal metal cores.

The elucidation of the binding modes of ligands to platinum nanoparticles reveals a strong binding of thiols, which seems to be of covalent character. In contrast, amines are found to bind in different modes to the particles. In acidic environment, amines are protonated to the corresponding ammonium species, which stabilize the nanoparticles through electrostatic interaction. Water or OH^- species are found to act as counterions for the ammonium ligands. In non-acidic environment amine ligands provide evidence for a binding mechanism of the nitrogen atom via hydrogen atoms to the particle. A direct bond between the nitrogen atom and the platinum nanoparticle surface is excluded based on the particle properties during functionalization. Phosphine ligands exhibit results, which are interpreted that both binding mechanisms are enabled at the same time, a hydrogen coordinated interaction and a direct bond to the particle. In acidic condition a similar binding mode is concluded as the amines, including protonated phosphine species as stabilizing agents. For gold and ruthenium nanoparticles first evidences hint to the occurrence of similar binding modes to the metal surface as proposed for platinum nanoparticles.

The binding modes of amines, phosphines and thiols to platinum nanoparticles are reflected by their stability during catalysis. In the selective hydrogenation of 3-hexyne to 3-hexene amine- and phosphine-stabilized particles precipitate, while thiol-protected particles remain stable in solution. However, the activity of thiol-protected platinum nanoparticles are strongly reduced in comparison with amine- and phosphine-

protected particles. For the highly stable thiol-protected nanoparticle samples the activity is tuned by reducing the ligand coverage. This is accomplished by either reducing the ligand concentration during the functionalization process or by the choice of thiol ligands with higher steric demands. Nanoparticles with a low ligand coverage reveal a high activity (TOFs up to 3996 h^{-1}), while the selectivity is maintained for all reactions at 84 – 91 %. Thiol ligands with bulky substituents, thus, give higher reaction rates under similar reaction conditions as the thiol ligand with an alkyl chain. Furthermore, all thiol-stabilized nanoparticle samples, including the ones comprising low ligand coverages, remain stable during the reaction. Even recycling is possible, which is tested for 8 runs, and constant conversion, selectivity and stability is obtained. In contrast, for the hydrogenation of a substrate comprising a bulky substituent a different behavior is observed. The selective hydrogenation of phenylacetylene to styrene obtains higher reaction rates for the OT-stabilized nanoparticles with a flexible, non-bulky alkyl chain, while the platinum nanoparticles stabilized by rigid CHT-ligands only give 3 % conversion even after 5 h reaction time. While the choice of the ligand does not seem to have an influence on the selectivity of the hydrogenation of 3-hexyne to 3-hexene, the Al_2O_3 support of ligand-functionalized platinum nanoparticles is assumed to affect this catalytic property of the catalyst.

In conclusion, a throughout characterization of ligand-stabilized platinum nanoparticles reveals the influence of both, the ligand binding modes and the structure of the ligand, on catalysis.

The results of this work supply potential directions for future research on this topic. For example, for platinum nanoparticles the proposal of the new binding mode for amine ligands leads to a new understanding of mechanisms taking place at metal nanoparticle surfaces. This knowledge can be considered for the rational design of catalysts for hydrogenation reactions. Furthermore, in this study only the influence of hydrogen was studied concerning the binding of amine ligands. Other small molecules, which interact with platinum surfaces and their impact on amine binding could be analyzed as well. In this work, first evidences were given regarding similar binding modes of amines to ruthenium nanoparticles compared to the binding of amines to platinum nanoparticles. Thus, a throughout investigation of ruthenium nanoparticles obtained from the polyol synthesis under inert atmosphere, may also reveal the binding mode of ligands or the behavior in selective hydrogenation reactions. Additionally, the obtained results of the immobilized nanoparticles applied in catalysis suggest an influence of the support material on the selectivity of the platinum nanoparticles in hydrogenation catalysis. The elucidation of this effect in detail is assumed to be helpful for tailoring new heterogeneous catalysts for the application in selective hydrogenation reactions.

Chapter 5

Experimental section

5.1 General remarks

$H_2PtCl_6 \cdot 6\ H_2O$ was purchased from Sigma Aldrich and used without further purification. For all reactions in hydrogen atmosphere, hydrogen 6.0 from Westfalen AG was used. All ligands were purchased from VWR International as "per analysis" grade or synthesized with a quality check by ^{1}H NMR. The phosphine was stored under an argon atmosphere. All ligands were used as received. All solvents were distilled prior to being used. Infrared absorption spectra were recorded using a Thermo Scientific Nicolet 380 FTIR spectroscope with a resolution of 4 cm^{-1} and 32 scans per measurement. The colloids and ligands were measured in transmission in a KBr liquid cell with CCl_4 as solvent. ^{1}H NMR spectra were recorded on a Bruker AVANCE III 400 instrument. For variable temperature NMR experiments, a Bruker DRX 400 was used. The ^{31}P magic-angle-spinning (MAS) NMR solid state spectrum were recorded on a Bruker Avance 300. Chemical shifts are reported in ppm relative to the signal of tetramethylsilane using the residual signals of $CDCl_3$ at 7.62 ppm and 1.73 ppm for *d*-THF for the ^{1}H NMR spectra, respectively. The resonance signal of solid ammonium dihydrogen phosphate was used as an external standard for all ^{31}P MAS NMR spectra at 1.1 ppm with respect to phosphoric acid. For thermogravimetric analysis all samples (about 8 mg) were measured under argon atmosphere in a TG/DAT Q5000 IR device (TA Instruments, Inc.). A heat rate of 10 °C/min was applied to the samples up to a maximum of 1200 °C. For TEM meaurements a JEM 2012 transmission electron microscope (JEOL) was employed to record the images of the platinum nanoparticles with an acceleration voltage of 120 kV. A drop of the colloid sample was applied to a carbon-coated copper grid and allowed to dry in air.

Nanoparticle sizes were determined from the diameter of 200 or 300 random particles by constructing a size-dependent histogram. GC Analysis of all samples were conducted at a Hewlett-Packard – HP 6890 Series GC System (Agilent Technologies Inc.) with an Astec® CHIRALDEX G-TA column and FID. The temperature gradient was started at 40 °C, which was held for 8 min. Then, heating of 20 °C/min up to 200 °C was applied followed by a hold at this temperature for 6 min. A cooling phase of 40 °C/min down to 150 °C finished the measurement. The XPS measurements have been performed at a UHV setup with a Leybold Heraeus LHS-IO XPS spectrometer. The X-ray tube was operated at an emission of 20 mA, at 12 kV to supply the Mg Kα radiation (1253.6 eV). The electron energy analyzer was used at a retarding factor B = 10 and E = constant. A voltage of 3.6 kV has constantly been applied to the detector. The measurements were recorded at a take-off angle of approximately 60°. Samples were deposited by casting a drop of the particle solution on a Si(111) wafer. UV/VIS measurements were carried out using a JASCO V-500 (JASCO Corp.). STM measurements were performed in a self-built Besocke beetle type STM. The scanning tips were prepared by mechanically cutting a Pt/Ir wire (80:20, Goodfellow, UK). All images were taken in constant current mode.

5.2 Synthesis of ligands

Synthesis of DPMT

In a 250 mL three-neck-flask equipped with a dropping funnel and reflux condenser 2.35 g thiourea (31 mmol, 1 eq.) was dissolved in 23 mL water. The reaction mixture was heated to 50 °C and 7.67 g bromodiphenylmethane (31 mmol, 1 eq.) was added. Then, the reaction mixture was heated for 5 minutes under reflux which resulted in the discoloration of the solution. Then, the solution was cooled to room temperature and 31 mL of a 2.5 M-sodium hydroxide solution was added dropwise with a dropping funnel. After that, the reaction mixture was heated again under reflux for 30 minutes. In the next step, the solution was cooled to room temperature and acidified with 7 mL concentrated hydrochloric acid. The solution was extracted three times with 20 mL diethyl ether. The organic phase was washed three times with 20 mL water, dried over magnesium sulfate and dried under reduced pressure to obtain 4.39 g of diphenylmethanethiol (21.9 mmol, 71 %).

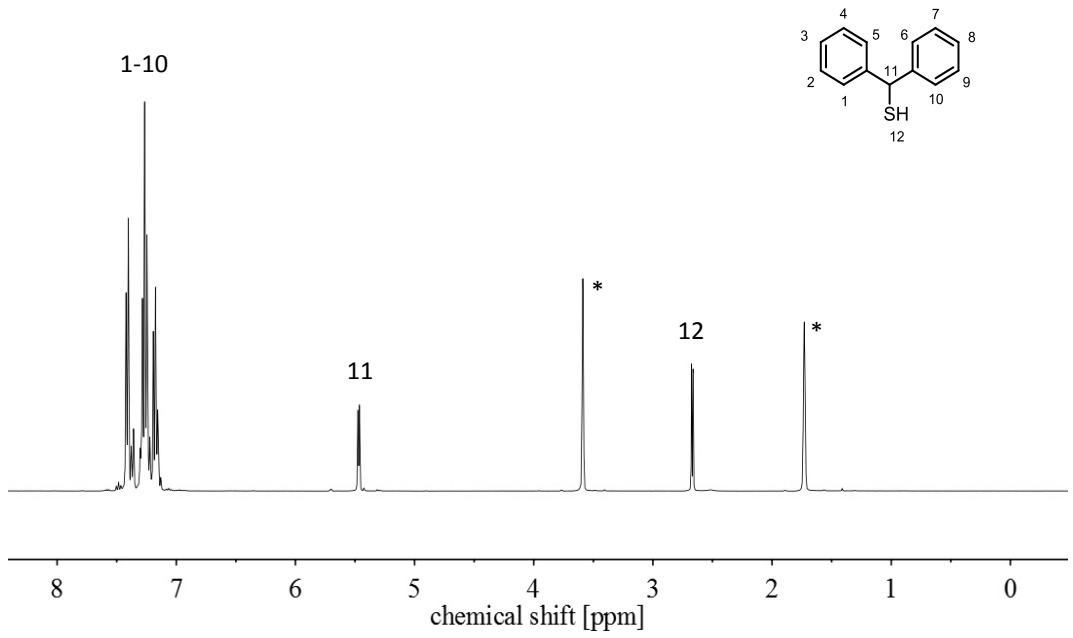

Figure 5.1: ^{1}H NMR of DPMT in d-THF (denotes solvent peaks).*

5.3 Synthesis and functionalization of nanoparticles

5.3.1 Platinum nanoparticles

Synthesis of "unprotected" platinum nanoparticles

The synthesis of "unprotected" platinum nanoparticles was carried out in analogy to the method of Wang et al.[46] In the standard experiment 0.25 g $H_2PtCl_6 \cdot 6\ H_2O$ (0.48 mmol) was placed under argon in a 250 mL-Schlenk flask and 25 mL ethylene glycol was added. A solution of sodium hydroxide in ethylene glycol (25 mL, 1.0 mol/L) was added and stirred vigorously to obtain a homogeneous mixture. The solution was heated to reflux at 150 °C for 1.5 h (500 rpm). The clear yellow solution turned black after 5 min. The colloidal solution of platinum nanoparticles was cooled down to room temperature and used as is.

Functionalization of "unprotected" platinum nanoparticles

To the obtained platinum nanoparticle/ethylene glycol solution a solution of 12 mmol of the respective ligand in 50 mL toluene was added. This solution was stirred vigorously so that the two phases are mixed properly until complete phase transfer of the nanoparticles was observed. Thereafter, the phases were allowed to separate in a separation funnel. The black-colored toluene phase containing the platinum colloids was washed three times with 20 mL water. Then, the toluene solution was concentrated to about 3 mL and 50 mL ethanol was added in order to precipitate the nanoparticles. The particles were separated via centrifugation, washed three times with 10 mL of an ethanol/water mixture (2:1), dried under reduced pressure and obtained as a black powder. The applied conditions during the functionalization process for all ligands are summarized in table 5.1 for the elucidation of the binding modes and in table 5.2 for the application in catalysis.

Table 5.1: Summary of the applied ligands and reaction conditions during the functionalization process of "unprotected" platinum nanoparticles for the elucidation of the binding modes.

ligand	n (ligand) mmol	ligand/Pt	V (ligand) mL	reaction condition	solvent	V (solvent) mL
OT	12	25	2.1	basic	toluene	50
OA	12	25	2.0	basic	toluene	50
DOA	12	25	3.6	basic	toluene	50
DOA	12	25	3.6	acidic	toluene	50
TOA	12	25	5.2	basic	toluene	50
TOA	12	25	5.2	acidic	toluene	50
TOA	12	25	5.2	basic/H_2-activation	toluene	50
TOP	12	25	5.4	basic	toluene	50
TOP	12	25	5.4	acidic	toluene	50
TOP	12	25	5.4	basic/H_2-activation	toluene	50

Table 5.2: Summary of the applied ligands and reaction conditions during the functionalization process of "unprotected" platinum nanoparticles for the application in the hydrogenation of 3-hexyne.

ligand	n (ligand) mmol	ligand/Pt	V (ligand) mL	reaction condition	solvent	V (solvent) mL
OT	0.024	0.05	0.042	basic	toluene	50
OT	0.24	0.5	0.416	basic	toluene	50
OT	0.48	1	0.083	basic	toluene	50
OT	2.4	5	0.42	basic	toluene	50
OT	12	25	2.1	basic	toluene	50
CHT	0.24	0.5	0.029	basic	toluene	50
CHT	2.4	5	0.294	basic	toluene	50
CHT	12	25	1.47	basic	toluene	50
DPMT	2.4	5	0.44	basic	toluene	50
DPMT	12	25	2.2	basic	toluene	50
PET	2.4	5	0.321	basic	toluene	50

5.3.2 Gold nanoparticles

Synthesis of gold nanoparticles

The synthesis of citrate-stabilized gold nanoparticles was carried out in analogy to the method of Turkevich et al.[128] In the standard experiment $HAuCl_4 \cdot 3\ H_2O$ (0.0833 mmol) was placed in a 2 L-flask and 1 L water was added. 25.9 mg sodium citrate dihydrate (0.0833 mmol) was added and the solution was stirred until the solid was completely dissolved. Then, 30 mL of a sodium borohydride solution (0.1 mol/L) was added and stirring was continued for 30 seconds (500 rpm). During the reaction the color of the solution changed from colorless to violet.

Functionalization of gold nanoparticles

To the obtained gold nanoparticle/water solution a solution of ligand dissolved in 150 ml toluene was added. For functionalization under acidic condition this solution was further stirred vigorously overnight. For a phase transfer reaction under basic condition 30 mL of a sodium hydroxide solution (1.0 mol/L) was added prior to the overnight stirring. Then, the phases were allowed to separate and the toluene phase was washed three times with 70 mL water. Then, the toluene solution was concentrated to about 3 mL and 50 mL ethanol was added in order to precipitate the nanoparticles. The particles were separated via centrifugation, washed three times with 10 mL ethanol, dried under reduced pressure and obtained as a black powder. The applied conditions during the functionalization process are summarized in table 5.3.

Table 5.3: Summary of the applied ligands and reaction conditions during the functionalization process of citrate-functionalized gold nanoparticles.

ligand	n (ligand) mmol	ligand/ Pt	V (ligand) mL	reaction condition	solvent	V (solvent) mL
OT	0.833 + 20[a]	10 + 240	0.145 + 3.5	basic	toluene	150
OT	0.833	10	0.145	acidic	toluene	150
OA	0.833 + 20[a]	10 + 240	0.138 + 3.3	basic	toluene	150
OA	0.833	10	0.138	acidic	toluene	150
DOA	0.833 + 20[a]	10 + 240	0.252 + 6.0	basic	toluene	150
DOA	0.833	10	0.252	acidic	toluene	150
TOA	0.833 + 20[a]	10 + 240	0.364 + 8.2	basic	toluene	150
TOA	0.833	10	0.364	acidic	toluene	150
TOA	0.833	10	0.364	acidic	hexane	150
TOA	0.833	10	0.364	acidic	ethanol	150

[a] After stirring for 3 h during the functionalization process and no phase transfer was visible, additionally ligand was added.

5.3.3 Ruthenium nanoparticles

Synthesis of ruthenium nanoparticles

The synthesis of "unprotected" ruthenium nanoparticles was carried out in analogy to the method of Wang et al.[46] In the standard experiment 0.0996 g $RuCl_3$ (0.48 mmol) was placed under argon in a 250 mL-Schlenk flask and 25 mL ethylene glycol was added. A solution of sodium hydroxide in ethylene glycol (25 mL, 1.0 mol/L) was added and stirred vigorously to obtain a homogeneous mixture. The solution was heated to reflux at 150 °C for 1.5 h (500 rpm). The colloidal solution of ruthenium nanoparticles was cooled down to room temperature and used as is.

Functionalization of ruthenium nanoparticles

To the obtained ruthenium nanoparticle/ethylene glycol solution a solution of 12 mmol of the respective ligand in 50 mL toluene was added and stirred vigorously so that the two phases are mixed properly overnight. Thereafter, the phases were allowed to separate in a separation funnel. The black-colored toluene phase containing the platinum colloids was washed three times with 20 mL water. Then, the toluene

solution was concentrated to about 3 mL and 50 mL ethanol was added in order to precipitate the nanoparticles. The particles were separated via centrifugation, washed three times with 10 mL ethanol, dried under reduced pressure and obtained as a black powder. The applied conditions during the functionalization process for all ligands are summarized in table 5.4.

Table 5.4: Summary of the applied ligands and reaction conditions during the functionalization process of "unprotected" ruthenium nanoparticles.

ligand	n (ligand) mmol	ligand/Pt	V (ligand) mL	reaction condition	solvent	V (solvent) mL
OT	12	25	2.1	basic	toluene	50
OA	12	25	2.0	basic	toluene	50
DOA	12	25	3.6	basic	toluene	50
TOA	12	25	5.2	basic	toluene	50
TOA	12	25	5.2	acidic	toluene	50
TOA	12	25	5.2	basic/H_2-activation	toluene	50

5.4 Functionalization and immobilization of platinum nanoparticles

Functionalization of platinum nanoparticles with water-soluble ligands

Syntheses of "unprotected" platinum nanoparticles was carried out as described in chapter 5.3.1. After cooling down to ambient temperature, the platinum nanoparticles were precipitated by adding 50 mL HCl (1 mol/L) and separated from the solvent by centrifugation. The particles were washed once with 10 mL HCl (1 mol/L) and then redissolved in 100 mL cyclohexanone. To this solution, four aliquots of an aqueous ligand solution containing 8.3 mmol/L of the respective ligand and 12.5 mmol/L NaOH, were added. The resulting emulsion was vigorously stirred for 30 min. During this time, the nanoparticles undergo a phase transfer into the ligand containing aqueous phase indicated by a color change of both phases. The nanoparticles were then separated from the cyclohexanone phase using a separation funnel. Then, the aqueous nanoparticle solution was concentrated in a rotary evaporator until the volume was reduced to about 1-2 mL. Upon the addition of an excess of acetone, the nanoparticles readily precipitated. The particles are centrifuged, the supernatant solvent removed and washed twice with 10 mL ethanol and once with 10 mL acetone. Table 5.5 gives a summary of the ligands applied during the functionalization process.

Table 5.5: Water-soluble ligands applied during the functionalization of platinum nanoparticles.

entry no	ligand
1	L-proline
2	(R)-3-pyrrolidinol
3	L-serine
4	L-thiazolidine-4-carboxylic acid
5	L-threonine
6	L-alpha-phenylglycine
7	cysteine

Immobilization of platinum nanoparticles on Al_2O_3

1/10 of the "unprotected" or water-soluble ligand-protected nanoparticles synthesized as described above were dissolved in 10 mL acetone. To this solution 5.22 g Al_2O_3 (PURALOX SCCa 150/200; Sasol) was added to obtain a metal loading of about 0.2 wt%. The resulting dispersion was stirred vigorously for 30 min. Then, the solvent was removed using a rotary evaporator. The ligand-functionalized supported nanoparticles were washed with ethanol twice and the "unprotected" nanoparticles were washed with acetone twice. The resulting solid was then dried under reduced pressure and kept in an desiccator until it was applied in the catalytic experiments.

5.5 Hydrogenation reactions

5.5.1 Hydrogenation of 3-hexyne

Thiol-, phosphine- and amine-capped platinum nanoparticles

In a standard procedure 4.6 µmol of the stabilized platinum nanoparticle sample was introduced into a Fischer-Porter bottle. The bottle was evacuated and purged with 1 bar hydrogen three times. Then, 5 mL THF was added via syringe. The mixture was stirred at room temperature and the hydrogen pressure was set to 1.5 bar. The reaction started immediately on the addition of 0.57 mL 3-hexyne (5 mmol, hexyne/Pt = 1093). Samples (0.1 mL) for GC analysis were taken via syringe in constant time intervals.

Platinum nanoparticles capped with different thiols

In a standard procedure 1 mg of the stabilized platinum nanoparticle sample was introduced into a Fischer-Porter bottle. The bottle was evacuated and purged with 1 bar hydrogen three times. Then, 5 mL THF was added via syringe. The mixture was stirred at room temperature and the hydrogen pressure was set to 1.5 bar. The reaction started immediately on the addition of 0.57 mL 3-hexyne (5 mmol). Samples (0.1 mL) for GC analysis were taken via syringe in constant time intervals.

Recycling of $CHT_{0.5}$-stabilized platinum nanoparticles

In the recycling experiment 1 mg of the $CHT_{0.5}$-stabilized platinum nanoparticles was introduced into a Fischer-Porter bottle. The bottle was evacuated and purged with 1 bar hydrogen three times. Then, 5 mL THF was added via syringe. The mixture was stirred at room temperature and the hydrogen pressure was set to 1.5 bar. The reaction started immediately on the addition of 0.57 mL 3-hexyne. After the first run

the particles were isolated by removing all reactants except for the particles from the flask under reduced pressure ($< 10^{-2}$ mbar). The bare nanoparticles were dispersed in THF again and readily used for the next recycling run. Samples (0.1 mL) for GC analysis were taken via syringe after 1 h each run.

Thiol- and amine-capped ruthenium nanoparticles

In a standard procedure 1.5 mg of the stabilized platinum nanoparticle sample was introduced into a Fischer-Porter bottle. The bottle was evacuated and purged with 1 bar hydrogen three times. Then, 5 mL THF was added via syringe. The mixture was stirred at room temperature and the hydrogen pressure was set to 1.5 bar. The reaction started immediately on the addition of 0.57 mL 3-hexyne (5 mmol). Samples (0.1 mL) for GC analysis were taken via syringe in constant time intervals.

Al_2O_3 immobilized platinum nanoparticles

In a standard procedure 20 mg of the Al_2O_3-supported platinum nanoparticle sample (ca. 0.2 wt%) was introduced into a Fischer-Porter bottle and 5 mL of an organic solvent and 0.57 mL 3-hexyne (5 mmol) was added. The bottle was evacuated and purged with 1 bar hydrogen three times followed by the final adjustment of the pressure to the reaction pressure. The reaction was carried out at room temperature and started upon the start of the magnetic stirrer. For the analysis of the products, aliquots (0.1 mL) for GC measurements were taken after constant time intervals.

5.5.2 Hydrogenation of phenylacetylene

In a standard procedure 1 mg of the stabilized platinum nanoparticle sample ($CHT_{0.5}$ or $OT_{0.5}$) was introduced into a Fischer-Porter bottle. The bottle was evacuated and purged with 1 bar hydrogen three times. Then, 5 mL THF was added via syringe. The mixture was stirred at room temperature and the hydrogen pressure was set to 1.5 bar. The reaction started immediately upon the addition of 0.55 mL phenylacetylene (5 mmol). Samples (0.1 mL) for GC analysis were taken via syringe in constant time intervals.

Chapter 6

References

(1) Rao, C. N. R.; Kulkarni, G. U.; Thomas, P. J.; Edwards, P. P. Size-dependent chemistry. *Chem. Eur. J.* **2002,** *8,* 28.

(2) Vajtai, R. *Springer handbook of nanomaterials;* Springer: Berlin, 2013.

(3) Singh, A. K. *Engineered nanoparticles: Structure, properties and mechanisms of toxicity;* Elsevier: Amsterdam, 2015.

(4) Long, Y.-T.; Jing, C. *Localized surface plasmon resonance based nanobiosensors;* Springer: Heidelberg, New York, 2014.

(5) Kerker, M. *The scattering of light and other electromagnetic radiation;* Academic Press: New York, N.Y., London, England, 1969.

(6) Kreibig, U.; Vollmer, M. *Optical properties of metal clusters;* Springer: Berlin, New York, 1995.

(7) Tyo, E. C.; Vajda, S. Catalysis by clusters with precise numbers of atoms. *Nat. Nanotechnol.* **2015,** *10,* 577.

(8) Habibpour, V.; Wang, Z. W.; Palmer, R. E.; Heiz, U. Size-selected metal clusters. *J. Applied Sci.* **2011,** *11,* 1164.

(9) Heiz, U.; Sanchez, A.; Abbet, S.; Schneider, W.-D. Catalytic oxidation of carbon monoxide on monodispersed platinum clusters. *J. Am. Chem. Soc.* **1999,** *121,* 3214.

(10) Crampton, A. S.; Rötzer, M. D.; Ridge, C. J.; Schweinberger, F. F.; Heiz, U.; Yoon, B.; Landman, U. Structure sensitivity in the nonscalable regime explored via catalysed ethylene hydrogenation on supported platinum nanoclusters. *Nat. Commun.* **2016,** *7,* 10389.

(11) Crespo-Quesada, M.; Cárdenas-Lizana, F.; Dessimoz, A.-L.; Kiwi-Minsker, L. Modern trends in catalyst and process design for alkyne hydrogenations. *ACS Catal.* **2012,** *2,* 1773.

(12) Jia, C.-J.; Schüth, F. Colloidal metal nanoparticles as a component of designed catalyst. *Phys. Chem. Chem. Phys.* **2011,** *13,* 2457.

(13) Derrien, M. L. In *Catalytic Hydrogenation.* Cervený, L., Ed.; Elsevier: Amsterdam, 1986; Vol. 27; pp 613–666.

(14) Fleming Harold W. Selective hydrogenation. 1964 (US3308180 A).

(15) Zack, R. S.; Skamser, R. O. Ethylene from NGL feedstocks. *Hydrocarb. Process.* **1983,** 99.

(16) Molnár, Á.; Sárkány, A.; Varga, M. Hydrogenation of carbon–carbon multiple bonds. *J. Mol. Catal. A-Chem.* **2001,** *173,* 185.

(17) Borodziński, A. The effect of palladium particle size on the kinetics of hydrogenation of acetylene–ethylene mixtures over Pd/SiO2 catalysts. *Catal. Lett.* **2001,** *71,* 169.

(18) Pellegatta, J.-L.; Blandy, C.; Collière, V.; Choukroun, R.; Chaudret, B.; Cheng, P.; Philippot, K. Catalytic investigation of rhodium nanoparticles in hydrogenation of benzene and phenylacetylene. *J. Mol. Catal. A-Chem.* **2002,** *178,* 55.

(19) Hori, J.; Murata, K.; Sugai, T.; Shinohara, H.; Noyori, R.; Arai, N.; Kurono, N.; Ohkuma, T. Highly active and selective semihydrogenation of alkynes with the palladium nanoparticles-tetrabutylammonium borohydride catalyst system. *Adv. Synth. Catal.* **2009,** *351,* 3143.

(20) Lee, J.-K.; Kim, D.-W.; Cheong, M.-S.; Lee, H.-J.; Cho, B.-W.; Kim, H.-S.; Mukherjee, D. Palladium nanoparticles suspended in an ionic liquid as reusable catalyst for alkyne semihydrogenation. *B. Kor. Chem. Soc.* **2010,** *31,* 2195.

(21) Boles, M. A.; Ling, D.; Hyeon, T.; Talapin, D. V. The surface science of nanocrystals. *Nat. Mater.* **2016,** *15,* 141.

(22) Kwon, S. G.; Krylova, G.; Sumer, A.; Schwartz, M. M.; Bunel, E. E.; Marshall, C. L.; Chattopadhyay, S.; Lee, B.; Jellinek, J.; Shevchenko, E. V. Capping ligands as selectivity switchers in hydrogenation reactions. *Nano Lett.* **2012,** *12,* 5382.

(23) Vargas, A.; Santarossa, G.; Baiker, A. Exchange of hydrogen between a platinum surface and a tertiary amine. *J. Phys. Chem. C.* **2011,** *115,* 1969.

(24) Bonhomme, C.; Gervais, C.; Laurencin, D. Recent NMR developments applied to organic–inorganic materials. *Prog. Nucl. Mag. Res Sp.* **2014,** *77,* 1.

(25) Heiz, U.; Vanolli, F.; Trento, L.; Schneider, W.-D. Chemical reactivity of size-selected supported clusters. *Rev. Sci. Instrum.* **1997,** *68,* 1986.

(26) LaMer, V. K.; Dinegar, R. H. Theory, production and mechanism of formation of monodispersed hydrosols. *J. Am. Chem. Soc.* **1950,** *72,* 4847.

(27) Brust, M.; Walker, M.; Bethell, D.; Schiffrin, D. J.; Whyman, R. Synthesis of thiol-derivatised gold nanoparticles in a two-phase liquid–liquid system. *J. Chem. Soc., Chem. Commun.* **1994,** *0,* 801.

(28) Teo, B. K.; Sloane, N. J. A. Magic numbers in polygonal and polyhedral clusters. *Inorg. Chem.* **1985,** *24,* 4545.

(29) Schmid, G.; Pfeil, R.; Boese, R.; Bandermann, F.; Meyer, S.; Calis, G. H. M.; van der Velden, Jan W. A. Au55[P(C6H5)3]12CI6 — ein Goldcluster ungewöhnlicher Größe. *Chem. Ber.* **1981,** *114,* 3634.

(30) Jadzinsky, P. D.; Calero, G.; Ackerson, C. J.; Bushnell, D. A.; Kornberg, R. D. Structure of a thiol monolayer-protected gold nanoparticle at 1.1 A resolution. *Science.* **2007,** *318,* 430.

(31) Zhu, M.; Aikens, C. M.; Hollander, F. J.; Schatz, G. C.; Jin, R. Correlating the crystal structure of a thiol-protected Au25 cluster and optical properties. *J. Am. Chem. Soc.* **2008,** *130,* 5883.

(32) Nunokawa, K.; Onaka, S.; Ito, M.; Horibe, M.; Yonezawa, T.; Nishihara, H.; Ozeki, T.; Chiba, H.; Watase, S.; Nakamoto, M. Synthesis, single crystal X-ray analysis, and TEM for a single-sized Au11 cluster stabilized by SR ligands. *J. Organomet. Chem.* **2006,** *691,* 638.

(33) Zeng, C.; Qian, H.; Li, T.; Li, G.; Rosi, N. L.; Yoon, B.; Barnett, R. N.; Whetten, R. L.; Landman, U.; Jin, R. Total structure and electronic properties of the gold nanocrystal Au36(SR)24. *Angew. Chem. Int. Ed.* **2012,** *51,* 13114.

(34) Qian, H.; Eckenhoff, W. T.; Zhu, Y.; Pintauer, T.; Jin, R. Total structure determination of thiolate-protected Au38 nanoparticles. *J. Am. Chem. Soc.* **2010,** *132,* 8280.

(35) Heaven, M. W.; Dass, A.; White, P. S.; Holt, K. M.; Murray, R. W. Crystal structure of the gold nanoparticle [N(C8H17)4][Au25(SCH2CH2Ph)18] *J. Am. Chem. Soc.* **2008,** *130,* 3754.

(36) Desireddy, A.; Conn, B. E.; Guo, J.; Yoon, B.; Barnett, R. N.; Monahan, B. M.; Kirschbaum, K.; Griffith, W. P.; Whetten, R. L.; Landman, U.; Bigioni, T. P. Ultrastable silver nanoparticles. *Nature.* **2013,** *501,* 399.

(37) Schmid, G.; Morun, B.; Malm, J.-O. Pt309Phen36*O30±10, a four-shell platinum cluster. *Angew. Chem. Int. Edit.* **1989,** *28,* 778.

(38) Roucoux, A.; Schulz, J.; Patin, H. Reduced transition metal colloids. *Chem. Rev.* **2002,** *102,* 3757.

(39) Teranishi, T.; Miyake, M. Size control of palladium nanoparticles and their crystal structures. *Chem. Mater.* **1998,** *10,* 594.

(40) Teranishi, T.; Miyake, M.; Hosoe, M. Formation of monodispersed ultrafine platinum particles and their electrophoretic deposition on electrodes. *Adv. Mater.* **1997,** *9,* 65.

(41) Tang, Z.; Geng, D.; Lu, G. Size-controlled synthesis of colloidal platinum nanoparticles and their activity for the electrocatalytic oxidation of carbon monoxide. *J. Colloid Interf. Sci.* **2005,** *287,* 159.

(42) Yu, W.; Tu, W.; Liu, H. Synthesis of nanoscale platinum colloids by microwave dielectric heating. *Langmuir.* **1999,** *15,* 6.

(43) Ahmadi, T. S.; Wang, Z. L.; Green, T. C.; Henglein, A.; El-Sayed, M. A. Shape-controlled synthesis of colloidal platinum nanoparticles. *Science.* **1996,** *272,* 1924.

(44) Burda, C.; Chen, X.; Narayanan, R.; El-Sayed, M. A. Chemistry and properties of nanocrystals of different shapes. *Chem. Rev.* **2005,** *105,* 1025.

(45) Tsung, C.-K.; Kuhn, J. N.; Huang, W.; Aliaga, C.; Hung, L.-I.; Somorjai, G. A.; Yang, P. Sub-10 nm platinum nanocrystals with size and shape control: catalytic study for ethylene and pyrrole hydrogenation. *J. Am. Chem. Soc.* **2009,** *131,* 5816.

(46) Wang, Y.; Ren, J.; Deng, K.; Gui, L.; Tang, Y. Preparation of tractable platinum, rhodium, and ruthenium nanoclusters with small particle size in organic media. *Chem. Mater.* **2000,** *12,* 1622.

(47) Schrader, I.; Warneke, J.; Neumann, S.; Grotheer, S.; Swane, A. A.; Kirkensgaard, J. J. K.; Arenz, M.; Kunz, S. Surface chemistry of "unprotected" nanoparticles. *J. Phys. Chem. C.* **2015,** *119,* 17655.

(48) Morris-Cohen, A. J.; Malicki, M.; Peterson, M. D.; Slavin, J. W. J.; Weiss, E. A. Chemical, structural, and quantitative analysis of the ligand shells of colloidal quantum dots. *Chem. Mater.* **2013,** *25,* 1155.

(49) Williams, D. B.; Carter, C. B. *Transmission electron microscopy: A textbook for materials science;* Plenum Press: New York, 1996.

(50) Wang, Z. L. Transmission electron microscopy of shape-controlled nanocrystals and their assemblies. *J. Phys. Chem. B.* **2000,** *104,* 1153.

(51) Khlebtsov, B. N.; Khlebtsov, N. G. On the measurement of gold nanoparticle sizes by the dynamic light scattering method. *Colloid J.* **2011,** *73,* 118.

(52) Hüfner, S. *Photoelectron Spectroscopy: Principles and Applications;* Springer Berlin Heidelberg: Berlin, Heidelberg, 2003.

(53) Li, X.-q.; Zhang, W.-x. Sequestration of metal cations with zerovalent iron nanoparticles - A study with high resolution X-ray photoelectron spectroscopy (HR-XPS). *J. Phys. Chem. C.* **2007,** *111,* 6939.

(54) Torelli, M. D.; Putans, R. A.; Tan, Y.; Lohse, S. E.; Murphy, C. J.; Hamers, R. J. Quantitative determination of ligand densities on nanomaterials by X-ray photoelectron spectroscopy. *ACS Appl. Mater. Interfaces.* **2015,** *7,* 1720.

(55) Cant, D. J. H.; Wang, Y.-C.; Castner, D. G.; Shard, A. G. A technique for calculation of shell thicknesses for core-shell-shell nanoparticles from XPS data. *Surf. Interface Anal.* **2016,** *48,* 274.

(56) Leff, D. V.; Brandt, L.; Heath, J. R. Synthesis and characterization of hydrophobic, organically-soluble gold nanocrystals functionalized with primary amines. *Langmuir.* **1996,** *12,* 4723.

(57) Günzler, H.; Gremlich, H.-U. *IR-Spektroskopie: Eine Einführung;* Wiley-VCH: Weinheim, 2003.

(58) Chen, S.; Kimura, K. Synthesis of thiolate-stabilized platinum nanoparticles in protolytic solvents as isolable colloids. *J. Phys. Chem. B.* **2001,** *105,* 5397.

(59) Cano, I.; Chapman, A. M.; Urakawa, A.; van Leeuwen, Piet W. N. M. Air-stable gold nanoparticles ligated by secondary phosphine oxides for the chemoselective hydrogenation of aldehydes. *J. Am. Chem. Soc.* **2014,** *136,* 2520.

(60) Sharma, A.; Singh, B. P.; Gathania Arvind K. Synthesis and characterization of dodecanethiol-stabilized gold nanoparticles. *Indian J. Pure Ap. Phy.* **2014,** 93.

(61) Sadeghmoghaddam, E.; Lam, C.; Choi, D.; Shon, Y.-S. Synthesis and catalytic properties of alkanethiolate-capped Pd nanoparticles generated from sodium S-dodecylthiosulfate. *J. Mater. Chem.* **2011,** *21,* 307.

(62) Hostetler, M. J.; Wingate, J. E.; Zhong, C.-J.; Harris, J. E.; Vachet, R. W.; Clark, M. R.; Londono, J. D.; Green, S. J.; Stokes, J. J.; Wignall, G. D.; Glish, G. L.; Porter, M. D.; Evans, N. D.; Murray, R. W. Alkanethiolate gold cluster molecules with core diameters from 1.5 to 5.2 nm. *Langmuir.* **1998,** *14,* 17.

(63) Shon, Y.-S.; Gross, S. M.; Dawson, B.; Porter, M.; Murray, R. W. Alkanethiolate-protected gold clusters generated from sodium S-dodecylthiosulfate (Bunte Salts). *Langmuir.* **2000,** *16,* 6555.

(64) Hens, Z.; Martins, J. C. A solution NMR toolbox for characterizing the surface chemistry of colloidal nanocrystals. *Chem. Mater.* **2013,** *25,* 1211.

(65) Glaria, A.; Cure, J.; Piettre, K.; Coppel, Y.; Turrin, C.-O.; Chaudret, B.; Fau, P. Deciphering ligands' interaction with Cu and Cu2O nanocrystal surfaces by NMR solution tools. *Chem. Eur. J.* **2015,** *21,* 1169.

(66) Liu, X.; Yu, M.; Kim, H.; Mameli, M.; Stellacci, F. Determination of monolayer-protected gold nanoparticle ligand–shell morphology using NMR. *Nat. Commun.* **2012,** *3,* 1182.

(67) Morris, G. A. In *Encyclopedia of magnetic resonance.* Harris, Robin K., Ed.; John Wiley & Sons, Ltd: Chichester, UK, 2007.

(68) Fritzinger, B.; Capek, R. K.; Lambert, K.; Martins, J. C.; Hens, Z. Utilizing self-exchange to address the binding of carboxylic acid ligands to CdSe quantum dots. *J. Am. Chem. Soc.* **2010,** *132,* 10195.

(69) Fiurasek, P.; Reven, L. Phosphonic and sulfonic acid-functionalized gold nanoparticles. *Langmuir.* **2007,** *23,* 2857.

(70) Badia, A.; Gao, W.; Singh, S.; Demers, L.; Cuccia, L.; Reven, L. Structure and chain dynamics of alkanethiol-capped gold colloids. *Langmuir.* **1996,** *12,* 1262.

(71) Sharma, R.; Holland, G. P.; Solomon, V. C.; Zimmermann, H.; Schiffenhaus, S.; Amin, S. A.; Buttry, D. A.; Yarger, J. L. NMR characterization of ligand binding and exchange dynamics in triphenylphosphine-capped gold nanoparticles. *J. Phys. Chem. C.* **2009,** *113,* 16387.

(72) Sharma, R.; Taylor, R. E.; Bouchard, L.-S. Intramolecular ligand dynamics in d15-(PPh3)-capped gold nanoparticles investigated by 2H NMR. *J. Phys. Chem. C.* **2011,** *115,* 3297.

(73) García-Antón, J.; Axet, M. R.; Jansat, S.; Philippot, K.; Chaudret, B.; Pery, T.; Buntkowsky, G.; Limbach, H.-H. Reactions of olefins with ruthenium hydride nanoparticles. *Angew. Chem. Int. Ed.* **2008,** *47,* 2074.

(74) Kumar, A.; Mandal, S.; Pasricha, R.; Mandale, A. B.; Sastry, M. Investigation into the interaction between surface-bound alkylamines and gold nanoparticles. *Langmuir.* **2003,** *19,* 6277.

(75) Song, Y.; Murray, R. W. Dynamics and extent of ligand exchange depend on electronic charge of metal nanoparticles. *J. Am. Chem. Soc.* **2002,** *124,* 7096.

(76) Prasad, B. L. V.; Stoeva, S. I.; Sorensen, C. M.; Klabunde, K. J. Digestive-ripening agents for gold nanoparticles. *Chem. Mater.* **2003,** *15,* 935.

(77) Samia, A. C. S.; Schlueter, J. A.; Jiang, J. S.; Bader, S. D.; Qin, C.-J.; Lin, X.-M. Effect of ligand−metal interactions on the growth of transition-metal and alloy nanoparticles. *Chem. Mater.* **2006,** *18,* 5203.

(78) Whetten, R. L.; Price, R. C. Nano-golden order. *Science.* **2007,** *318,* 407.

(79) Pearson, R. G. Absolute electronegativity and hardness. *Inorg. Chem.* **1988,** *27,* 734.

(80) Anderson, N. C.; Hendricks, M. P.; Choi, J. J.; Owen, J. S. Ligand exchange and the stoichiometry of metal chalcogenide nanocrystals. *J. Am. Chem. Soc.* **2013,** *135,* 18536.

(81) Owen, J. The coordination chemistry of nanocrystal surfaces. *Science.* **2015,** *347,* 615.

(82) La Llave, E.; Clarenc, R.; Schiffrin, D. J.; Williams, F. J. Organization of alkane amines on a gold surface. *J. Phys. Chem. C.* **2014,** *118,* 468.

(83) Gavia, D. J.; Shon, Y.-S. Catalytic properties of unsupported palladium nanoparticle surfaces capped with small organic ligands. *ChemCatChem.* **2015,** *7,* 892.

(84) Böker, A.; He, J.; Emrick, T.; Russell, T. P. Self-assembly of nanoparticles at interfaces. *Soft Matter.* **2007,** *3,* 1231.

(85) Albani, D.; Vilé, G.; Mitchell, S.; Witte, P. T.; Almora-Barrios, N.; Verel, R.; López, N.; Pérez-Ramírez, J. Ligand ordering determines the catalytic response

of hybrid palladium nanoparticles in hydrogenation. *Catal. Sci. Technol.* **2016,** *6,* 1621.

(86) Frederick, M. T.; Achtyl, J. L.; Knowles, K. E.; Weiss, E. A.; Geiger, F. M. Surface-amplified ligand disorder in CdSe quantum dots determined by electron and coherent vibrational spectroscopies. *J. Am. Chem. Soc.* **2011,** *133,* 7476.

(87) Knoppe, S.; Bürgi, T. Chirality in thiolate-protected gold clusters. *Acc. Chem. Res.* **2014,** *47,* 1318.

(88) Dolamic, I.; Knoppe, S.; Dass, A.; Bürgi, T. First enantioseparation and circular dichroism spectra of Au38 clusters protected by achiral ligands. *Nat. Commun.* **2012,** *3,* 798.

(89) Knoppe, S.; Dolamic, I.; Dass, A.; Bürgi, T. Separation of enantiomers and CD spectra of Au40(SCH2CH2Ph)24. *Angew. Chem. Int. Ed.* **2012,** *51,* 7589.

(90) Gautier, C.; Bürgi, T. Vibrational circular dichroism of N-acetyl-l-cysteine protected gold nanoparticles. *Chem. Commun.* **2005,** 5393.

(91) Knoppe, S.; Dharmaratne, A. C.; Schreiner, E.; Dass, A.; Bürgi, T. Ligand exchange reactions on Au38 and Au40 clusters. *J. Am. Chem. Soc.* **2010,** *132,* 16783.

(92) Horiuti, I.; Polanyi, M. Exchange reactions of hydrogen on metallic catalysts. *Trans. Faraday Soc.* **1934,** *30,* 1164.

(93) Vilé, G.; Albani, D.; Almora-Barrios, N.; López, N.; Pérez-Ramírez, J. Advances in the design of nanostructured catalysts for selective hydrogenation. *ChemCatChem.* **2016,** *8,* 21.

(94) Borodziński, A.; Bond, G. C. Selective hydrogenation of ethyne in ethene-rich streams on palladium catalysts. Part 1. Effect of changes to the catalyst during reaction. *Cataly. Rev.* **2006,** *48,* 91.

(95) Witte, P. T.; Berben, P. H.; Boland, S.; Boymans, E. H.; Vogt, D.; Geus, J. W.; Donkervoort, J. G. BASF NanoSelect™ technology. *Top. Catal.* **2012,** *55,* 505.

(96) Alonso, F.; Osante, I.; Yus, M. Highly stereoselective semihydrogenation of alkynes promoted by nickel(0) nanoparticles. *Adv. Synth. Catal.* **2006,** *348,* 305.

(97) Abu-Reziq, R.; Wang, D.; Post, M.; Alper, H. Platinum nanoparticles supported on ionic liquid-modified magnetic nanoparticles. *Adv. Synth. Catal.* **2007,** *349,* 2145.

(98) Evangelisti, C.; Panziera, N.; D'Alessio, A.; Bertinetti, L.; Botavina, M.; Vitulli, G. New monodispersed palladium nanoparticles stabilized by poly-(N-vinyl-2-pyrrolidone). *J. Catal.* **2010,** *272,* 246.

(99) Venkatesan, R.; Prechtl, M. H. G.; Scholten, J. D.; Pezzi, R. P.; Machado, G.; Dupont, J. Palladium nanoparticle catalysts in ionic liquids. *J. Mater. Chem.* **2011,** *21,* 3030.

(100) Niu, M.; Wang, Y.; Li, W.; Jiang, J.; Jin, Z. Highly efficient and recyclable ruthenium nanoparticle catalyst for semihydrogenation of alkynes. *Catal. Commun.* **2013,** *38,* 77.

(101) Gieshoff, T. N.; Welther, A.; Kessler, M. T.; Prechtl, M. H. G.; Jacobi von Wangelin, A. Stereoselective iron-catalyzed alkyne hydrogenation in ionic liquids. *Chem. Commun.* **2014,** *50,* 2261.

(102) Konnerth, H.; Prechtl, M. H. G. Selective partial hydrogenation of alkynes to (Z)-alkenes with ionic liquid-doped nickel nanocatalysts at near ambient conditions. *Chem. Commun.* **2016**.

(103) Fievet, F.; Lagier, J.; Blin, B.; Beaudoin, B.; Figlarz, M. Homogeneous and heterogeneous nucleations in the polyol process for the preparation of micron and submicron size metal particles. *Solid State Ionics.* **1989,** *32-33,* 198.

(104) Yang, J.; Deivaraj, T. C.; Too, H.-P.; Lee, J. Y. Acetate stabilization of metal nanoparticles and its role in the preparation of metal nanoparticles in ethylene glycol. *Langmuir.* **2004,** *20,* 4241.

(105) Bock, C.; Paquet, C.; Couillard, M.; Botton, G. A.; MacDougall, B. R. Size-selected synthesis of PtRu nano-catalysts: reaction and size control mechanism. *J. Am. Chem. Soc.* **2004,** *126,* 8028.

(106) Fu, X.; Wang, Y.; Wu, N.; Gui, L.; Tang, Y. Surface modification of small platinum nanoclusters with alkylamine and alkylthiol. *J. Colloid Interf. Sci.* **2001,** *243,* 326.

(107) Kunz, S.; Schreiber, P.; Ludwig, M.; Maturi, M. M.; Ackermann, O.; Tschurl, M.; Heiz, U. Rational design, characterization and catalytic application of metal clusters functionalized with hydrophilic, chiral ligands: a proof of principle study. *Phys. Chem. Chem. Phys.* **2013,** *15,* 19253.

(108) Chen, S.; Kimura, K. Synthesis and characterization of carboxylate-modified gold nanoparticle powders dispersible in water. *Langmuir.* **1999,** *15,* 1075.

(109) Kim, K.-S.; Demberelnyamba, D.; Lee, H. Size-selective synthesis of gold and platinum nanoparticles using novel thiol-functionalized ionic liquids. *Langmuir.* **2004,** *20,* 556.

(110) Adams, B.; Lerner, L. Observation of hydroxyl protons of sucrose in aqueous solution. *J. Am. Chem. Soc.* **1992,** *114,* 4827.

(111) Exarchou, V.; Troganis, A.; Gerothanassis, I. P.; Tsimidou, M.; Boskou, D. Do strong intramolecular hydrogen bonds persist in aqueous solution? *Tetrahedron.* **2002,** *58,* 7423.

(112) Rocha-Santos, T.; Duarte, A. C. *Analysis of marine samples in search of bioactive compounds;* Elsevier: Amsterdam, 2014.

(113) Morris, K. F.; Stilbs, P.; Johnson, C. S. Analysis of mixtures based on molecular size and hydrophobicity by means of diffusion-ordered 2D NMR. *Anal. Chem.* **1994,** *66,* 211.

(114) Pery, T.; Pelzer, K.; Buntkowsky, G.; Philippot, K.; Limbach, H.-H.; Chaudret, B. Direct NMR evidence for the presence of mobile surface hydrides on ruthenium nanoparticles. *ChemPhysChem.* **2005,** *6,* 605.

(115) Paquette, L. A. *Encyclopedia of reagents for organic synthesis;* Wiley: Chichester, 1995.

(116) Kolbert, A. C.; Groot, H. J. M.; Putten, D.; Brom, H. B.; Jongh, L. J.; Schmid, G.; Krautscheid, H.; Fenske, D. Solid state magic angle spinning 13C and 31P NMR of organic ligand stabilized high nuclearity metal clusters. *Z. Phys. D Atom Mol. Cl.* **1993,** *26,* 24.

(117) Melke, J.; Peter, B.; Habereder, A.; Ziegler, J.; Fasel, C.; Nefedov, A.; Sezen, H.; Wöll, C.; Ehrenberg, H.; Roth, C. Metal–support interactions of platinum nanoparticles decorated N-doped carbon nanofibers for the oxygen reduction reaction. *ACS Appl. Mater. Interfaces.* **2016,** *8,* 82.

(118) Kumar, A.; Joshi, H. M.; Mandale, A. B.; Srivastava, R.; Adyanthaya, S. D.; Pasricha, R.; Sastry, M. Phase transfer of platinum nanoparticles from aqueous to organic solutions using fatty amine molecules. *J. Chem. Sci.* **2004,** *116,* 293.

(119) Jaouen, F.; Herranz, J.; Lefèvre, M.; Dodelet, J.-P.; Kramm, U. I.; Herrmann, I.; Bogdanoff, P.; Maruyama, J.; Nagaoka, T.; Garsuch, A.; Dahn, J. R.; Olson, T.; Pylypenko, S.; Atanassov, P.; Ustinov, E. A. Cross-laboratory experimental study of non-noble-metal electrocatalysts for the oxygen reduction Reaction. *ACS Appl. Mater. Interfaces.* **2009,** *1,* 1623.

(120) Fink, J.; Kiely, C. J.; Bethell, D.; Schiffrin, D. J. Self-organization of nanosized gold particles. *Chem. Mater.* **1998,** *10,* 922.

(121) Özkar, S.; Finke, R. G. Nanocluster formation and stabilization fundamental studies. *J. Am. Chem. Soc.* **2002,** *124,* 5796.

(122) Thomas, K. G.; Zajicek, J.; Kamat, P. V. Surface binding properties of tetraoctylammonium bromide-capped gold nanoparticles. *Langmuir.* **2002,** *18,* 3722.

(123) Astruc, D.; Lu, F.; Aranzaes, J. R. Nanoparticles as recyclable catalysts: the frontier between homogeneous and heterogeneous catalysis. *Angew. Chem. Int. Edit.* **2005,** *44,* 7852.

(124) Yonezawa, T.; Tominaga, T.; Richard, D. Stabilizing structure of tertiary amine-protected rhodium colloid dispersions in chloroform. *J. Chem. Soc., Dalton Trans.* **1996,** 783.

(125) Ryu, J. H.; Han, S. S.; Kim, D. H.; Henkelman, G.; Lee, H. M. Ligand-induced structural evolution of Pt55 nanoparticles: amine versus thiol. *ACS nano.* **2011,** *5,* 8515.

(126) Schrader, I.; Warneke, J.; Backenköhler, J.; Kunz, S. Functionalization of platinum nanoparticles with L-proline: simultaneous enhancements of catalytic activity and selectivity. *J. Am. Chem. Soc.* **2015,** *137,* 905.

(127) Sherman, J. The heats of hydrogenation of unsaturated hydrocarbons. *Oil Soap.* **1939,** *16,* 28.

(128) Turkevich, J. Colloidal gold. Part I. *Gold Bull.* **1985,** *18,* 86.

(129) Turkevich, J. Colloidal gold. Part II. *Gold Bull.* **1985,** *18,* 125.

(130) Frens, G. Controlled nucleation for the regulation of the particle size in monodisperse gold suspensions. *Nat. Phys. Sci.* **1973,** *241,* 20.

(131) Bohren, C. F.; Huffman, D. R. *Absorption and scattering of light by small particles;* Wiley-VCH Verlag GmbH: Weinheim, Germany, 1998.

(132) Kunze, J.; Burgess, I.; Nichols, R.; Buess-Herman, C.; Lipkowski, J. Electrochemical evaluation of citrate adsorption on Au(111) and the stability of citrate-reduced gold colloids. *J. Electroanal. Chem.* **2007,** *599,* 147.

(133) Park, J.-W.; Shumaker-Parry, J. S. Structural study of citrate layers on gold nanoparticles: role of intermolecular interactions in stabilizing nanoparticles. *J. Am. Chem. Soc.* **2014,** *136,* 1907.

(134) Willey, T. M.; Vance, A. L.; Bostedt, C.; van Buuren, T.; Meulenberg, R. W.; Terminello, L. J.; Fadley, C. S. Surface structure and chemical switching of thioctic acid adsorbed on Au(111) as observed using near-edge X-ray absorption fine structure. *Langmuir.* **2004,** *20,* 4939.

(135) Lara, P.; Philippot, K.; Chaudret, B. Organometallic Ruthenium Nanoparticles. *ChemCatChem.* **2013,** *5,* 28.

(136) Tschan, M. J.-L.; Diebolt, O.; van Leeuwen, P. W. N. M. Ruthenium metal nanoparticles in hydrogenation. *Top. Catal.* **2014,** *57,* 1054.

(137) Pan, C.; Pelzer, K.; Philippot, K.; Chaudret, B.; Dassenoy, F.; Lecante, P.; Casanove, M.-J. Ligand-stabilized ruthenium nanoparticles. *J. Am. Chem. Soc.* **2001,** *123,* 7584.

(138) Raspolli Galletti, A. M.; Antonetti, C.; Longo, I.; Capannelli, G.; Venezia, A. M. A novel microwave assisted process for the synthesis of nanostructured ruthenium catalysts active in the hydrogenation of phenol to cyclohexanone☆. *Appl. Catal. A-Gen.* **2008,** *350,* 46.

(139) Kim, J.-Y.; Kim, K.-H.; Park, S.-H.; Kim, K.-B. Microwave-polyol synthesis of nanocrystalline ruthenium oxide nanoparticles on carbon nanotubes for electrochemical capacitors. *Electrochim. Acta.* **2010,** *55,* 8056.

(140) Umpierre, A. P.; de Jesús, E.; Dupont, J. Turnover numbers and soluble metal nanoparticles. *ChemCatChem.* **2011,** *3,* 1413.

(141) Eklund, S. E.; Cliffel, D. E. Synthesis and catalytic properties of soluble platinum nanoparticles protected by a thiol monolayer. *Langmuir.* **2004,** *20,* 6012.

(142) Schoenbaum, C. A.; Schwartz, D. K.; Medlin, J. W. Controlling surface crowding on a Pd catalyst with thiolate self-assembled monolayers. *J. Catal.* **2013,** *303,* 92.

(143) Marshall, S. T.; O'Brien, M.; Oetter, B.; Corpuz, A.; Richards, R. M.; Schwartz, D. K.; Medlin, J. W. Controlled selectivity for palladium Cctalysts using self-assembled monolayers. *Nat. Mater.* **2010,** *9,* 853.

(144) Vilé, G.; Almora-Barrios, N.; Mitchell, S.; López, N.; Pérez-Ramírez, J. From the lindlar catalyst to supported ligand-modified palladium nanoparticles: selectivity patterns and accessibility constraints in the continuous-flow three-phase hydrogenation of acetylenic compounds. *Chem. Eur. J.* **2014,** *20,* 5926.

(145) Schoenbaum, C. A.; Schwartz, D. K.; Medlin, J. W. Controlling the surface environment of heterogeneous catalysts using self-assembled monolayers. *Accounts Chem. Res.* **2014,** *47,* 1438.

(146) Corpuz, A. R.; Pang, S. H.; Schoenbaum, C. A.; Medlin, J. W. Hydrogen exposure effects on Pt/Al_2O_3 catalysts coated with thiolate monolayers. *Langmuir.* **2014,** *30,* 14104.

(147) Isaacs, S. R.; Cutler, E. C.; Park, J.-S.; Lee, T. R.; Shon, Y.-S. Synthesis of tetraoctylammonium-protected gold nanoparticles with improved stability. *Langmuir.* **2005,** *21,* 5689.

(148) Niu, Z.; Li, Y. Removal and utilization of capping agents in nanocatalysis. *Chem. Mater.* **2014,** *26,* 72.

(149) Ross, J. R. H. *Heterogeneous catalysis: Fundamentals and applications;* Elsevier: Amsterdam, 2012.

(150) Perego, C. Experimental methods in catalytic kinetics. *Catal. Today.* **1999,** *52,* 133.

Acknowledgments

Many people contributed significantly to this project. In particular, I have to thank:
Prof. Ueli Heiz for giving me the opportunity to work in his group.
Dr. Mirza Cokoja and Dr. Martin Tschurl for supervising my project and giving me the freedom to work independently. It is great to have two supervisors from different fields for scientific discussions, although they may sometimes suffer from communication issues. I further deeply respect your delight and enthusiasm for research in general and your patience, particularly when working on a manuscript, which splits the opinion of the readership.
Sarah Wieghold (STM), Maria Weindl (TGA, NMR), Jürgen Kudermann (NMR, GC), Dr. Gabriele Raudaschl-Sieber (solid state MAS NMR), Dr. Marianne Hanzlik (TEM), Prof. Sebastian Günther (XPS), Dr. Florian Schweinberger (XPS), Ulrike Ammari (EA), Petra Ankenbauer (EA) and Bircan Dilki (EA) for their time and patience in measuring my samples with techniques and machines, that I am just not able to operate, explaining and discussing the results with me.
Imke Schrader (cooperation partner for immobilization experiments) for the great working environment during her stay in Munich and very productive two weeks.
Dr. Marlene Kaposi, Markus Anneser, Dr. Daniel Weiß and Anja Lindhorst for spending lunchtime every day with me at the bakery and thus, escaping the chemistry building for some time of the day.
Thank you to all groups, which warmly welcomed me at the university, the inorganic chemistry group of Prof. Kühn, the physical chemistry group of Prof. Heiz and the Herzig group. It was great spending barbecue sessions, coffee breaks, after-work hours or Hütten-trips with you.
Anke Korte and Jenny Lebert for just being friends during our studies in Bremen and Cologne. Jenny even made it to Munich with me. Thank you so much for discussing work and life with me during coffee breaks, beer drinking or chatty wine events.
My parents Rita und Arthur Wand for their support no matter which city I moved to or country I visited. You always gave me the freedom to do everything that I liked to do.
Finally, I deeply thank my fiancé Maurice Laboureur for his never ending encouragement and trying to find solutions for unsolvable problems. I am very happy spending the future with you.